Application of Numerical Modelling in Choosing Container Spacing, Placement-Room Spacing and Placement-Room Shape for a Deep Geological Repository Using the In-Floor Borehole Placement Method

NWMO TR-2009-28 October 2009

R. Guo

Atomic Energy of Canada Limited

nwmo
NUCLEAR WASTE MANAGEMENT ORGANIZATION
SOCIÉTÉ DE GESTION DES DÉCHETS NUCLÉAIRES

Nuclear Waste Management Organization
22 St. Clair Avenue East, 6th Floor
Toronto, Ontario
M4T 2S3
Canada

Tel: 416-934-9814
Web: www.nwmo.ca

Application of Numerical Modelling in Choosing Container Spacing, Placement-Room Spacing and Placement-Room Shape for a Deep Geological Repository Using the In-Floor Borehole Placement Method

NWMO TR-2009-28

October 2009

R. Guo
Atomic Energy of Canada Limited

Disclaimer:

This report does not necessarily reflect the views or position of the Nuclear Waste Management Organization, its directors, officers, employees and agents (the “NWMO”) and unless otherwise specifically stated, is made available to the public by the NWMO for information only. The contents of this report reflect the views of the author(s) who are solely responsible for the text and its conclusions as well as the accuracy of any data used in its creation. The NWMO does not make any warranty, express or implied, or assume any legal liability or responsibility for the accuracy, completeness, or usefulness of any information disclosed, or represent that the use of any information would not infringe privately owned rights. Any reference to a specific commercial product, process or service by trade name, trademark, manufacturer, or otherwise, does not constitute or imply its endorsement, recommendation, or preference by NWMO.

ABSTRACT

Title: **Application of Numerical Modelling in Choosing Container Spacing, Placement-Room Spacing and Placement-Room Shape for a Deep Geological Repository Using the In-Floor Borehole Placement Method**
Report No.: **NWMO TR-2009-28**
Author(s): R. Guo
Company: Atomic Energy of Canada Limited
Date: October 2009

Abstract
A series of three-dimensional thermal transient and thermal-mechanical (T-M) stress analyses was performed on a deep geological repository (DGR) for used CANDU fuel using the in-floor borehole placement method. The DGR is assumed to be located at a depth of 500 m in crystalline rock. Near-field thermal analyses were carried out to develop a number of thermally acceptable repository layouts. Among these repository layouts, a specific repository layout design with a container spacing of 4.2 m and a placement room-spacing of 40 m was selected for further excavation stability analyses. This specific repository layout design requires the shortest total length of placement rooms and access tunnels.

A coupled near-field T-M model was conducted for the first 1,000 years after placement of the used fuel in a DGR. Excavation-induced mechanical stresses in the rock around the placement room and the placement borehole were studied for circular and elliptical shaped placement-rooms. The stability of the rock mass was evaluated using the Hoek and Brown empirical failure criterion. Excavation of placement room would not cause any significant failure in the rock surrounding the placement room. Some localized damage would occur at the roof of the placement room. The drilling of the in-floor boreholes within the placement room could cause localized damage around the boreholes and in the rock web between two adjacent boreholes. In comparison with the elliptical-shaped room, the localised damage is more severe in the circular-shaped room. For the circular-shaped placement room, the thickness of the damage zone is estimated to be less than 0.125 m at the roof of the placement room, about 0.24 m near the borehole and decreases to 0.02 m at the mid-point of the rock web between two boreholes and less than 0.07 m around the boreholes.

Based on coupled T-M far-field analyses, the peak temperatures at various regions in the repository were determined. The maximum thermally induced uplift at the ground surface above the centre of the repository would be about 0.2 m. The maximum subsidence induced by ice load on the ground surface would be about 6.4 m at 96,000 years.

.

TABLE OF CONTENTS

Page

ABSTRACT ..... **v**

1. INTRODUCTION **1**

2. DESCRIPTION OF A PROPOSED DEEP GEOLOGICAL REPOSITORY **2**

3. METHODS OF ANALYSES AND MATERIAL PROPERTIES **3**

3.1 METHODS OF ANALYSES **3**
3.2 ASSUMPTIONS **4**
3.3 MATERIAL PROPERTIES **4**

4. THERMAL SENSITIVITY ANALYSES FOR CHOOSING PLACEMENT-ROOM SPACING AND CONTAINER SPACING **9**

4.1 MODEL GEOMETRY, THERMAL AND MECHANICAL BOUNDARY CONDITIONS **9**
4.1.1 Model Geometry 9
4.1.2 Thermal and Mechanical Boundary Conditions 10
4.2 THERMAL MODELLING RESULTS FOR CHOOSING PLACEMENT-ROOM SPACING AND CONTAINER SPACING **14**

5. THE FAR-FIELD MODEL **16**

5.1 MODEL GEOMETRY, THERMAL AND MECHANICAL BOUNDARY CONDITIONS **17**
5.1.1 Far-Field Model Geometry 17
5.1.2 Far-Field Model Boundary Conditions 18
5.1.2.1 Far-Field Model Thermal Boundary Conditions 18
5.1.2.2 Far-Field Model Mechanical Boundary Conditions 19
5.1.3 Initial Conditions for the Far-Field Modelling 20
5.1.4 Finite Element Discretization 20
5.2 NUMERICAL RESULTS FROM FAR-FIELD MODELLING **22**
5.2.1 Thermal Results from Far-Field Modelling 22
5.2.2 Mechanical Results from Far-Field Modelling 26

6. NEAR-FIELD MODELLING **47**

6.1 NEAR-FIELD THERMAL MODELLING **48**
6.1.1 The Near-Field Thermal Model 48
6.1.2 Thermal Results from Near-Field Thermal Modelling 48
6.1.3 50
6.2 NEAR-FIELD MECHANICAL AND COUPLED T-M MODELLING **53**
6.2.1 Excavation Analyses 53
6.2.2 Coupled T-M Analyses for the Circular-Shaped Placement Room 58
6.2.2.1 Coupled T-M Near-Field Model 58
6.2.2.2 Thermal Results from the Coupled T-M Modelling 59
6.2.2.3 Thermally Induced Near-Field Stresses 59
6.2.2.4 Thermally Induced Near-Field Displacements 67
6.2.3 Combination of Excavation-Mechanical and Thermally Induced Stresses 74

6.2.4 Near-Field Stability Analyses 82

7. SUMMARY AND CONCLUSIONS 87

ACKNOWLEDGEMENTS 88

REFERENCES 89

LIST OF TABLES

Page

Table 1: Heat Output of Containers of Reference Used CANDU Fuel at Different Times 7
Table 2: Thermal and Mechanical Parameters for the Materials Considered in the Modelling 8
Table 3: Modelling Cases for Sensitivity Analyses 9
Table 4: Peak Temperatures and Time for All Cases 16
Table 5: Glacial-Ice Ground Pressure..... 17

LIST OF FIGURES

Page

Figure 1: Sectional View of Placement Room using the In-Floor Placement Method with a Circular Placement Room 2
Figure 2: Sectional View of Placement Room using the In-Floor Placement Method with an Elliptical Placement Room 3
Figure 3: Placement Room showing General Arrangement of Sealing System Blocks and Used Fuel Containers (After RWE NUKEM Limited 2003b) 4
Figure 4: Finite Element Discretization of the Central Part of the Unit Cell using a Circular-Room Cross Section for Near- Field Analyses 11
Figure 5: Thermal Boundary Conditions for Near-Field Unit Cell..... 12
Figure 6: Mechanical Boundary Conditions for Near-Field Unit Cell..... 13
Figure 7: Temperatures on a Container Surface for a Horizontally Infinite Repository with a Placement-Room Spacing of 20 m 14
Figure 8: Temperatures on a Container Surface for a Horizontally Infinite Repository with a Placement-Room Spacing of 25 m 14
Figure 9: Temperatures on a Container Surface for a Horizontally Infinite Repository with a Placement-Room Spacing of 30 m 15
Figure 10: Temperatures on a Container Surface for a Horizontally Infinite Repository with a Placement-Room Spacing of 40 m 15
Figure 11: Isometric View of Far-Field Model of a DGR using the In-Floor Borehole Placement Method..... 18
Figure 12: Thermal Boundary Conditions for Far-Field Model..... 19
Figure 13: Mechanical Boundary Conditions for Far-Field Model..... 20
Figure 14: Mesh for the Far-Field Thermal Model 21
Figure 15: Simulated Temperatures from Far-Field Analyses at Different Locations..... 22
Figure 16: Far-Field Temperature Profiles at Different Times along Horizontal Symmetry Line OR 23
Figure 17: Far-Field Temperature Rise versus Time at Selected Points along the Vertical Line through the Repository Centre 23
Figure 18: Temperature Distributions along the Vertical Axis of the Repository 24
Figure 19: Thermally Induced Temperature Rise Distributions along the Vertical Axis of the Repository 25
Figure 20: Temperature Response at Five Different Times (The bottom of the figures is 4,000 m below ground surface)..... 26

continued…

LIST OF FIGURES (continued)

Page

Figure 21: Thermally Induced Stresses at the Repository Centre without Considering the Ice Load (Reduction of compressive stress is negative) 27
Figure 22: Total Stresses at the Repository Centre without Considering the Ice Load (Reduction of compressive stress is negative) 27
Figure 23: Total Stresses at the Repository Centre Considering the Ice Load (Reduction of compressive stress is negative) 28
Figure 24: Thermally Induced Stresses in the X-Direction along a Horizontal Line (OR) through the Repository Centre (Reduction of compressive stress is negative) 28
Figure 25: Total Stresses in the X-Direction along a Horizontal Line through the Repository Centre (OR) (Reduction of compressive stress is negative) 29
Figure 26: Thermally Induced Stresses in the Y-Direction along a Horizontal Line through the Repository Centre (Reduction of compressive stress is negative) 29
Figure 27: Total Stresses in the Y-Direction along a Horizontal Line through the Repository Centre (Reduction of compressive stress is negative) 30
Figure 28: Thermally Induced Stress Changes in the Z-Direction along a Horizontal Line through the Repository Centre (Reduction of compressive stress is negative) 31
Figure 29: Total Stresses in the Z-Direction along a Horizontal Line through the Repository Centre (Reduction of compressive stress is negative) 31
Figure 30: Thermally Induced Stresses in the X-Direction along a Vertical Line through the Repository Centre (Reduction of compressive stress is negative) 32
Figure 31: Total Stresses in the X-Direction along a Vertical Line through the Repository Centre (Reduction of compressive stress is negative) 33
Figure 32: Thermally Induced Stress Changes in the Y-Direction along a Vertical Line through the Repository Centre (Reduction of compressive stress is negative) 33
Figure 33: Total Stresses in the Y-Direction along a Vertical Line through the Repository Centre (Reduction of compressive stress is negative) 34
Figure 34: Thermally Induced Stress Changes in the Z-Direction along a Vertical Line through the Repository Centre (Reduction of compressive stress is negative) 35
Figure 35: Total Stresses in the Z-Direction along a Vertical Line through the Repository Centre (Reduction of compressive stress is negative) 35
Figure 36: Thermally Induced Horizontal Stresses (X-direction) on the Ground Surface above the Repository Centre without Considering the Ice Load (Reduction of compressive stress is negative) 36
Figure 37: Thermally Induced Horizontal Stresses (X-direction) on the Ground Surface above the Repository Centre Considering the Ice Load (Reduction of compressive stress is negative) 36
Figure 38: Thermally Induced Horizontal Stresses (X-direction) along Line AB (Reduction of compressive stress is negative) 37
Figure 39: Distributions of Thermally Induced Stresses in the X-Direction on the Vertical Cross-Section through the Centre of the Repository at Four Different Times (Compressive stress is negative) 38
Figure 40: Distributions of Thermally Induced Stresses in the Y-Direction on the Vertical Cross-Section through the Centre of the Repository at Four Different Times (Compressive stress is negative) 39

.....continued…

LIST OF FIGURES (continued)

Page

Figure 41: Distributions of Thermally Induced Stresses in the Z-Direction on the Vertical Cross-Section through the Centre of the Repository at Four Different Times (Compressive stress is negative) 40
Figure 42: Thermally Induced Maximum Principal Stresses at Different Times (Compressive stress is negative) 41
Figure 43: Thermally Induced Minimum Principal Stresses at Different Times (Compressive stress is negative) 42
Figure 44: Thermally Induced Vertical Displacements along the Vertical Line through the Repository Centre without Considering Ice Load (Upward displacement is positive) 43
Figure 45: Comparison of Vertical Displacement along the Vertical Line through Repository Centre at 96,000 Years without and with Considering the Ice Load (Upward displacement is positive) 44
Figure 46: Thermally Induced Vertical Displacement along Ground Surface without Considering Ice Load (Upward displacement is positive) 44
Figure 47: Thermally Induced Vertical Displacement at Ground Surface above the Repository Centre without Considering Ice Load (Upward displacement is positive) 45
Figure 48: Vertical Displacement at Ground Surface above the Repository Centre Considering Ice Load (Upward displacement is positive) 46
Figure 49: Thermally Induced Vertical Displacements at 5,000 Years with a Maximum Value of 0.2 m 46
Figure 50: Thermally Induced Vertical Displacement at the Repository Centre without Considering Ice Load (Upward displacement is positive) 47
Figure 51: Locations for Presentation of Near-Field Modelling Results 49
Figure 52: Temperatures along Horizontal Line EI through the Mid-Height of the Container between Two Placement Rooms 50
Figure 53: Temperature versus Time at Different Locations along Horizontal Line EI 50
Figure 54: Temperatures at Locations of A, B, C, D and E in the Vicinity of the Container and Placement Room 51
Figure 55: Temperature along Line BH at Different Times 51
Figure 56: Temperature along Vertical Line through the Axis of the Container at Seven Different Times 52
Figure 57: Temperatures in the Buffer, Light Backfill, Dense Backfill and Pellets at Four Different Times 53
Figure 58: Temperatures in the Rock near the Container at Four Different Times 54
Figure 59: Stresses along Line AG after Excavation for Two Different Placement-Room Shapes 55
Figure 60: Stresses along Line BH after Excavation for Two Placement-Room Shapes 56
Figure 61: Stresses along Line EI after Excavation for Two Different Placement-Room Shapes 56

continued…

LIST OF FIGURES (continued)

Page

Figure 62: Stresses along Line FK after Excavation for Two Different Placement-Room Shapes 57
Figure 63: Stresses along Line CJ after Excavation for Two Placement-Room Shapes 58
Figure 64: Stresses along Line QS after Excavation for Two Placement-Room Shapes 58
Figure 65: Thermally Induced Stresses in the X-Direction along Line AG 59
Figure 66: Thermally Induced Stresses in the Y-Direction along Line AG 60
Figure 67: Thermally Induced Stresses in the Z-Direction along Line AG 60
Figure 68: Thermally Induced Stresses in the X-Direction along Line BH 61
Figure 69: Thermally Induced Stresses in the Y-Direction along Line BH 61
Figure 70: Thermally Induced Stresses in the Z-Direction along Line BH 62
Figure 71: Thermally Induced Stresses in the X-Direction along Line EI 62
Figure 72: Thermally Induced Stresses in the Y-Direction along Line EI 63
Figure 73: Thermally Induced Stresses in the Z-Direction along Line EI 63
Figure 74: Thermally Induced Stresses in the X-Direction along Line FK 64
Figure 75: Thermally Induced Stresses in the Y-Direction along Line FK 64
Figure 76: Thermally Induced Stresses in the Z-Direction along Line FK 64
Figure 77: Thermally Induced Stresses in the X-Direction along Line CJ 65
Figure 78: Thermally Induced Stresses in the Y-Direction along Line CJ 65
Figure 79: Thermally Induced Stresses in the X-Direction along Line QS 66
Figure 80: Thermally Induced Stresses in the Y-Direction along Line QS 66
Figure 81: Thermally Induced Stresses in the Z-Direction along Line QS 67
Figure 82: Thermally Induced Displacements in the Z-Direction along Line AG 68
Figure 83: Vertical Displacement v.s. Time at Four Different Locations along Line AG 68
Figure 84: Thermally Induced Displacements in the X-Direction along Line BH 69
Figure 85: Thermally Induced Displacement in the X-Direction at Different Locations along Line BH 69
Figure 86: Thermally Induced Displacements in the X-Direction along Line EI 70
Figure 87: Thermally Induced Displacement in the X-Direction at Different Locations along Line EI 70
Figure 88: Thermally Induced Displacements in the Y-Direction along Line FK 71
Figure 89: Thermally Induced Displacement in the Y-Direction at Different Locations along Line FK 71
Figure 90: Thermally Induced Displacements in the Z-Direction along Line CJ 72
Figure 91: Thermally Induced Vertical Displacement at Point C 72
Figure 92: Thermally Induced Displacements in the Y-Direction along Line CJ 73
Figure 93: Thermally Induced Displacement in the Y-Direction at Different Locations along Line CJ 73
Figure 94: Profiles of Total Stresses in the X-Direction along Line AG 74
Figure 95: Profiles of Total Stresses in the Y-Direction along Line AG 75

continued…

LIST OF FIGURES (concluded)

Page

Figure 96: Profiles of Total Stresses in the Z-Direction along Line AG....75
Figure 97: Profiles of Total Stresses in the X-Direction along Line BH....76
Figure 98: Profiles of Total Stresses in the Y-Direction along Line BH....76
Figure 99: Profiles of Total Stresses in the Z-Direction along Line BH....77
Figure 100: Profiles of Total Stresses in the X-Direction along Line EI....77
Figure 101: Profiles of Total Stresses in the Y-Direction along Line EI....78
Figure 102: Profiles of Total Stresses in the Z-Direction along Line EI....78
Figure 103: Profiles of Total Stresses in the X-Direction along Line FK....79
Figure 104: Profiles of Total Stresses in the Y-Direction along Line FK....79
Figure 105: Profiles of Total Stresses in the Z-Direction along Line FK....80
Figure 106: Profiles of Total Stresses in the X-Direction along Line CJ....80
Figure 107: Profiles of Total Stresses in the Y-Direction along Line CJ....81
Figure 108: Profiles of Total Stresses in the X-Direction along Line QS....81
Figure 109: Profiles of Total Stresses in the Y-Direction along Line QS....82
Figure 110: Profiles of Total Stresses in the Z-Direction along Line QS....82
Figure 111: Safety Factors along Line AG at Four Different Times....83
Figure 112: Safety Factors along Line BH at Four Different Times....83
Figure 113: Safety Factors along Line EI at Four Different Times....84
Figure 114: Safety Factors along Line FK at Four Different Times....85
Figure 115: Safety Factors along Line CJ after Excavation....86
Figure 116: Safety Factors along Line QS at Five Different Times Time....86
Figure 117: Thickness of the EDZ at the Floor of the Placement Room....87

1. INTRODUCTION

The Adaptive Phased Management (APM) approach proposed by the Nuclear Waste Management Organization (NWMO) (NWMO 2005) and accepted by the Government of Canada (NRCan 2007) for long-term management of Canada's used nuclear fuel includes placement of the waste in engineered excavations around 500 m m deep in either crystalline rock or sedimentary rock. A design concept for deep geological placement of used CANDU fuel was first developed by Atomic Energy of Canada Limited (AECL) during the period of 1978 to 1996, under the Canadian Nuclear Fuel Waste Management Program (Joint Statement 1978, 1981). The waste owners and the NWMO have continued to develop the deep geological repository (DGR) concept for the long-term safe management of used fuel. A conceptual design and cost estimate for a DGR based on an in-room placement method was prepared in 2002 (CTECH 2002). The DGR concept using the in-floor borehole placement method for used-fuel containers was developed by RWE NUKEM Limited (2003a) based on the Swedish KBS-3V design (Birgersson et al. 2001).

A series of conceptual design studies for a DGR have been carried out in the past (Acres et al. 1985, 1993; Golder Associates Ltd. 1993; Tsai 1986; Tsui and Tsai 1982; 1985; 1994a, b, c). These studies include two- and three-dimensional thermal transient and thermo-mechanical (T-M) analyses for the far-field and near-field of a repository. More recently, RWE NUKEM Limited (2003b) performed T-M analyses using ABAQUS[1] (a finite-element computer program) as part of the assessment of the updated conceptual design for in-floor borehole placement of used nuclear fuel in a DGR.

The CODE_BRIGHT finite-element program[2] was used in 2007 to assess the T-M response of the in-floor borehole placement method for used-fuel containers in a DGR at a depth of 1,000 m in crystalline rock (Guo 2007). Sensitivity analyses were performed in 2008 to investigate the influence of the container spacing and placement-room spacing on the thermal response in a DGR located in limestone at an assumed depth of 750 m below ground surface using a horizontal placement method, also using CODE_BRIGHT (Guo 2008). To further investigate the T-M response in a DGR, CODE_BRIGHT (version 23beta) is used in choosing placement-room spacing, container spacing and placement-room shape and T-M response of a used fuel DGR in granite using the in-floor placement method at an assumed depth of 500-m below ground surface.

This report contains the following.

- A description of the modelled DGR scenarios.
- Material properties.
- Thermal sensitivity analyses for selecting the placement-room spacing and the container spacing.

---

[1] ABAQUS is a general-purpose nonlinear finite element analysis program for mechanical, structural, civil, biomedical, and related engineering applications and is available from SIMULIA France**,** 10, Rue Marcel Dassault, CS70504, 78946 Velizy Villacoublay Cedex, France.

2 CODE_BRIGHT is a general-purpose finite-element program for the analysis of coupled thermal-hydro-mechanical (THM) phenomena in geological media, including moisture transfer in unsaturated soils. It is developed and maintained by the Universidad Politécnica de Cataluña (Olivella et al. 1996).

- Mechanical modelling of the placement room and borehole excavation-induced stress redistribution for both a circular-shaped and elliptical-shaped placement rooms.
- Coupled T-M analytical results from far-field modelling of a DGR.
- Numerical modelling of the coupled T-M response of an in-floor DGR with a circular placement-room shape.
- Summary and conclusions.

2. DESCRIPTION OF A PROPOSED DEEP GEOLOGICAL REPOSITORY

The DGR layout to be modelled consists of an array of horizontal, circular-shaped placement rooms (Figure 1) or elliptical-shaped placement rooms with an aspect ratio (i.e., width to height) of approximately 1.7 (Figure 2). The diameter of the circular placement room is 4.2 m. The elliptical placement room is set at 4.05-m high and 6.89-m wide (Guo 2007).

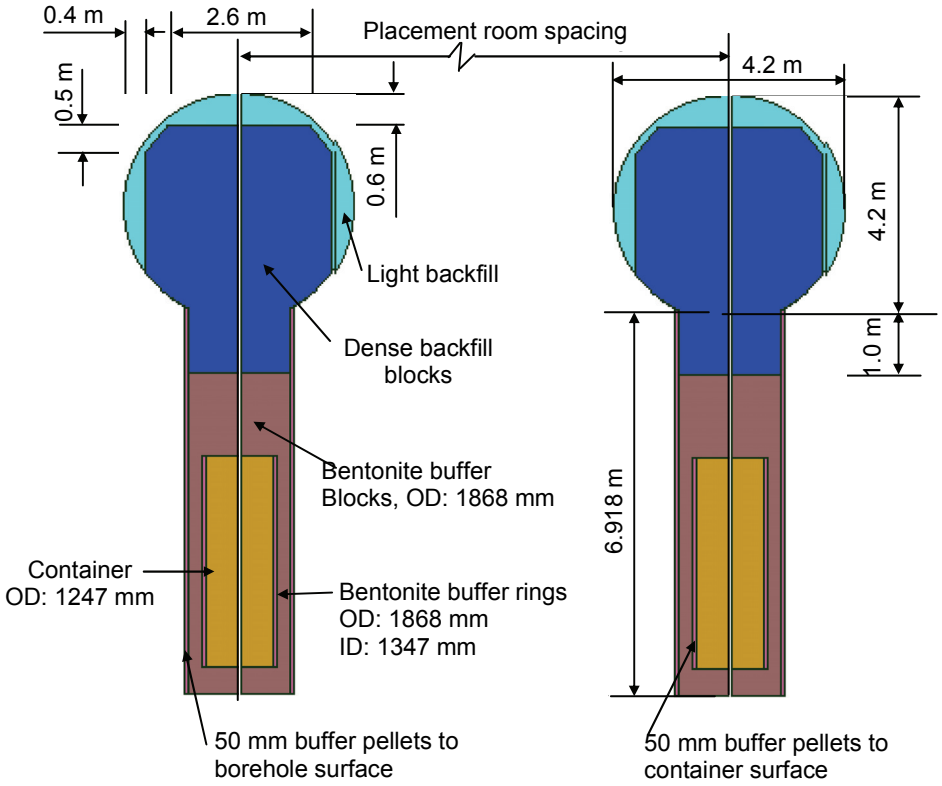


Figure 1: Sectional View of Placement Room using the In-Floor Placement Method with a Circular Placement Room

Access tunnels connect the placement rooms for moving personnel, material, excavated rock, waste containers and backfilling materials. These rooms are arranged into several distinct sections or panels. Each panel consists of a number of rooms, each room containing a number of in-floor boreholes at a specified spacing along the centreline of the placement-room floor. One used-fuel container is placed in each borehole (Figure 3). Each container is 3,909 mm

long with a diameter of 1,247 mm and accommodates 360 used CANDU® fuel bundles. The container design consists of a 25-mm-thick copper outer corrosion-barrier and an inner, carbon-steel load-bearing component (Maak and Simmons 2001). The DGR has a minimum total capacity of about 3.6-million intact fuel bundles or about 10,000 used-fuel containers (UFCs).

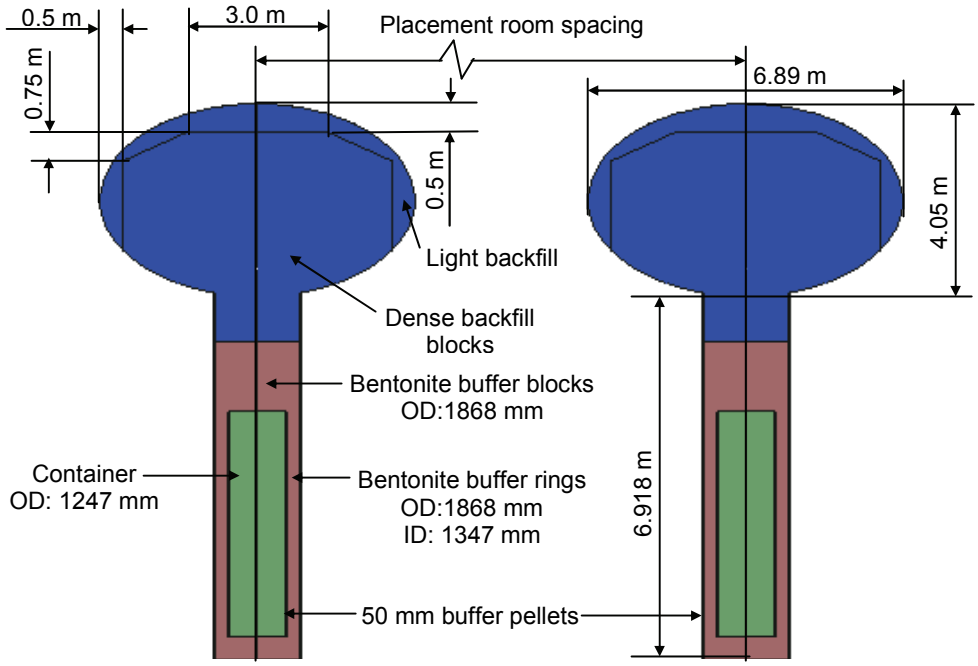


Figure 2: Sectional View of Placement Room using the In-Floor Placement Method with an Elliptical Placement Room

The placement room should be oriented with its long axis parallel to the maximum principal stress direction to minimize the tangential-stress concentrations around the room perimeter. The repository is located at a depth of 500 m in granite with geological and hydrogeologic conditions similar to those of the sparsely fractured rock of the Whiteshell Research Area near Pinawa, Manitoba.

3. METHODS OF ANALYSES AND MATERIAL PROPERTIES

3.1 METHODS OF ANALYSES

The analyses in the report include thermal and coupled T-M modelling to choose the suitable placement room spacing and container spacing. Therefore, the process of these analyses is iterative. For example, although a series of thermal (T) analyses may suggest a certain borehole spacing based on the specification that the temperature at the container surface does not exceed 100°C, the thermal-mechanical (T-M) analyses provide feedback on whether the boreholes will be stable at that spacing or whether the spacing needs to be increased to achieve stability. In this report, a series of near-field thermal analyses was performed to select a combination of suitable placement-room and container spacings such that the temperature on

the container outer surface in a repository will not exceed 100°C. A case for the placement-room spacing and container spacing was then derived based on the preliminary analyses from near-field coupled T-M modelling for the cases with placement-room spacings and container spacings that met the thermal requirement. Then detailed near-field and far-field thermal and coupled T-M analyses were performed.

The CODE_BRIGHT computer program is used in these analyses. GiD (Version 8.0.9)[3] is used in pre-processing and post-processing the input and output data from CODE_BRIGHT.

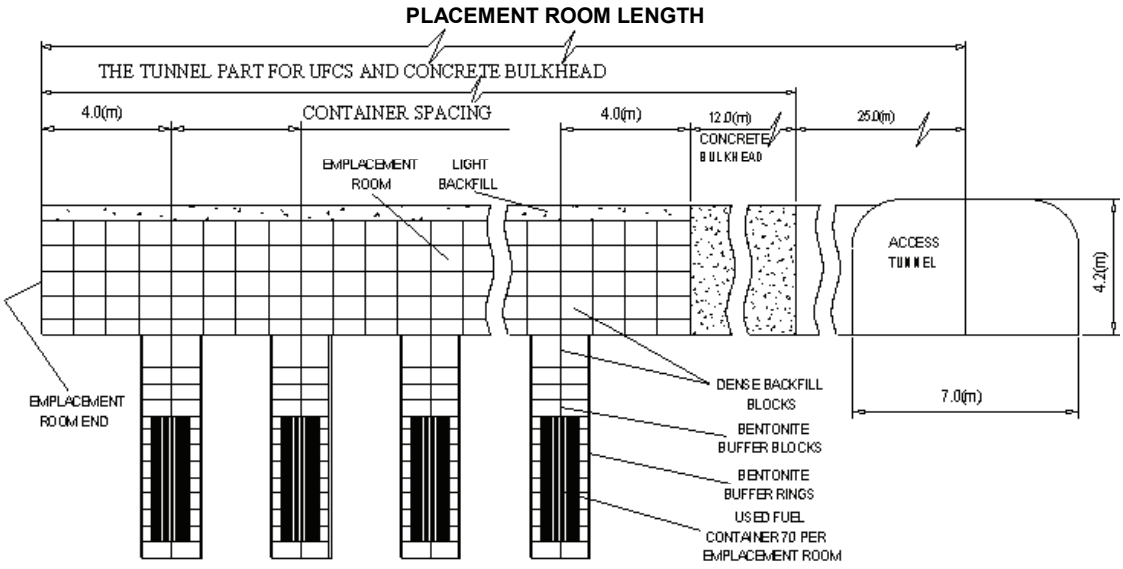


Figure 3: Placement Room showing General Arrangement of Sealing System Blocks and Used Fuel Containers (After RWE NUKEM Limited 2003b)

3.2 ASSUMPTIONS

Each of the materials used in the modelling is assumed to be homogeneous, isotropic, temperature-independent and linearly elastic. The rock mass around the DGR is assumed to be infinite in the horizontal extent.

3.3 MATERIAL PROPERTIES

USED-FUEL PROPERTIES

The heat output from the used fuel from each UFC is as shown in Table 1. All of used fuel is assumed to undergo an initial cooling period of 30 years in surface facilities prior to placement

[3] GiD is a commercial graphical user interface, developed by the International Centre for Numerical Methods in Engineering of Universidad Politècnica de Cataluña, for the definition, preparation and visualization of the data related to numerical simulations (http://gid/cimne.upc.es).

within the DGR and the DGR is assumed to be filled instantaneously with 30-year-out-of-reactor fuel at the reference conditions.

ROCK-MASS PROPERTIES

The material properties of the rock mass are based on measurements from Lac du Bonnet granite at the Underground Research Laboratory (Martin 1993) and are included in Table 2.

The Hoek and Brown empirical failure criterion (Hoek and Brown 1980, 1988) is adopted to evaluate the stability of the rock mass near the placement room and the in-floor borehole. The empirical equation of the Hoek and Brown failure criterion is given by:

$$\sigma_{1f} = \sigma_3 + (m \cdot \sigma_c \cdot \sigma_3 + s \cdot \sigma_c^2)^{\frac{1}{2}} \quad (1)$$

where σ_{1f} is the major principal stress at failure;

σ_3 is the minor principal stress;

σ_c is the uniaxial compressive strength of the intact rock materials from which the rock mass is made up; and

m and s are empirical constants.

Two failure criteria are considered. The first failure criteria or strength model is applied for the case of excavation at ambient temperature to assess whether or not failure may occur from the complex excavation geometry of an advancing tunnel or room face. For this criterion, the parameters of Eqn. 1 are m = 12.5, s = 0.1 and σ_c = 140 MPa,. No damage is assumed if the calculated σ_{1f} is greater than the applied major principal stress σ_1. The second failure criterion or strength model is used for the peak strength of the rock that is not damaged by excavation under the full thermal-mechanical loads. The second set of strength parameters are m = 17, s = 0.1 and σ_c = 210 MPa and these can only be applied if the rock excavation stresses do not exceed the initial design parameters during excavation

The ambient in-situ stresses (Kaiser and Maloney 2005) used in these analyses are as follows:

$$\sigma_1 = \begin{cases} 0.071\ MPa/m \cdot depth + 5.768\ MPa & < 300\ m \\ 0.041\ MPa/m \cdot depth + 14.9\ MPa & from\ 300\ m\ to\ 600\ m \\ 0.026\ MPa/m \cdot depth + 23.636\ MPa & from\ 600\ m\ to\ 1500\ m \end{cases} \quad (2)$$

$$\sigma_2 = \begin{cases} 0.043\ MPa/m \cdot depth + 3.287\ MPa & < 300\ m \\ 0.035\ MPa/m \cdot depth + 5.67\ MPa & from\ 300\ m\ to\ 600\ m \\ 0.016\ MPa/m \cdot depth + 17.104\ MPa & from\ 600\ m\ to\ 1500\ m \end{cases} \quad (3)$$

$$\sigma_3 = \begin{cases} 0.034\ MPa/m \cdot depth & < 300\ m \\ 0.0096\ MPa/m \cdot depth + 7.334\ MPa & from\ 300\ m\ to\ 600\ m \\ 0.020\ MPa/m \cdot depth + 1.066\ MPa & from\ 600\ m\ to\ 1500\ m \end{cases} \quad (4)$$

where σ_1, σ_2 and σ_3 are the major, intermediate and minor principal stresses, respectively.

The ambient in-situ stress, σ_1, is applied in the Y-direction; the stress, σ_2, is applied in the X-direction; and the stress, σ_3, is applied in the Z-direction as shown in Figure 4.

SEALING-MATERIAL PROPERTIES

There are four bentonite clay-based sealing materials for the in-floor borehole placement design: buffer material, dense backfill, light backfill and buffer pellets. For the in-floor borehole placement method, the buffer is placed around the container in the form of close-fitting, pre-compacted rings. The 50-mm gap between the UFC and the buffer rings, and the 50-mm gap between the rings and the rock formation will be filled using a pelletized form of the buffer material. The specifications for the basic physical properties of clay-based sealing materials are presented in Table 2.

USED-FUEL CONTAINER PROPERTIES

The thermal conductivity of the used-fuel container is 300 W/(m°C). The density of the used-fuel container is 7800 kg/m^3. The specific heat of the used-fuel container is 500 J/(kg°C). The Young's modulus is 200,000 MPa and its Poisson's ratio is 0.2.

Table 1: Heat Output of Containers of Reference Used CANDU Fuel at Different Times

Time Out-of-reactor (years)	Heat Generation (220 MWh/kg U Burn-up)		
	Watts per kg U	Watts per bundle	(W/container) (360 bundles)
30	1.83E-01	3.52	1268.2
35	1.68E-01	3.23	1164.2
40	1.54E-01	2.97	1069.2
45	1.42E-01	2.74	986.4
50	1.32E-01	2.53	910.8
55	1.22E-01	2.35	846.0
60	1.14E-01	2.19	788.4
70	9.91E-02	1.908	686.9
75	9.30E-02	1.791	644.8
80	8.75E-02	1.685	606.6
90	7.82E-02	1.505	541.8
100	7.07E-02	1.361	490.0
110	6.47E-02	1.245	448.2
135	5.41E-02	1.041	374.8
150	4.99E-02	0.96	345.6
160	4.77E-02	0.918	330.5
200	4.19E-02	0.806	290.2
300	3.55E-02	0.684	246.2
500	2.91E-02	0.56	201.6
1,000	2.02E-02	0.388	139.7
2,000	1.38E-02	0.265	95.40
5,000	1.00E-02	0.1926	69.34
10,000	7.19E-03	0.1385	49.86
20,000	4.16E-03	0.0801	28.84
35,000	2.27E-03	0.0437	15.73
50,000	1.43E-03	0.0274	9.864
100,000	4.41E-04	0.00849	3.056
200,000	1.65E-04	0.00317	1.141
250,000	1.52E-04	0.00293	1.055
500,000	1.48E-04	0.00285	1.026
1,000,000	1.48E-04	0.00285	1.026

Table 2: Thermal and Mechanical Parameters for the Materials Considered in the Modelling (after Garisto et al. 2004)

Property	Granite [4]	Buffer	Buffer Pellets	Dense backfill	Light backfill
Composition	N/A[2]	100% bentonite	100% bentonite	70:25:5 aggregate, clay, bentonite	50:50 bentonite, crushed granite sand
Thermal conductivity (W/m°C)	3.00	1.00	0.5	2.00	0.70
Specific heat (J/kg°C)	845	1440	910	1100	1280
Bulk Density (kg/m^3)	2700	1950	1410	2280	1400
Dry Density (kg/m^3)	2700	1610	1410	2120	1240
Porosity (%)	0.3	41	49	22	50
Saturation Level (%)	N/A	65	6	80	33
Moisture content (Gravimetric, %)	N/A	17	2	8.5	15
Young's modulus (GPa)	45	0.10	0.10	0.20	0.10
Poisson's ratio	0.25	0.10	0.10	0.10	0.10
Coefficient of thermal expansion (10^{-6}/°C)	10	N/A	N/A	N/A	N/A

[4] P. Baumgartner *et al.* "The in-room emplacement method for a used fuel disposal facility – preliminary design consideration", AECL TR-655, COG-94-533, 1995

[2] NA - not applicable.

4. THERMAL SENSITIVITY ANALYSES FOR CHOOSING PLACEMENT-ROOM SPACING AND CONTAINER SPACING

A series of near-field thermal analyses was performed to select a suitable combination of placement-room and container spacings such that the temperature on the container outer surface in a repository will not exceed 100°C. Table 3 shows the cases of near-field thermal modelling for selecting container spacing and room spacing conducted in this section.

Table 3: Modelling Cases for Sensitivity Analyses

Room spacing (m) / Cases / Container spacing (m)	20	V 25	30	40
3.2			X	
4.0			X	X
4.2				X
4.5			X	X
4.6			X	
4.7			X	
5.0	X	X		
5.3		X		
6.0	X			
6.2	X			

4.1 MODEL GEOMETRY, THERMAL AND MECHANICAL BOUNDARY CONDITIONS

4.1.1 Model Geometry

The finite-element discretization of a unit cell using the in-floor borehole method for the near-field modelling is shown in Figure 4. There are six kinds of materials, granite rock; light backfill, dense backfill blocks, bentonite buffer blocks, container and bentonite pellets (Note that the colours in Figure 4 do not relate to these materials). The dimensions of the placement room and the in-floor borehole are the same as shown in Figure 1. The horizontal dimensions of a unit cell are b x d (b=1/2 of container spacing, d=1/2 of placement-room spacing. Placement-room spacing (d) and container spacing (b) are shown in Table 3. The vertical dimension of the model unit cell is 5,000 m. The depth of the crown of the placement room is 500 m. Eight-noded elements are used through the model. The elements are more densely distributed in the region of high thermal and stress gradients as shown in Figure 4 (near the placement room and the in-floor borehole). Dimensions of a typical solid element around the in-floor borehole are approximately 0.15 m x 0.18 m x 0.28 m.

4.1.2 Thermal and Mechanical Boundary Conditions

Thermal Boundary Conditions shown in Figure 5 are as follows.

- The temperature on the top surface (ground surface) is 5°C for the first 60,000 years. The temperature is 0°C after 60,000 years, assuming glaciation.
- An isothermal condition is applied at bottom of the model (i.e., 5,000 metres below ground surface) at a temperature of 65°C.
- An adiabatic condition is applied on the four vertical surfaces of the model due to mirror symmetry, which represents the thermal conditions associated with this unit cell within an infinite tabular array of placement rooms.
- A uniform thermal load is applied at the nodes (12 nodes) along the axis of the container. The total thermal load applied to the 12 nodes is one quarter (1/4) of a container thermal load (Table 1) due to the intersection of two adiabatic planes at the container centreline.

Mechanical Boundary Conditions shown in Figure 6 are as follows.

- The ground surface is free to move in the vertical direction.
- The four vertical surfaces are fixed in the horizontal direction and are free to move vertically.
- The bottom surface is fixed in the vertical direction.

The thermal and mechanical boundary conditions described above represent boundary conditions for a unit cell in a horizontally infinite repository. Based on the study in Guo (2007), the results from the near-field model using thermal-mechanical boundary conditions described above are accurate only for the first 1,000 years for a horizontally finite repository.

Initial Boundary Conditions are as follows.

- The initial ambient temperature of the model is based on geothermal gradient of 0.012°C/m of depth and a ground surface temperature of 5°C resulting in an ambient temperature of 65°C at the bottom of the model (i.e., at a depth of 5,000 m).
- The initial stresses and displacements are assumed to be zero.

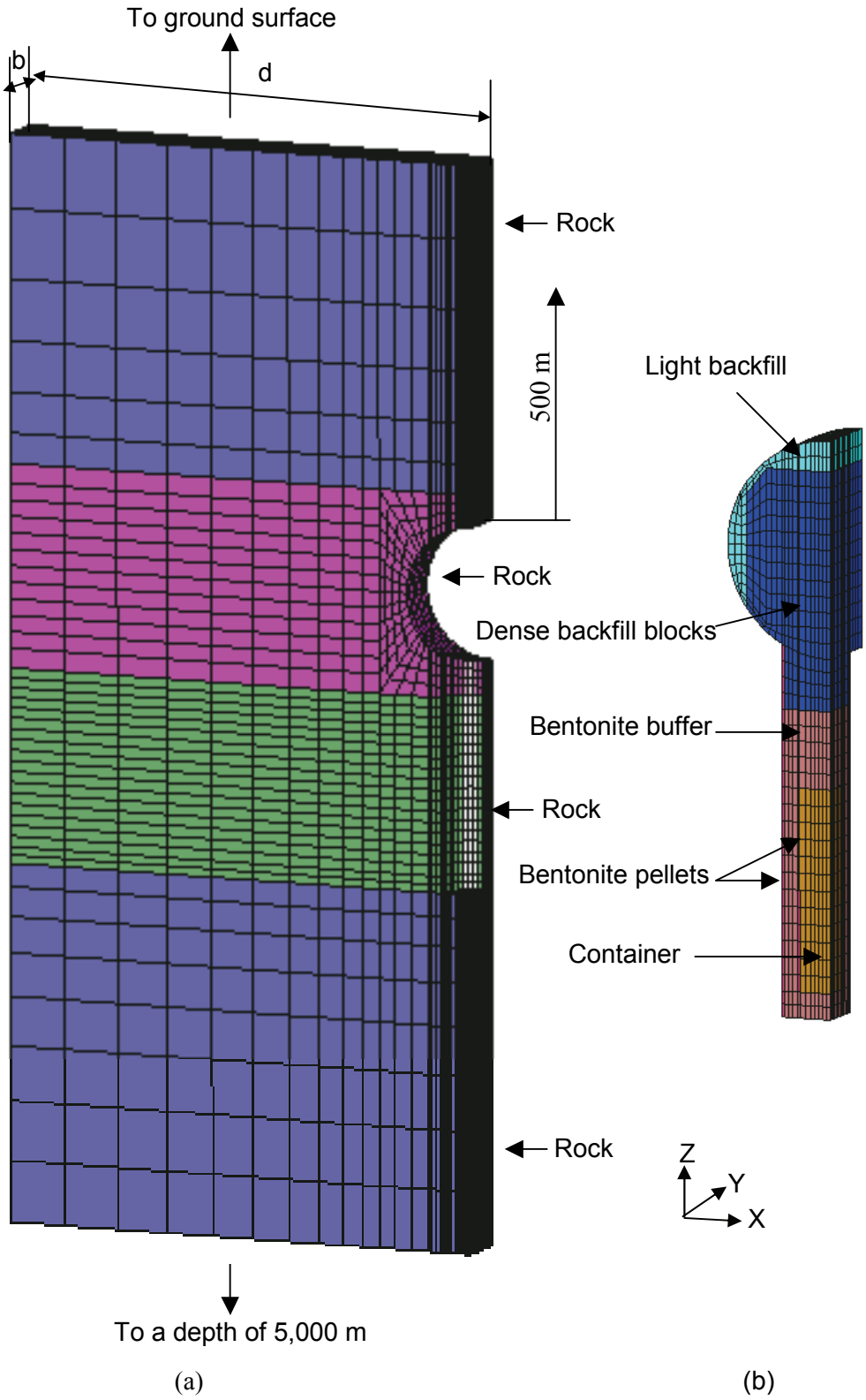


Figure 4: Finite Element Discretization of the Central Part of the Unit Cell Using a Circular-Room Cross Section for Near-Field Analyses

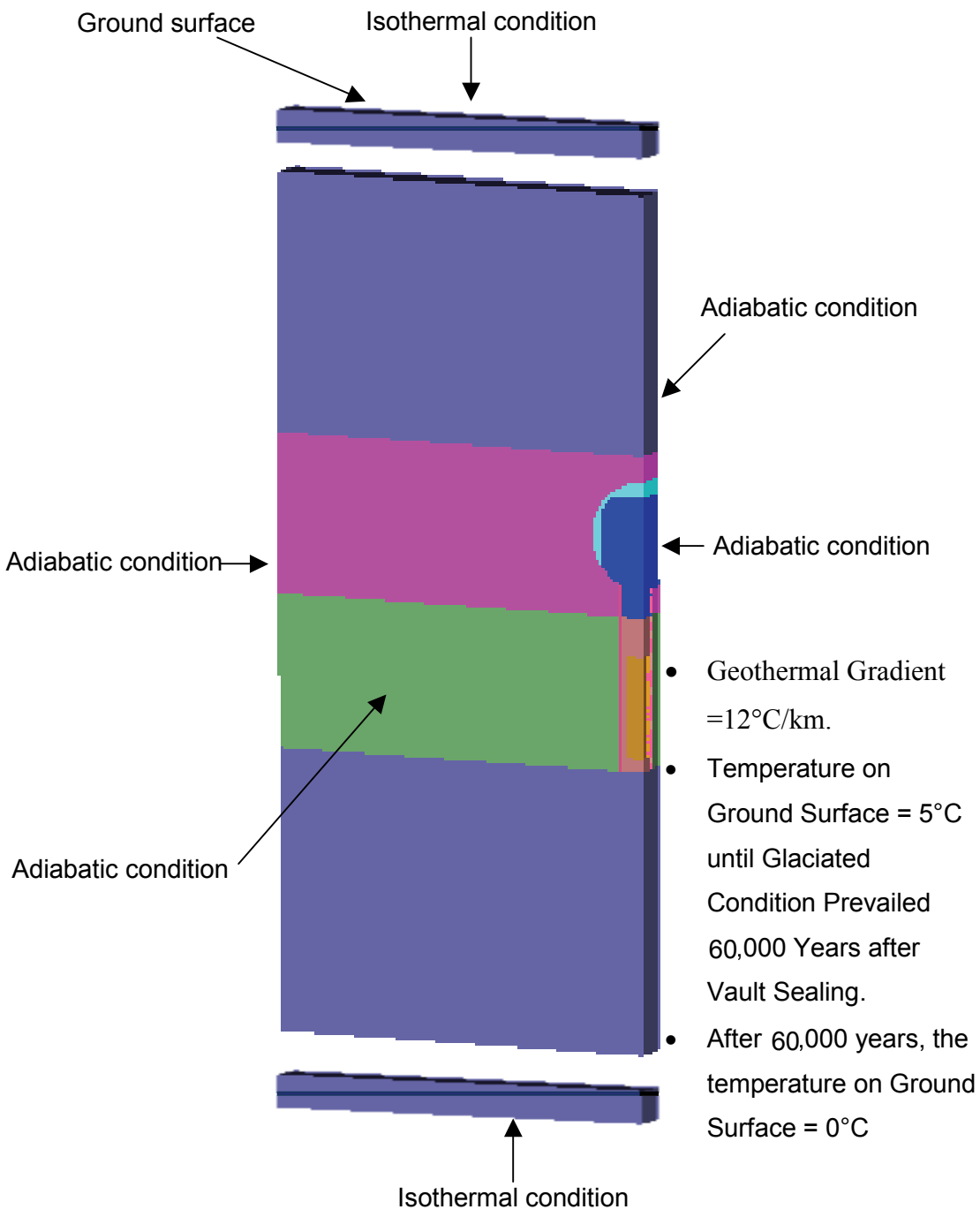


Figure 5: Thermal Boundary Conditions for Near-Field Unit Cell

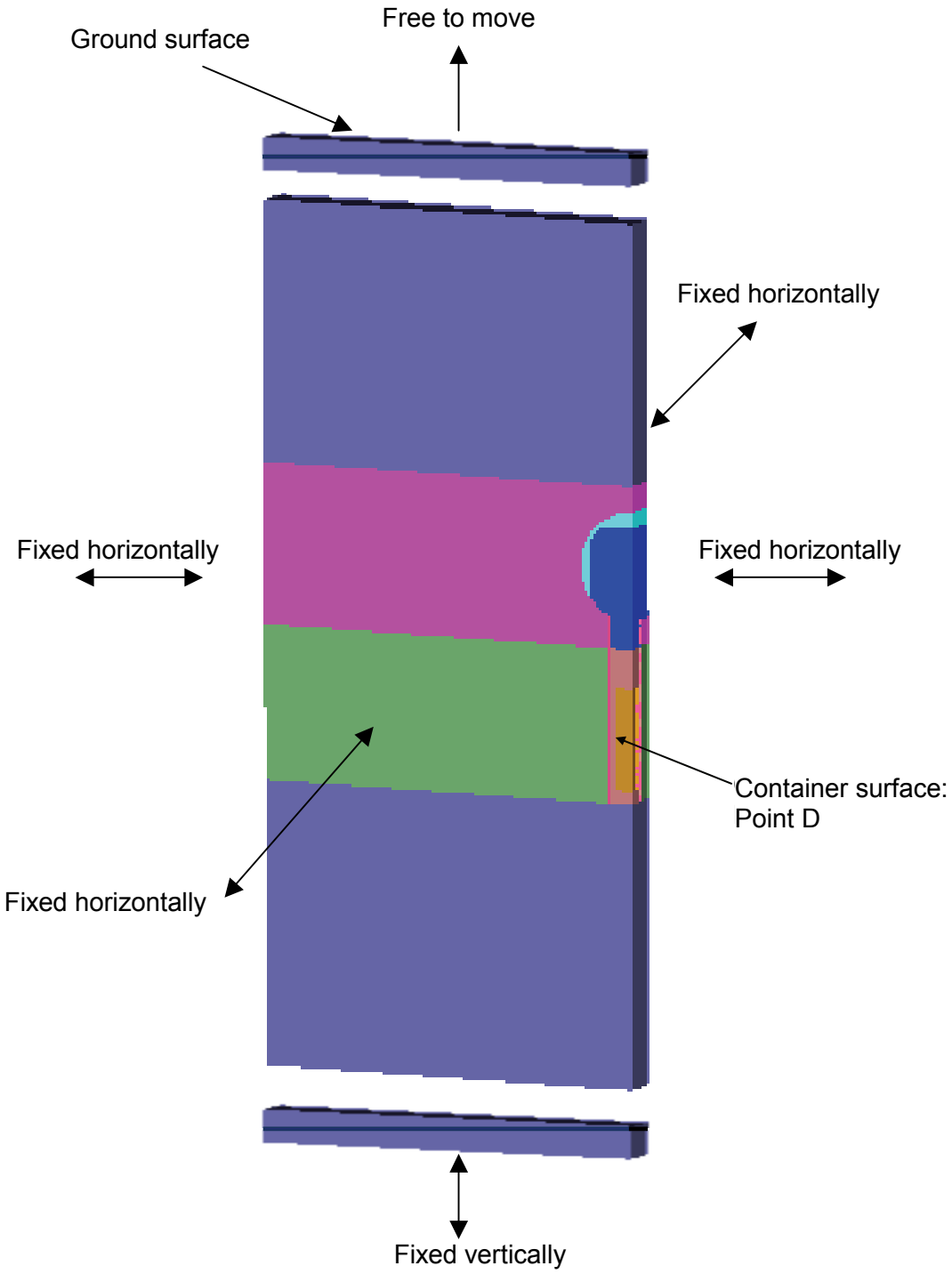


Figure 6: Mechanical Boundary Conditions for Near-Field Unit Cell

4.2 THERMAL MODELLING RESULTS FOR CHOOSING PLACEMENT-ROOM SPACING AND CONTAINER SPACING

Figures 7 through 10 show the calculated temperatures on the container surface in a horizontally infinite repository at various container spacings for placement-room spacings of 20, 25, 30 and 40 m, respectively. For the cases with a room spacing of 20 m, the first peak temperatures are higher than 100°C when container spacing is less than 6.2 m. For the cases with a room spacing of 25 m, the first peak temperature is higher than 100°C when container spacing is less than 5.3 m.

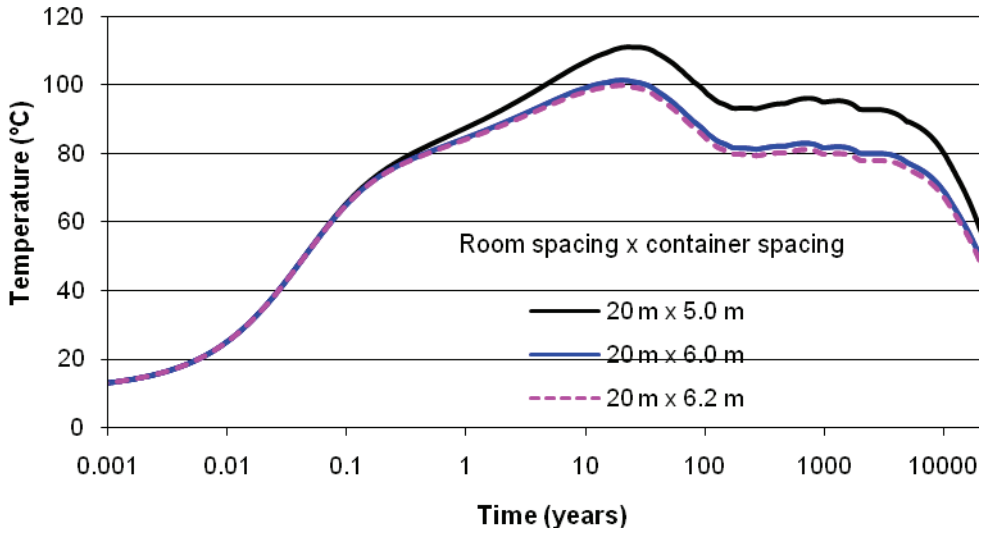


Figure 7: Temperatures on a Container Surface for a Horizontally Infinite Repository with a Placement-Room Spacing of 20 m

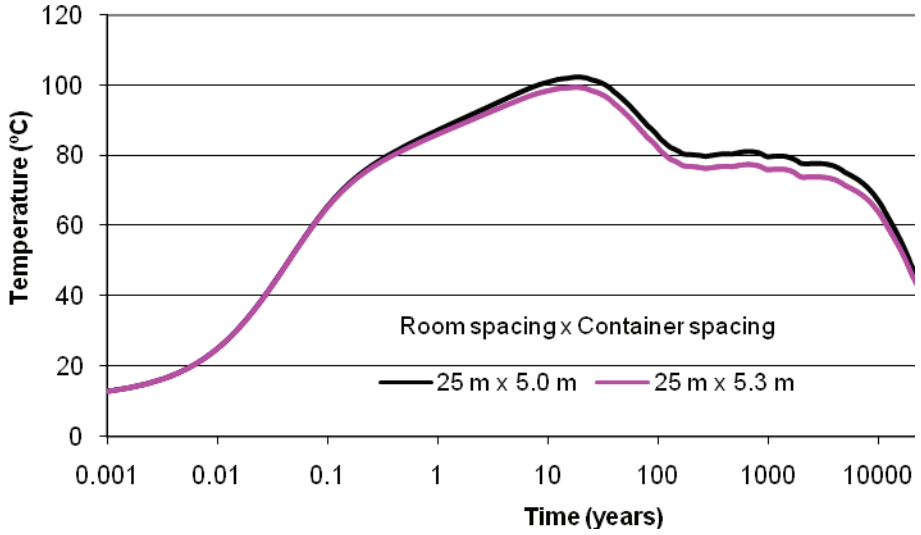


Figure 8: Temperatures on a Container Surface for a Horizontally Infinite Repository with a Placement-Room Spacing of 25 m

For the cases with a room spacing of 30 m, the first peak temperature is higher than 100°C when container spacing is less than 4.7 m. For the cases with a room spacing of 40 m, the first peak temperature is higher than 100°C when container spacing is less than 4.2 m.

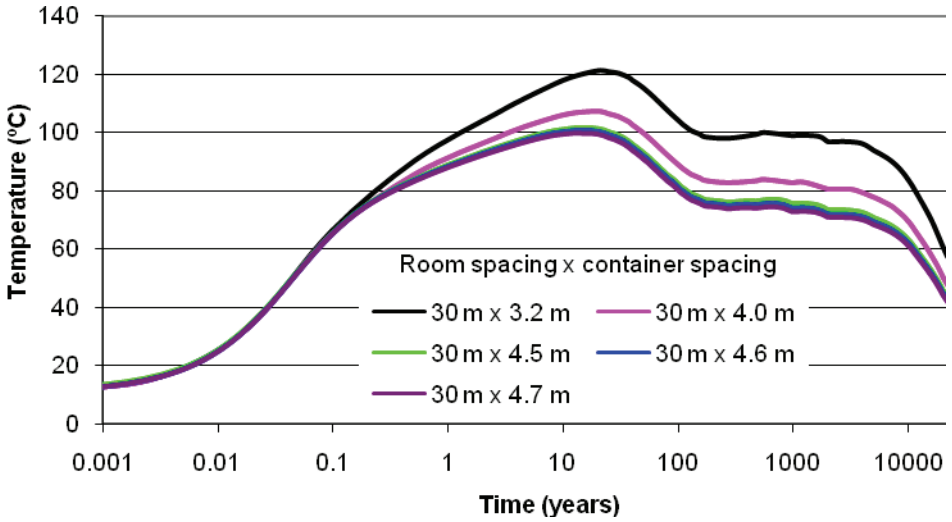


Figure 9: Temperatures on a Container Surface for a Horizontally Infinite Repository with a Placement-Room Spacing of 30 m

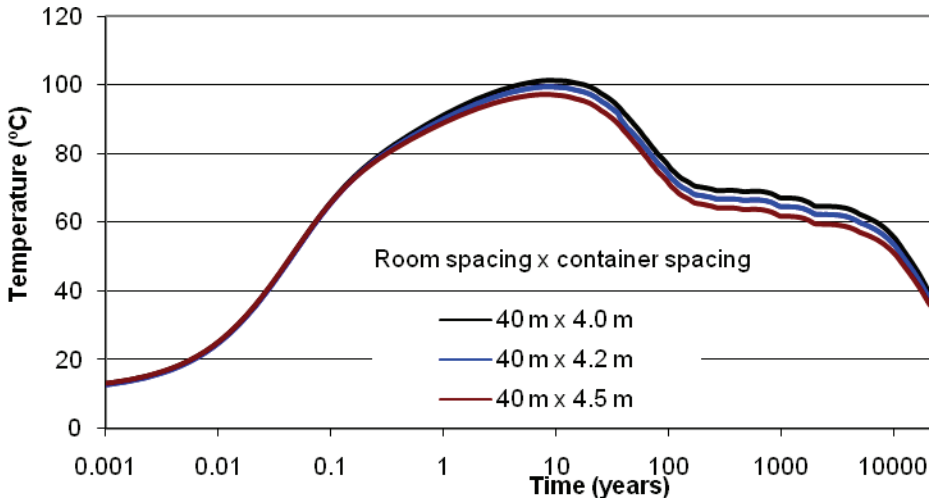


Figure 10: Temperatures on a Container Surface for a Horizontally Infinite Repository with a Placement-Room Spacing of 40 m

Table 4 shows the peak temperatures for all of the cases. For each room-spacing case, a container-spacing case was found that satisfies the thermal requirement of a maximum container outer-surface temperature of 100°C. Among all four thermally acceptable repository layout designs, the layout design with a room-spacing of 40 m and a container spacing of 4.2 m has been selected for further modelling analyses since this layout design requires the shortest total length of placement room and access tunnels. In order to reduce the excavation and backfilling costs, it is desirable to select repository layout designs with relatively shorter lengths of placement rooms and access tunnels.

Table 4: Peak Temperatures and Time for All Cases

PRS x CS (m x m)	Peak temperature (°C)	Time (years)	PRS x CS (m x m)	Peak temperature (°C)	Time (years)
20 x 5.0	111	27.5	20 x 6.0	102	20.0
20 x 6.2	100	20.0	25 x 5.0	102	20.0
25 x 5.3	100	17.5	30 x 3.2	121	22.5
30 x 4.0	107	20.0	30 x 4.5	102	17.5
30 x 4.6	101	12.4	30 x 4.7	100	12.4
40 x 4.0	102	8.3	40 x 4.2	100	8.3
40 x 4.5	97	8.3			

Note: PRS: Placement-Room Spacing; CS: Container Spacing

5. THE FAR-FIELD MODEL

This section describes the far-field modeling for a repository with a placement-room spacing of 40 m and a container spacing of 4.2 m. This repository has 165 placement rooms in eight panels. Each panel has 21 placement rooms. There are 67 containers in each placement room. Therefore, there are total 11,055 containers in the geometry associated with this repository (i.e., the minimum of ~10,000 containers was specified in Section 2 and a contingency to account for borehole that cannot be used). The plan area of the repository is 1,820 m by 1,450 m and the depth of the repository is fixed at 500 m to the crown of the placement room.

The thermal response was calculated using finite-element program CODE_BRIGHT, in which the influence of glaciation on the thermal response was reflected by application of thermal boundary condition on the ground surface that the temperature was 5^{o}C during the first 60,000 years and 0^{o}C after 60,000 years although the time of glaciations will be only from 60,000 years to 105,000 years. Using 0^{o}C as the thermal boundary condition on the ground surface after 105,000 years will not affect the conclusions from the far-field modelling because the temperatures in the rock near the repository after 105,000 years will be very low. For the near-field modelling, the results after 105,000 years are only good for a horizontally infinite repository, not for the case of a horizontally finite DGR.

The thermally induced mechanical response caused by thermal load released by the used-fuel and the decrease of the temperature on the ground surface during the period of glaciation was calculated. The mechanical response caused by ice load (Table 5) during the period of glaciation was calculated using Hooke's law under the K_0 condition (there is no horizontal displacement). The total stresses were obtained by adding the initial stress vectors, ice-load induced stress vectors and thermally induced stress vectors based on the principle of superposition. The total displacements were obtained by adding the displacement induced by ice load during the period of glaciation to the thermally induced displacements.

Table 5: Glacial-Ice Ground Pressure (Baumgartner 2005)

Time Following Waste Placement (a)	Glacial Ice Thickness (m)	Ground Pressure* (MPa)
60,000	0	0.0
66,000	1,500	13.5
86,000	3,000	27.1
96,000	3,200	28.9
104,000	2,100	18.9
105,000	0	0.0

5.1 MODEL GEOMETRY, THERMAL AND MECHANICAL BOUNDARY CONDITIONS

The far-field analyses provide an assessment of the thermal and stress conditions in the rock mass surrounding a repository of finite dimensions. Uplift of the rock mass due to thermal expansion effects can be estimated including the potential for near-surface fracturing or the opening of pre-existing near-vertical fractures.

5.1.1 Far-Field Model Geometry

The isometric view of the far-field model of a repository using the in-floor-borehole placement method is shown in Figure 11. Due to symmetry, only a quarter section of a DGR needs to be modelled. The model is bounded vertically by the ground surface on the upper side and by a plane 10,000 m below the ground surface, at the bottom. The horizontal dimensions of the model in the X- and Y-directions are 7,000 m x 7,000 m. These dimensions should be sufficient such that the T-M response of the rock at the boundaries remains unaffected by the presence of the DGR during the simulation time period. The DGR is represented by a 3.918-m-thick plate of material generating heat load and the details of the placement rooms are ignored. The horizontal dimensions of a quarter of a DGR are 910 m x 725 m.

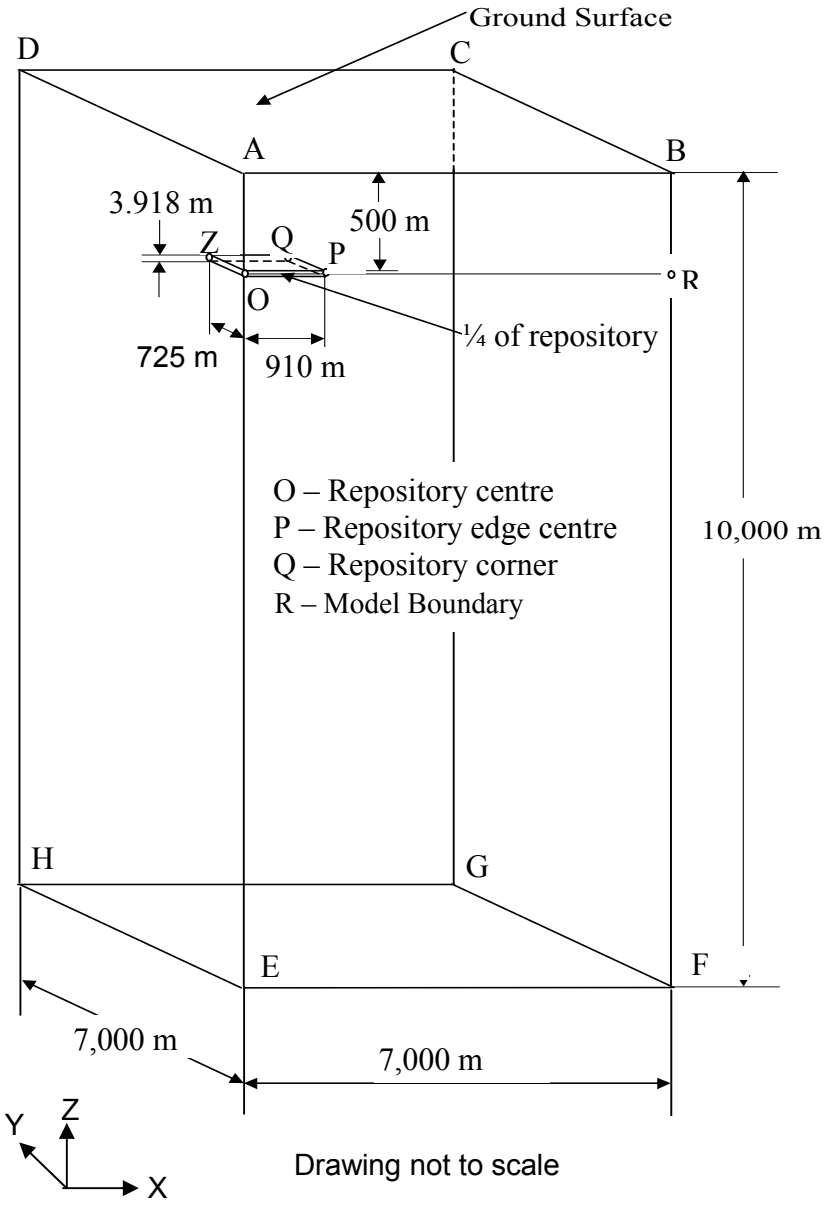


Figure 11: Isometric View of Far-Field Model of a DGR using the In-Floor Borehole Placement Method

5.1.2 Far-Field Model Boundary Conditions

5.1.2.1 Far-Field Model Thermal Boundary Conditions

As with the near-field model, the thermal boundary conditions are defined as follows (Figure 12).

- The upper surface boundary condition is modelled as an isothermal boundary, at a temperature of 5°C, representing the average Canadian Shield surface temperature, reducing to 0°C after 60,000 years to account for a period of glaciation.

- The lower boundary is also modelled as an isothermal boundary set at a temperature of 125°C, based on a geothermal gradient of 0.012°C/m of depth plus the ground surface temperature of 5°C.
- The vertical boundaries are modelled as adiabatic planes of symmetry as shown in Figure 12.
- The heat generated from the used-fuel containers in one-quarter of a repository is uniformly distributed throughout one-quarter of the repository (i.e., a rectangular plate of 910-m long by 725-m wide by 3.918-m high (3.918 m is the height of the used-fuel container).

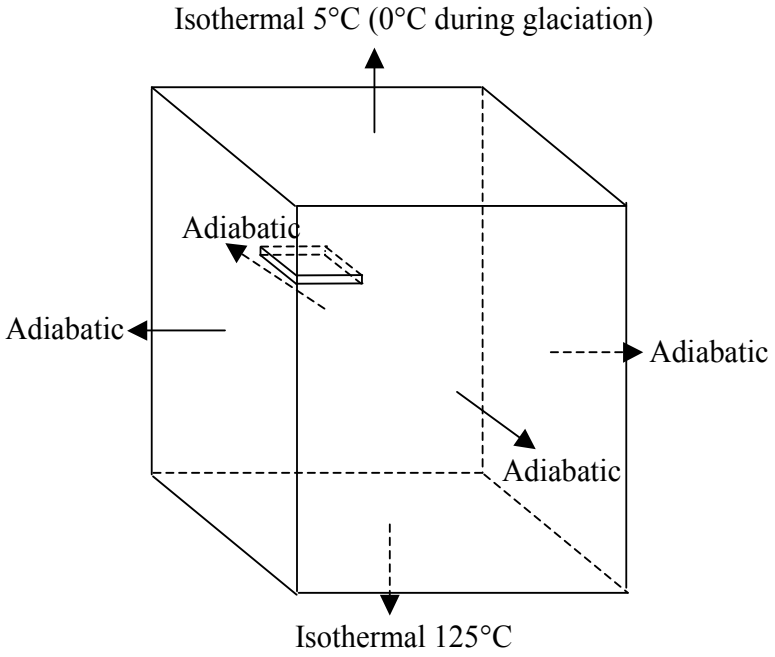


Figure 12: Thermal Boundary Conditions for Far-Field Model

5.1.2.2 Far-Field Model Mechanical Boundary Conditions

The mechanical boundary conditions are defined as follows (Figure 13).

- The vertical planes of the model are constrained not to move in the horizontal direction.
- The bottom plane of the model is fixed in the vertical direction.
- The upper horizontal plane, the ground surface, is free to move in the vertical direction during the first 60,000 years.
- Glacial gravitational loads are applied on the ground surface beginning 60,000 years after waste placement (Table 5).

The model is representative of a DGR positioned in an infinite extent of granite.

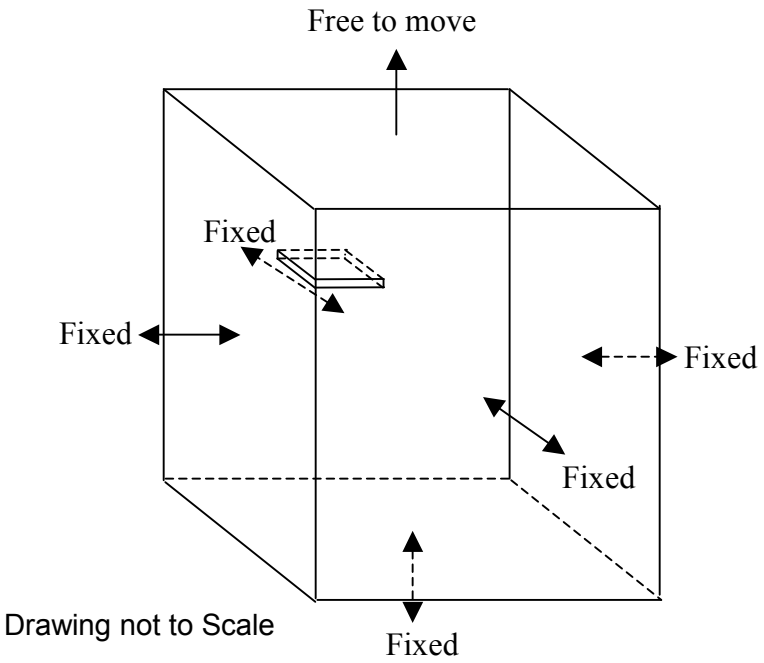


Figure 13: Mechanical Boundary Conditions for Far-Field Model

5.1.3 Initial Conditions for the Far-Field Modelling

The initial temperature of the model is that the geothermal gradient is 0.012°C/m of depth, with the ground surface temperature being 5°C and the model bottom temperature of 125°C. The initial stresses and displacement are assumed to be zero.

5.1.4 Finite Element Discretization

The finite-element discretization of the far-field model is shown in Figure 14. The domain is discretized such that the elements are more densely distributed in the rock mass just above and beneath the repository level where the thermal and mechanical gradients are expected to be the greatest. Dimensions of a typical element within the repository are 60.7 m x 40.8 m x 0.9795 m. The model has 16,900 nodes and 15,000 eight-noded elements.

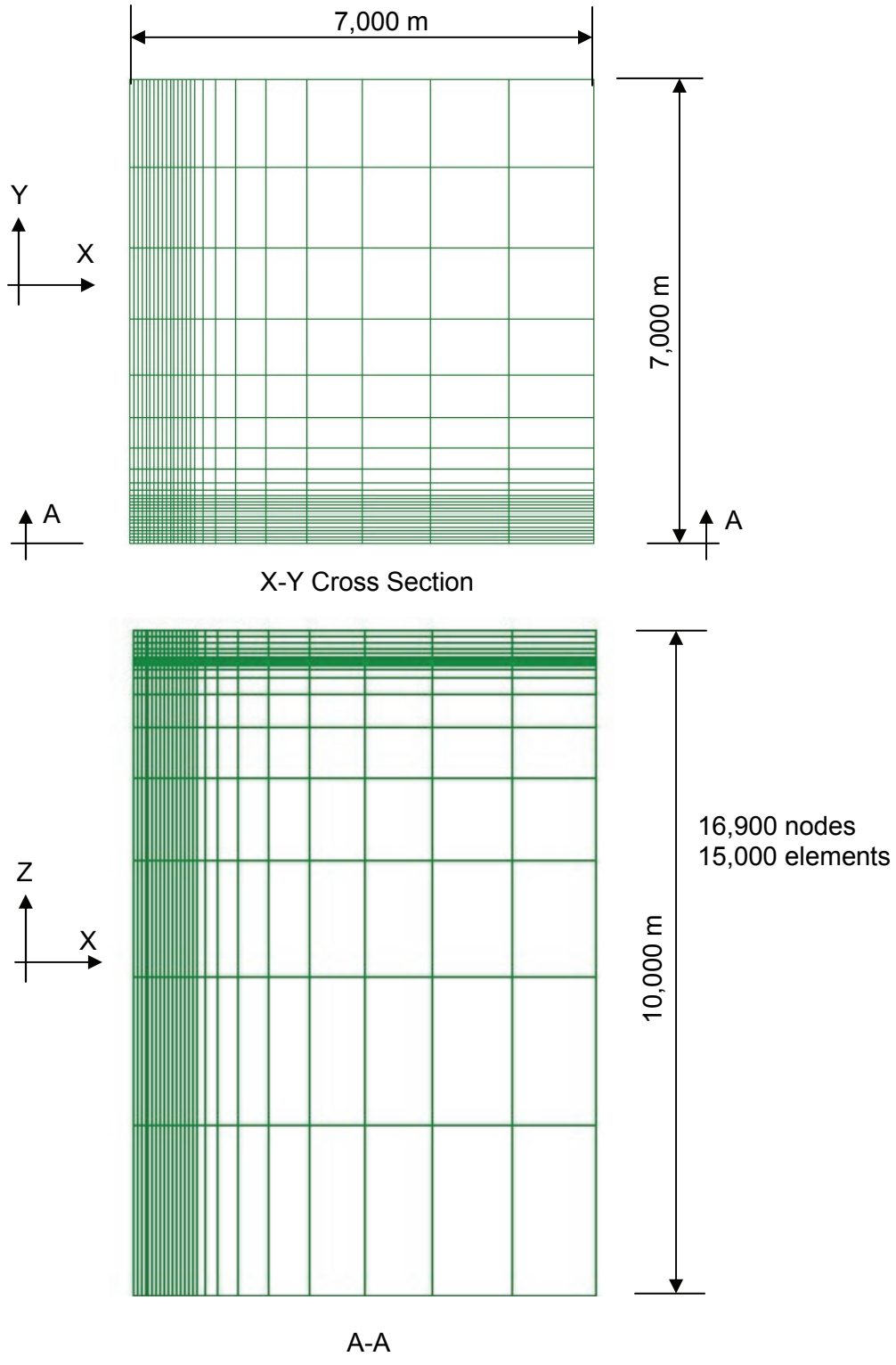


Figure 14: Mesh for the Far-Field Thermal Model

5.2 NUMERICAL RESULTS FROM FAR-FIELD MODELLING

The results from far-field numerical simulation of a repository with finite-horizontal dimensions are presented in this Section. The modelled results include temperatures, thermally induced stresses, total thermal and in-situ stresses, and thermally induced displacements at selected locations.

5.2.1 Thermal Results from Far-Field Modelling

Figure 15 illustrates the temperatures at the four different locations O, P, Q and R shown in Figure 11. The peak temperature occurs at 1,500 years at the repository centre with a magnitude of 42°C. The peak temperatures at the centre of a repository edge and repository corner are 27°C and 19°C, respectively. The temperature at Point R decreases after 60,000 years because of the thermal boundary change on the ground surface to account for a period of glaciation.

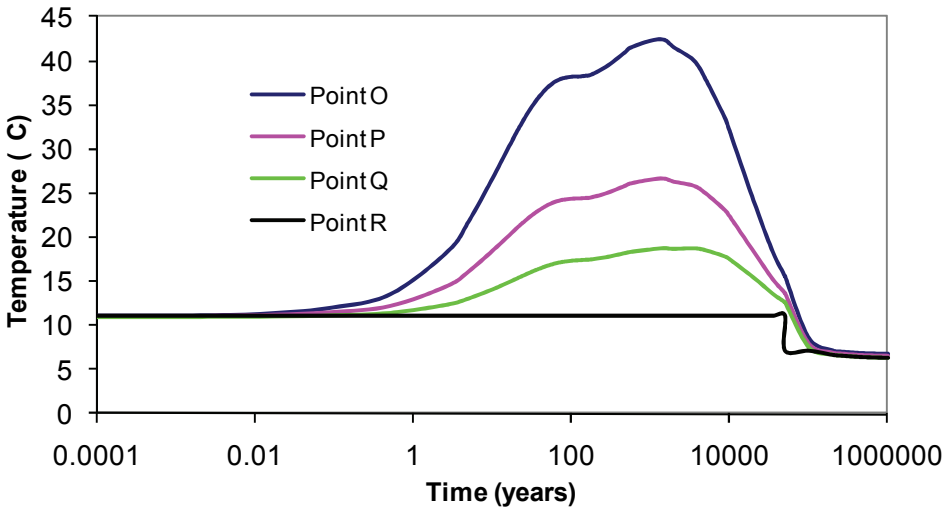


Figure 15: Simulated Temperatures from Far-Field Analyses at Different Locations

Temperature profiles along the horizontal symmetry line OR (refer to Figure 11 for location) at six different times are shown in Figure 16. The thermal load caused by used nuclear fuel influences the temperature of the rock in a range of 2,000 m or less from the centre of the repository. Therefore, the horizontal dimensions of 7,000 m of the model are sufficient to conduct the far-field modelling.

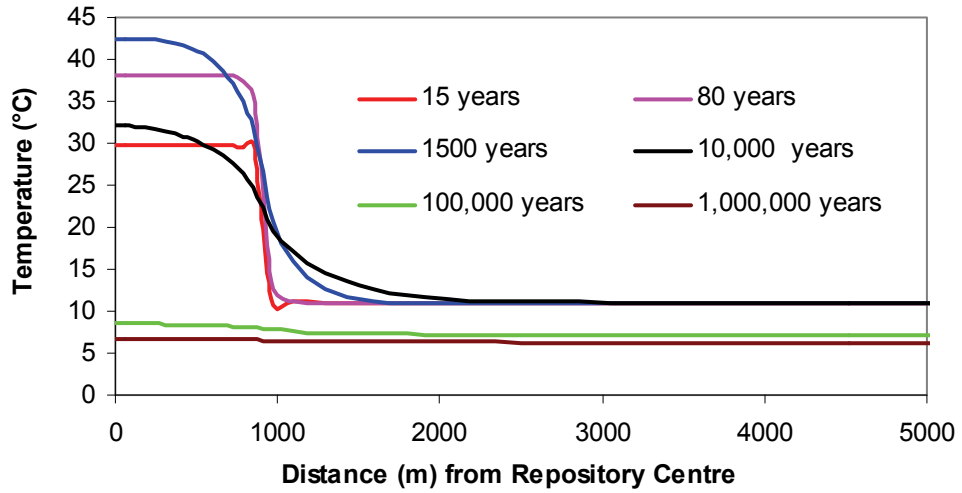


Figure 16: **Far-Field Temperature Profiles at Different Times along Horizontal Symmetry Line OR**

Temperatures versus time at selected points along the vertical line through the repository centre are shown in Figure 17. At the centre of the repository (i.e., 500 m below the ground surface), the net rise of the temperature is about 31°C. At a location 1,440 m below the ground surface, the temperature rise is only 4°C.

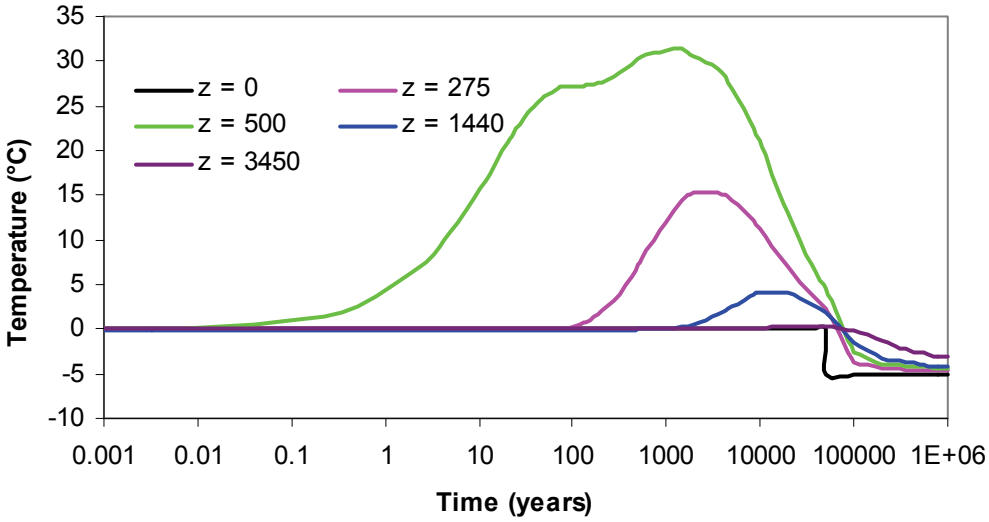


Figure 17: **Far-Field Temperature Rise versus Time at Selected Points along the Vertical Line through the Repository Centre**

Temperature profiles and the temperature rise along the vertical axis through the centre of the DGR at different times are shown in Figure 18 and Figure 19, respectively. The thermal influence of the DGR only appears to reach a maximum depth of 2200 m at 5,000 years after placement. The thermal response shown by the 1,000,000 year curve is due to the reduction of surface temperature from 5°C to 0°C caused by the return of glaciations.

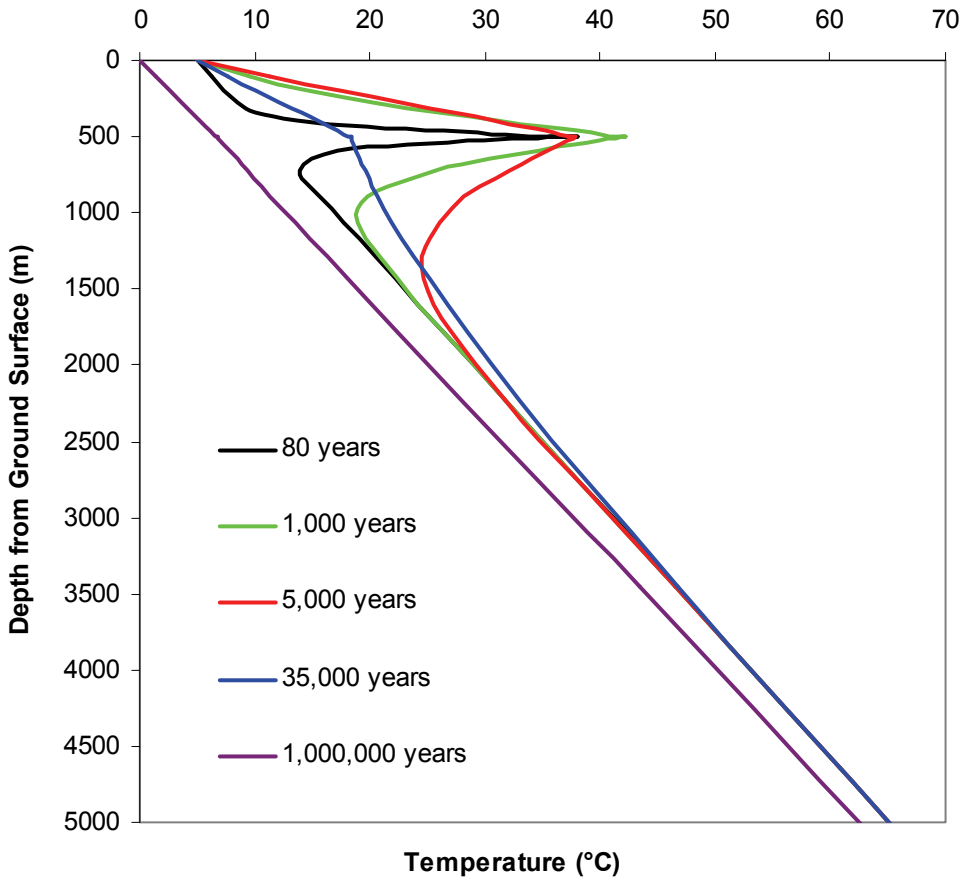


Figure 18: **Temperature Distributions along the Vertical Axis of the Repository**

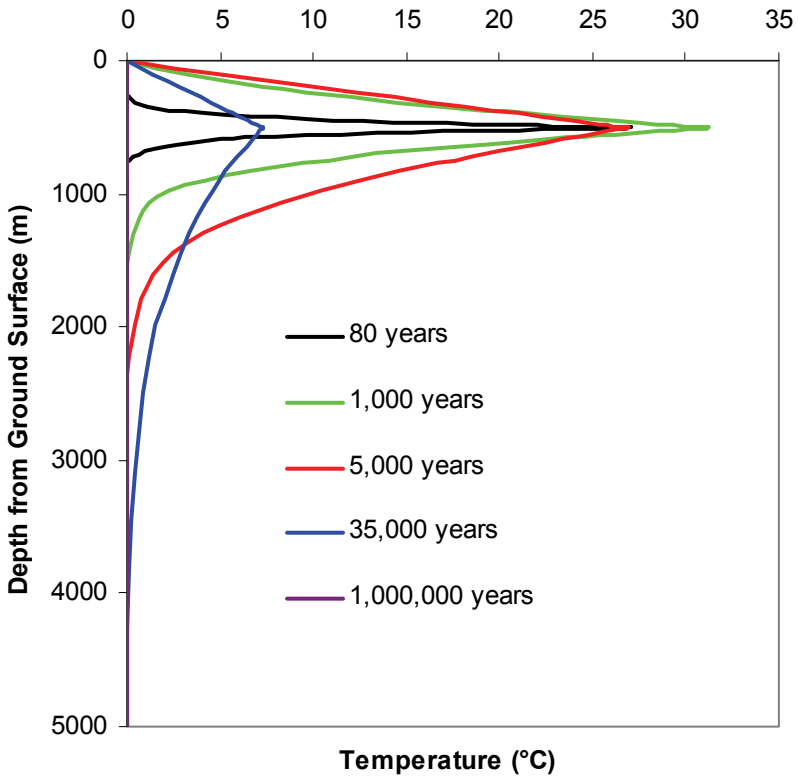


Figure 19: **Thermally Induced Temperature Rise Distributions along the Vertical Axis of the Repository**

The temperature rise occurs only near the repository area for the first 100 years as shown in Figure 20. After 1,000,000 years, the temperature around the repository approaches ambient temperatures.

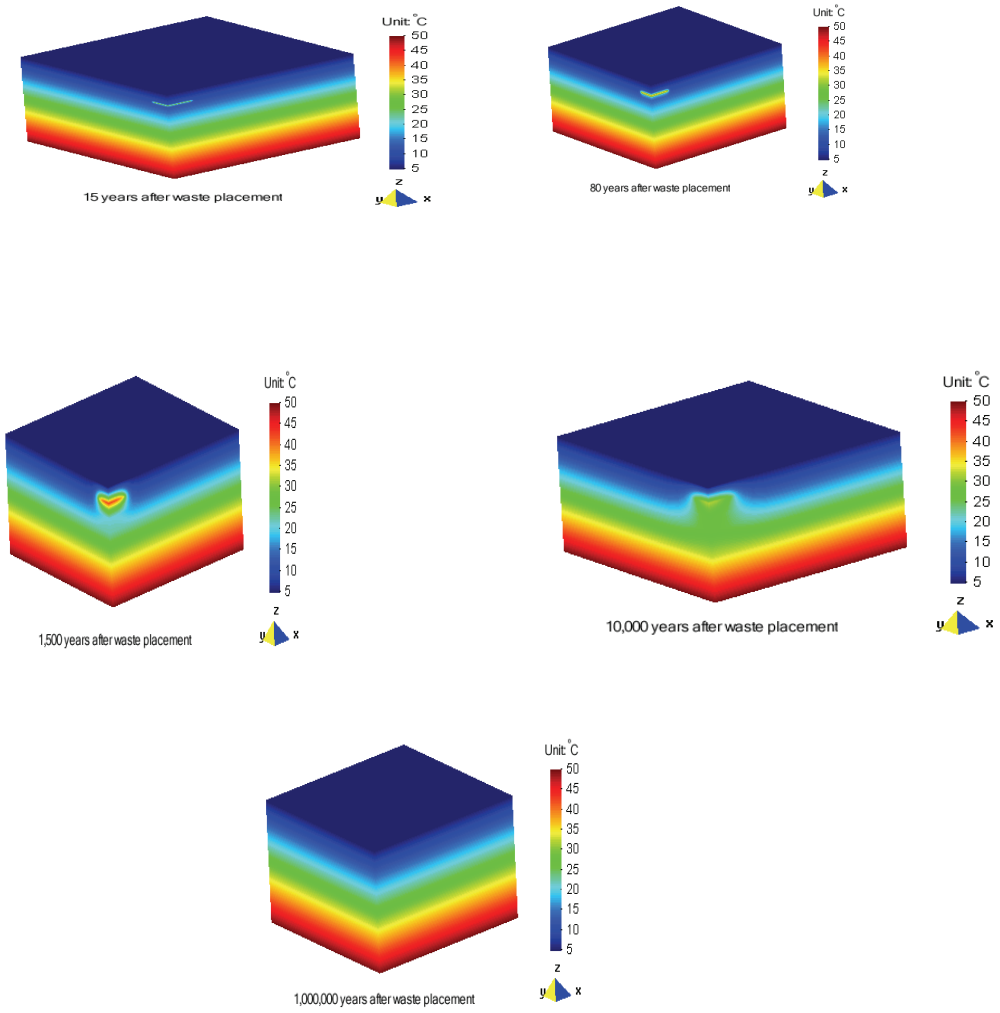


Figure 20: Temperature Response at Five Different Times (The bottom of the figures is 4,000 m below ground surface)

5.2.2 Mechanical Results from Far-Field Modelling

Figure 21 shows the thermally induced stresses at the repository centre without considering the ice load. The first peak thermally induced horizontal stress in the X-directional is 15.4 MPa at 80 years and the second peak thermally induced horizontal stress in the X-direction is 15.8 MPa at 500 years (refer to Figure 17 to see the time for peak temperatures). The thermally induced horizontal stress in the Y-direction is similar to that in the X-direction. The thermally induced horizontal stress decreases to -2.6 MPa at 1,000,000 years. The thermally induced vertical stress only has one peak value, which is 2 MPa at 5,000 years.

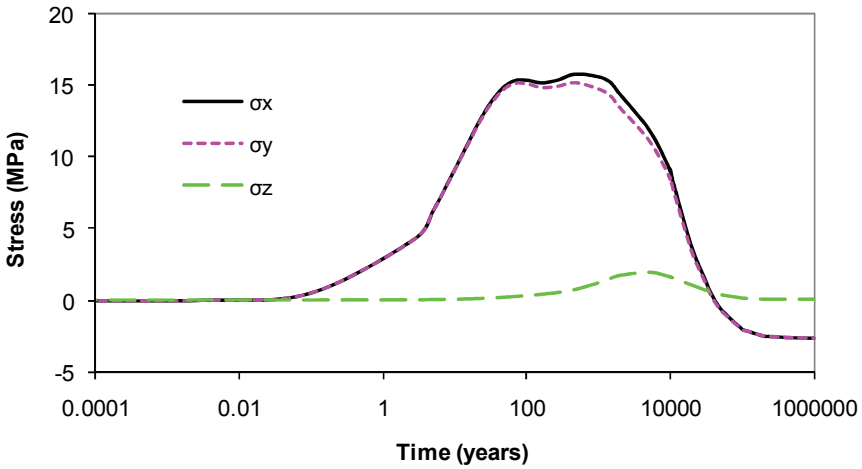


Figure 21: Thermally Induced Stresses at the Repository Centre without Considering the Ice Load (Reduction of compressive stress is negative)

Figure 22 shows the total stresses at the repository centre without considering the ice load. The peak values of the horizontal stresses in the X-direction are 38.6 MPa at 80 years and 39 MPa at 500 years. The peak value of the horizontal stresses in the Y-direction is 50.4 MPa at both 80 years and 500 years. The peak vertical stress is 14 MPa at 5,000 years.

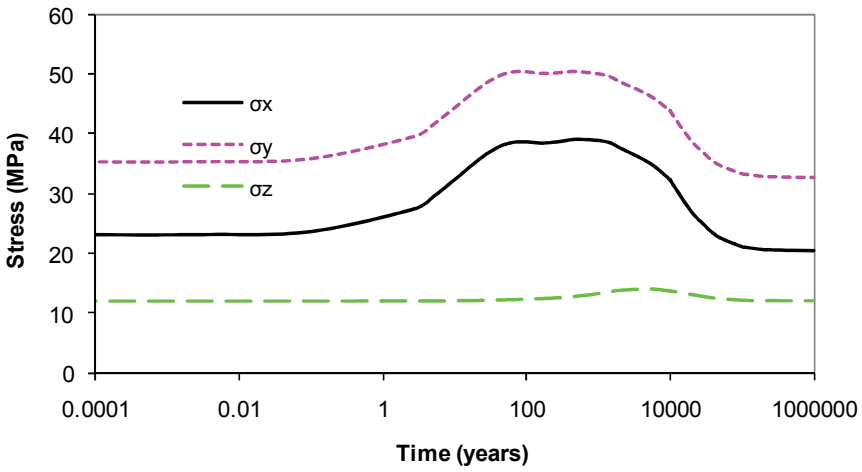


Figure 22: Total Stresses at the Repository Centre without Considering the Ice Load (Reduction of compressive stress is negative)

Figure 23 shows total stresses at the repository centre considering the ice load. The difference between Figure 23 and Figure 22 is that during the period of glaciation, the stresses include the stresses caused by ice load. Therefore, the third peak horizontal stresses are 31 MPa and 42 MPa at 96,000 years in the X- and Y-directions, respectively. The second peak vertical stresses 41 MPa at 96,000 years.

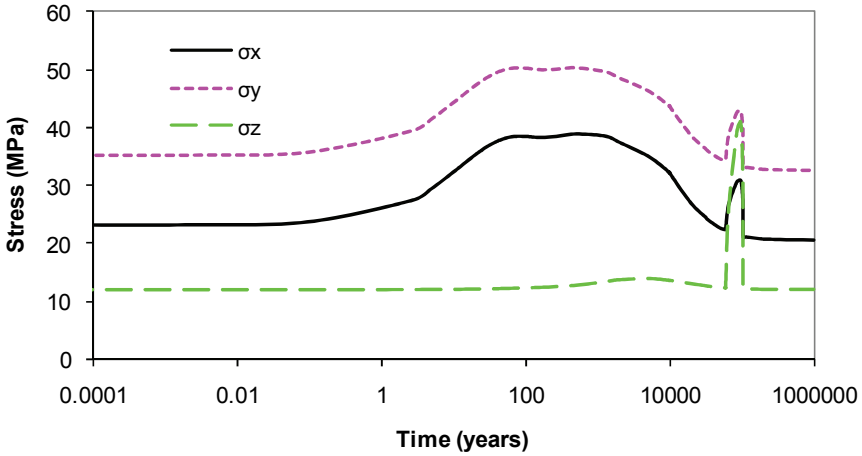


Figure 23: Total Stresses at the Repository Centre Considering the Ice Load (Reduction of compressive stress is negative)

The thermally induced stresses in the X-direction along the horizontal line (Line OR in Figure 11) at four different times are shown in Figure 24. The peak thermally induced stress in the X-direction is about 16 MPa at 1,000 years. Note the reduction of the thermally induced stress beyond 60,000 years (i.e., 1,000,000 years) due to glacial cooling.

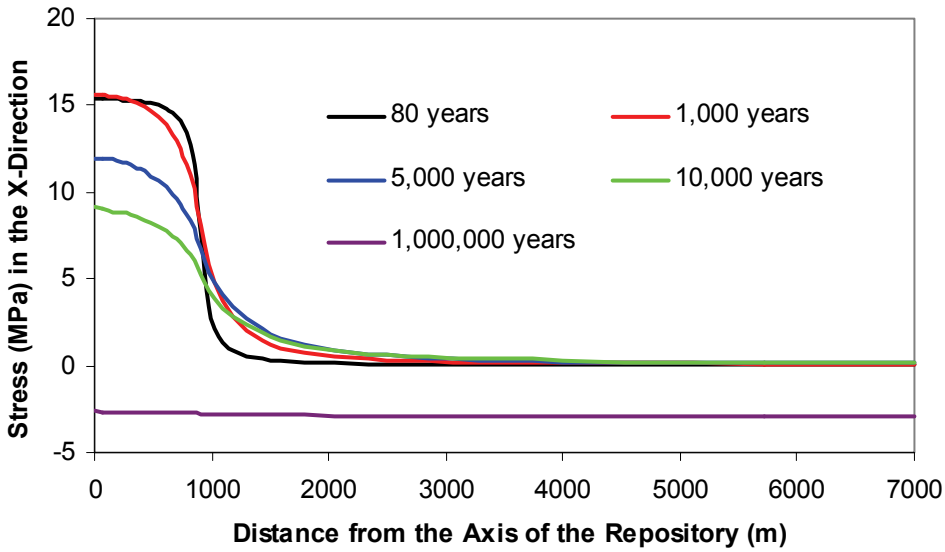


Figure 24: **Thermally Induced Stresses in the X-Direction along a Horizontal Line (OR) through the Repository Centre** (Reduction of compressive stress is negative)

Profiles of total stresses in the X-direction along a horizontal line (Line OR) through the repository centre, which include the intermediate-principal stresses (σ_2) in the same direction, are illustrated in Figure 25. From the mechanical point of view, the influence of the repository thermal load exists only in the area less than 2,500 m horizontally from the centre of the repository. The horizontal stress in the X-direction peaks at 39 MPa at 1,000 years.

The thermally induced stresses in the Y-direction along the horizontal line (Line OR in Figure 11) at four different times are shown in Figure 26. The peak thermally induced stress in the Y-direction is about 15 MPa at 80 years.

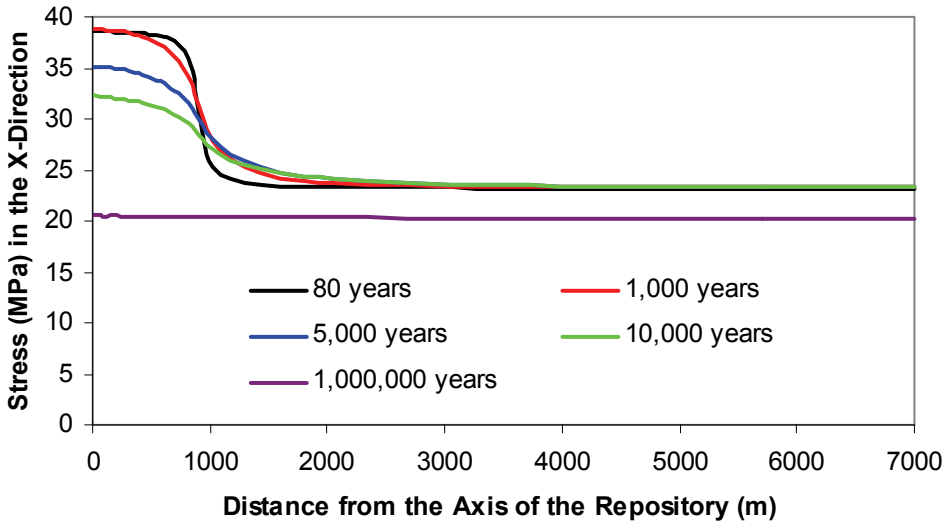


Figure 25: **Total Stresses in the X-Direction along a Horizontal Line through the Repository Centre (OR)** (Reduction of compressive stress is negative)

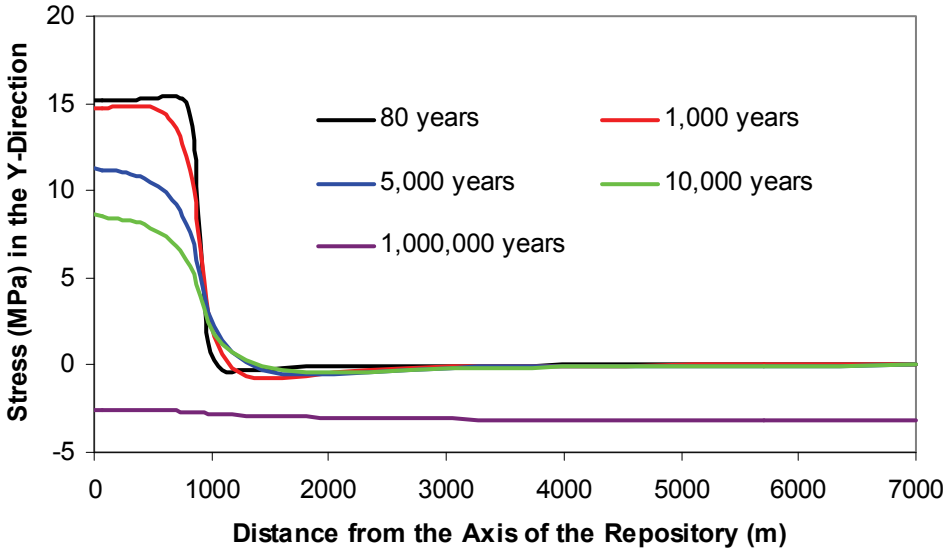


Figure 26: **Thermally Induced Stresses in the Y-Direction along a Horizontal Line through the Repository Centre** (Reduction of compressive stress is negative)

Profiles of total stresses in the Y-direction along the horizontal line (Line OR in Figure 11), which include the major principal stresses (σ_1) in the same direction, at four different times are shown in Figure 27. The peak stress in the Y-direction is 51 MPa at the centre of the repository. At a time of 1,000,000 years after UFC placement, the stress in the Y-direction drops to about 33 MPa at the centre of the repository.

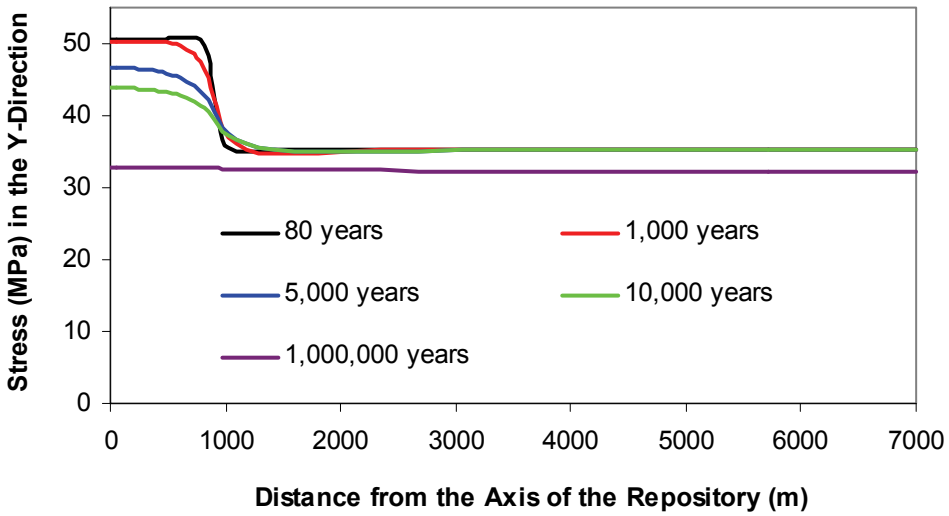


Figure 27: **Total Stresses in the Y-Direction along a Horizontal Line through the Repository Centre** (Reduction of compressive stress is negative)

The thermally induced stress changes in the Z-direction along the horizontal line OR (Figure 11) can be seen in Figure 28. The peak thermally induced stress in the Z-direction is about 2.5 MPa at about 1,000 years near the edge of repository. The thermally induced peak stress reduction is about 1.6 MPa from 100 to 1,000 years near the edge of repository. The reduction at 1,000,000 years is due to glacial cooling.

Profiles of total stresses in the Z-direction along horizontal line (Line OR in Figure 11), which include the minor principal stresses (σ_3) in the same direction, are shown in Figure 29. The stress in the Z-direction peaks at about 14.6 MPa near the edge of repository at about 1,000 years.

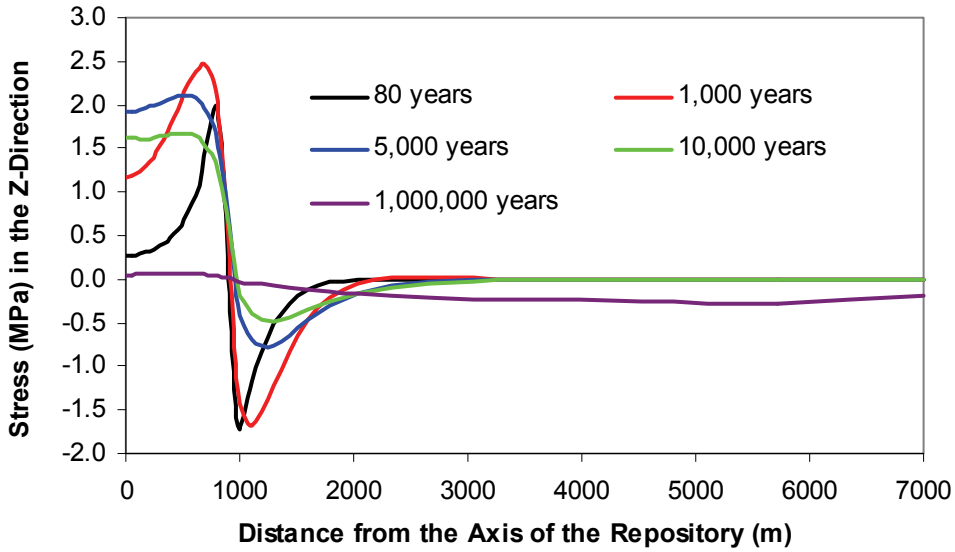


Figure 28: **Thermally Induced Stress Changes in the Z-Direction along a Horizontal Line through the Repository Centre** (Reduction of compressive stress is negative)

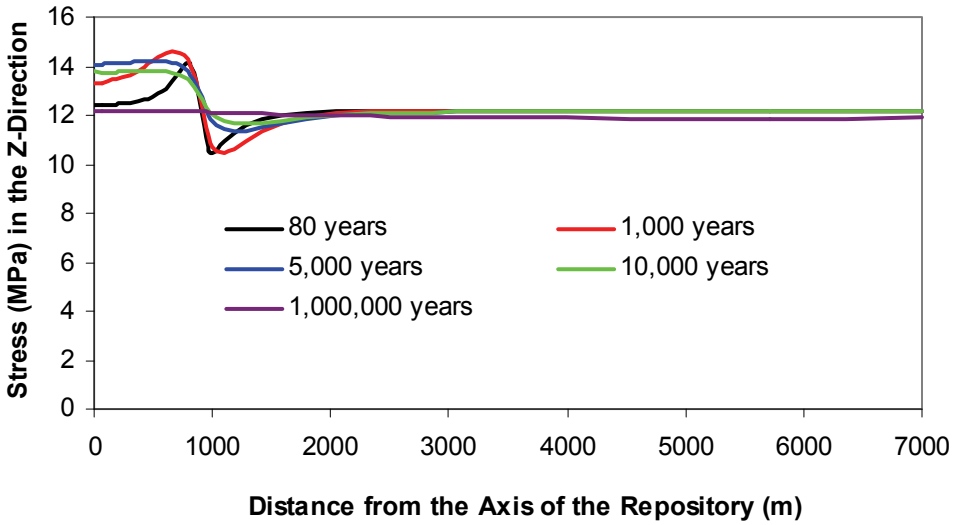


Figure 29: **Total Stresses in the Z-Direction along a Horizontal Line through the Repository Centre** (Reduction of compressive stress is negative)

The apparent influence of heating caused by the used nuclear fuel on the X-direction stress exists only in the depth from the ground surface to about 2,500 m, as shown in Figure 30. Figure 31 shows the total stress in the X-direction along the vertical line through the repository centre. The peak thermally induced compressive stress in the X-direction is 15.6 MPa. At the ground surface, the thermally induced stress reduction in the X-direction is 5.6 MPa at 5,000 years. The thermally induced stress reduction at the centre of the repository is 2.7 MPa

at 1,000,000 years, while at the ground surface, the thermally induced stress is reduced to 3 MPa. The greatest tensile total stress in the X-direction is 2.3 MPa, which occurs on the ground surface at 5,000 years. The depth of the rock with a calculated tensile stress is about 37 m. It is likely that the depth of this zone is similar or slightly greater than the depth of 37 m because the model does not includes “no-tension” analyses. This may result in the closed fractures in the rock in this zone reopening, causing the permeability of the rock in this zone to increase.

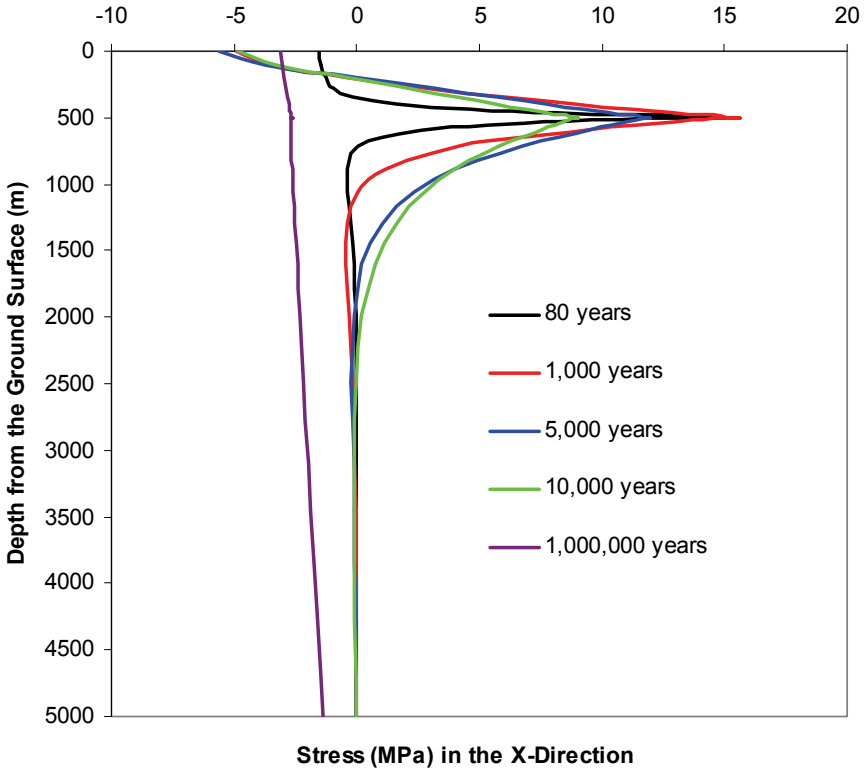


Figure 30: **Thermally Induced Stresses in the X-Direction along a Vertical Line through the Repository Centre** (Reduction of compressive stress is negative)

Thermally induced stresses and profiles of total stresses in the Y-direction along the vertical line through the repository centre are shown in Figures 32 and 33, respectively. The thermally induced compressive stress increase in the Y-direction peaks at 15 MPa at 80 years and the stress decrease in the Y-direction peaks at 2.6 MPa at the repository horizon at 1,000,000 years. The thermally induced compressive stress decrease peaks at 6.7 MPa at 5,000 years on the ground surface. The greatest total tensile stress in the Y-direction is 1 MPa, which occurs on the ground surface at 5,000 years.

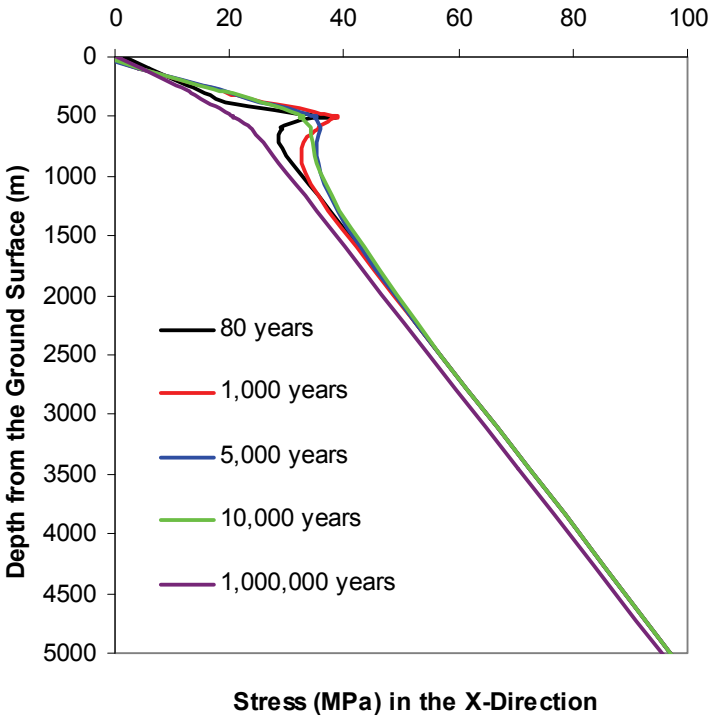


Figure 31: **Total Stresses in the X-Direction along a Vertical Line through the Repository Centre** (Reduction of compressive stress is negative)

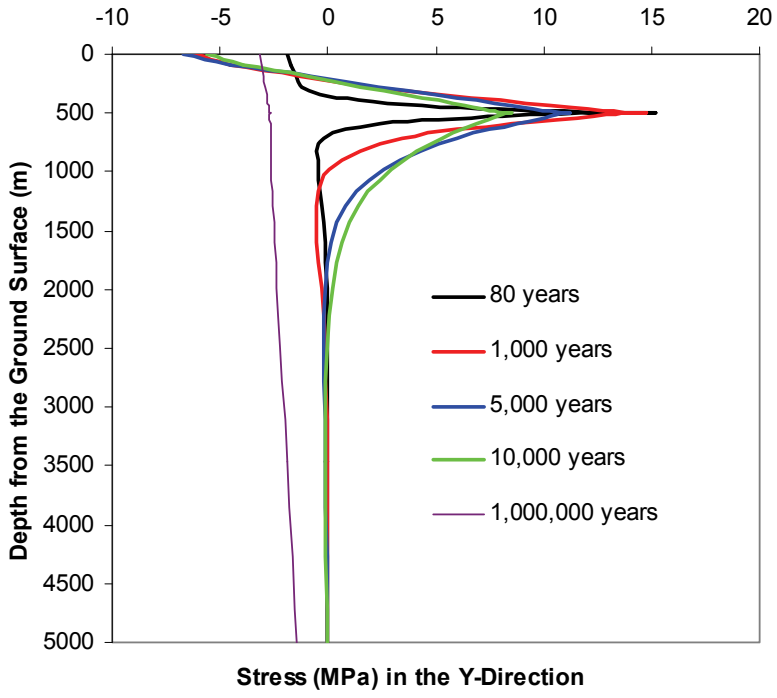


Figure 32: **Thermally Induced Stress Changes in the Y-Direction along a Vertical Line through the Repository Centre** (Reduction of compressive stress is negative)

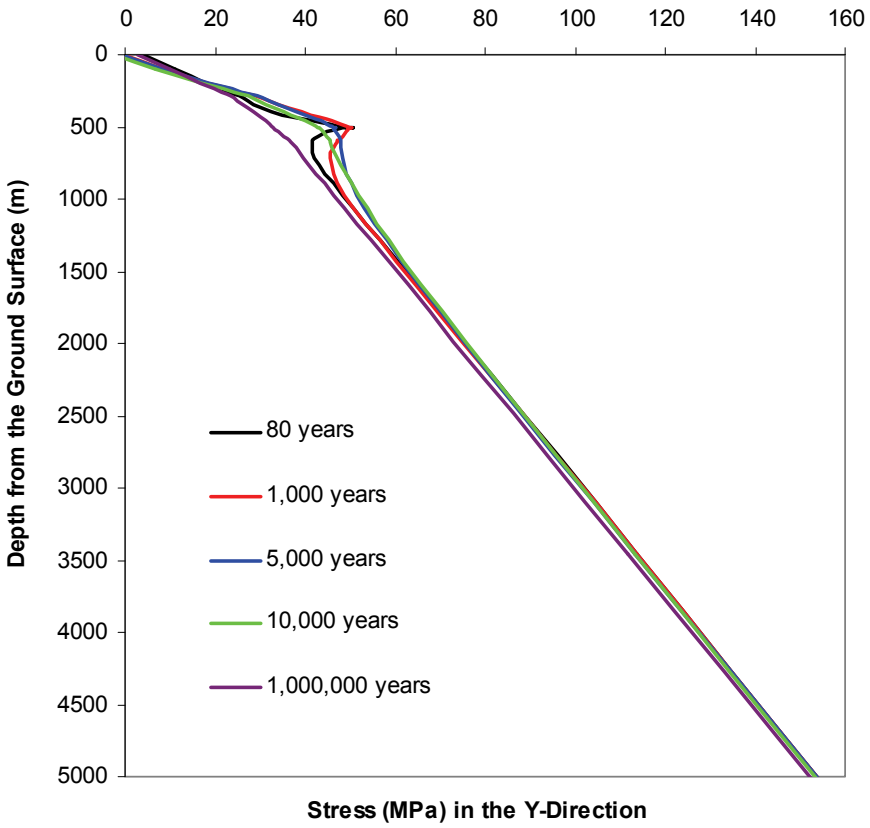


Figure 33: **Total Stresses in the Y-Direction along a Vertical Line through the Repository Centre** (Reduction of compressive stress is negative)

Thermally induced stresses and profiles of stress changes in the Z-direction along the vertical line through the repository centre are shown in Figures 34 and 35, respectively. The thermally induced compressive stress increase in the Z-direction at the repository level peaks at 2.4 MPa at 5,000 years and the thermally induced compressive stress reduction peaks at 0.2 MPa at 1,000,000 years.

Thermally induced horizontal stresses on the ground surface above the repository centre with time without considering ice load are shown in Figure 36. The first and second peak thermally induced stress reductions at ground surface induced by thermal expansion of the rock mass near the repository are 5.6 MPa and 4 MPa at 5,000 years and 60,000 years after waste placement.

Thermally induced horizontal stresses on the ground surface above the repository centre with time considering ice load are shown in Figure 37. The peak value of the thermally induced stress on the ground surface induced by thermal expansion of the rock mass near the repository and the stress caused by ice load are 6.2 MPa at 96,000 years after waste placement.

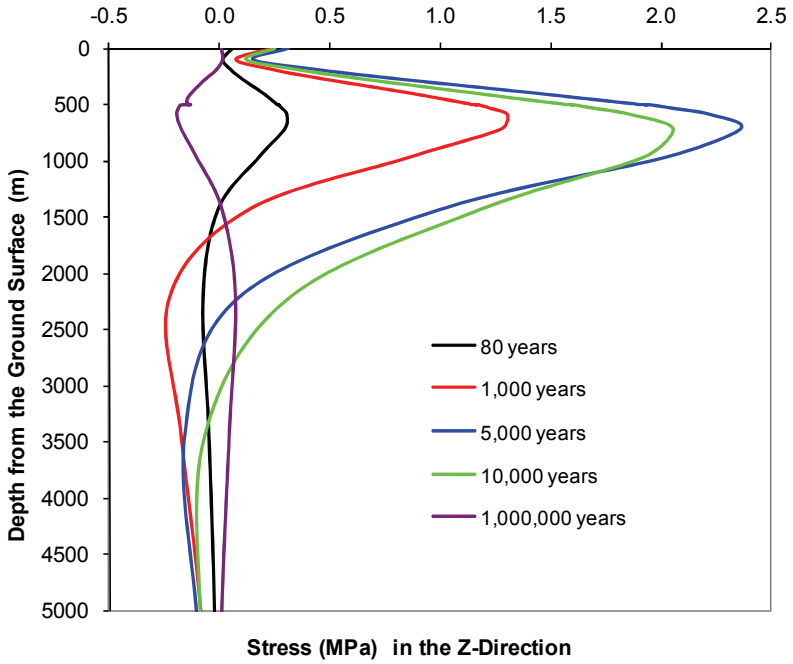


Figure 34: **Thermally Induced Stress Changes in the Z-Direction along a Vertical Line through the Repository Centre** (Reduction of compressive stress is negative)

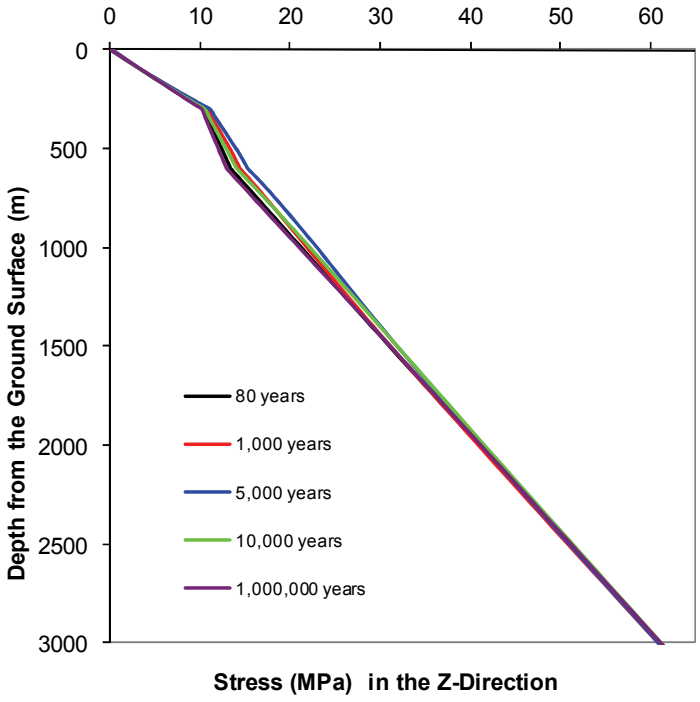


Figure 35: **Total Stresses in the Z-Direction along a Vertical Line through the Repository Centre** (Reduction of compressive stress is negative)

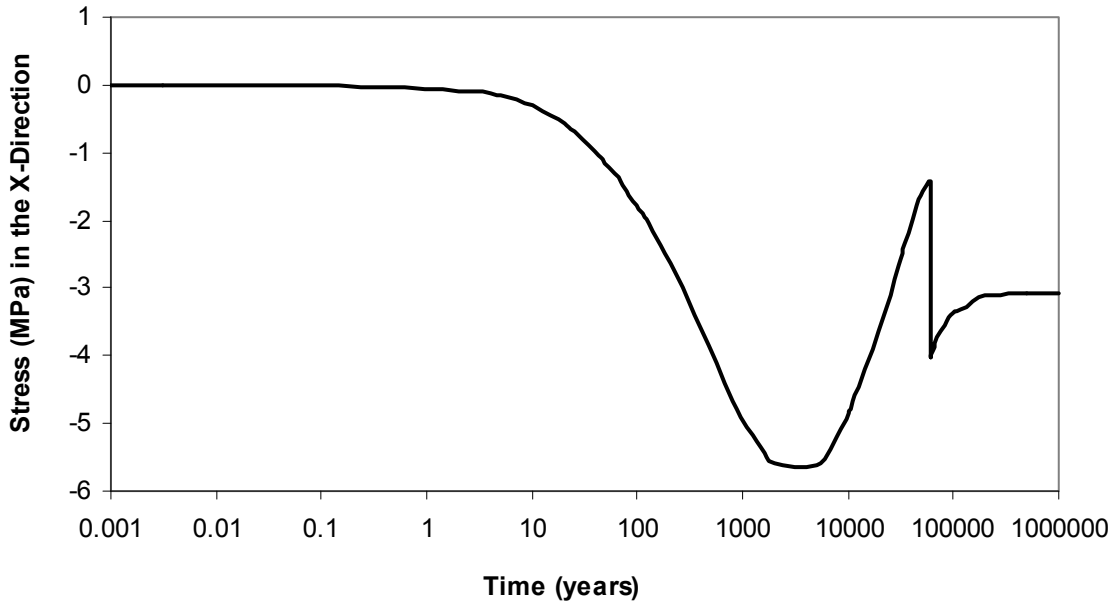


Figure 36: Thermally Induced Horizontal Stresses (X-direction) on the Ground Surface above the Repository Centre without Considering the Ice Load (Reduction of compressive stress is negative)

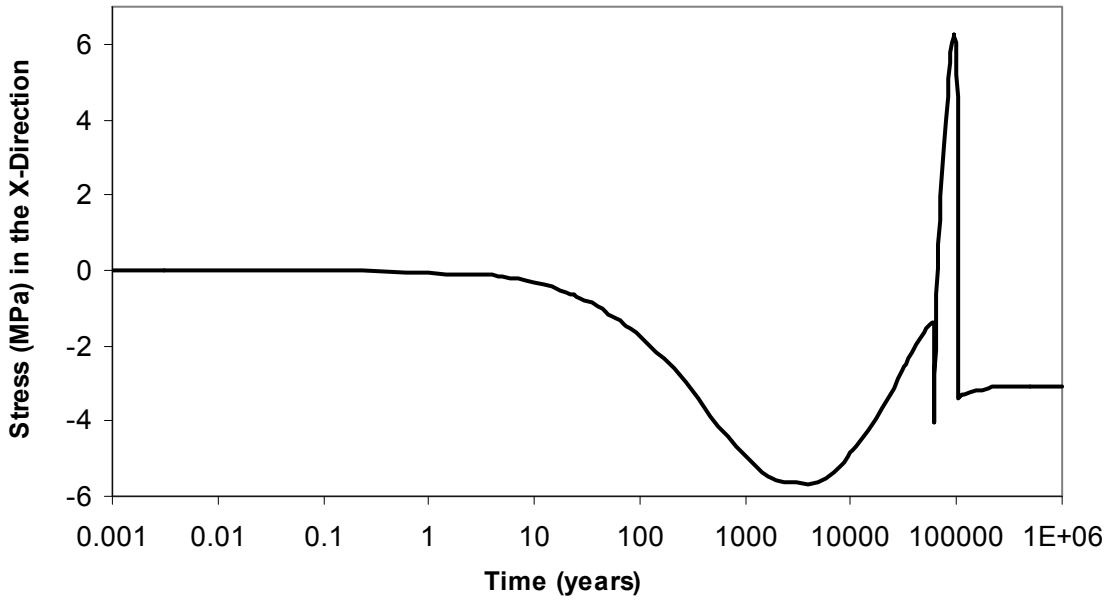


Figure 37: Thermally Induced Horizontal Stresses (X-direction) on the Ground Surface above the Repository Centre Considering the Ice Load (Reduction of compressive stress is negative)

Figure 38 shows the thermally induced stresses in the X-direction along Line AB (refer to Figure 11 for location). Although in the area above the repository, the stress is reduced by thermal load to tensile values and, at about 1,300 m horizontally from the repository axis, the compressive thermal stresses in the rock increase (i.e., by 2 MPa at 1,000 years).

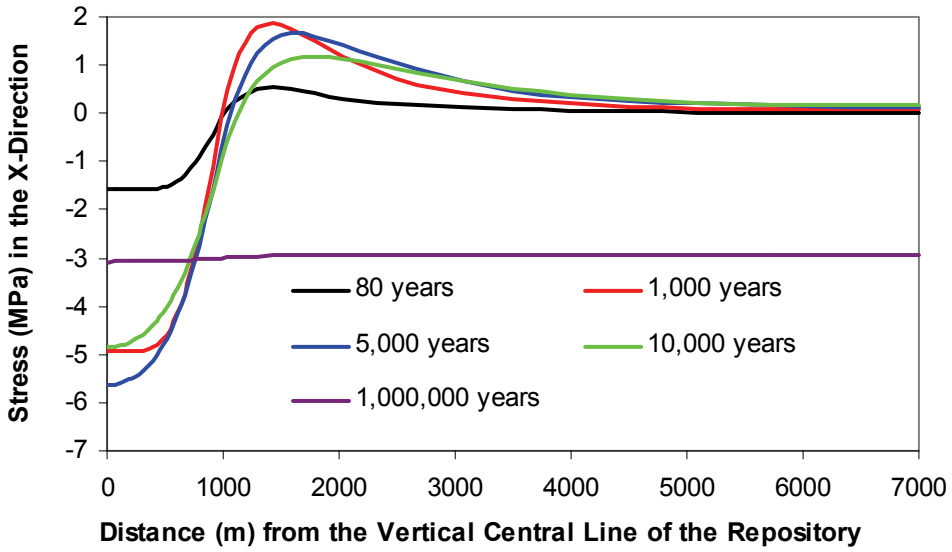


Figure 38: Thermally Induced Horizontal Stresses (X-direction) along Line AB
(Reduction of compressive stress is negative)

The thermally induced stress distributions in the X-, Y-, and Z-directions on the vertical cross section (i.e., Plane ABFE, in Figure 11) at selected times are presented in Figures 39, 40 and 41, respectively. They show the stress reductions in the X- and Y-directions near ground surface and in the Z-direction near the edge of the repository. (Note that compressive stress is negative and tensile stress is positive on the scale).

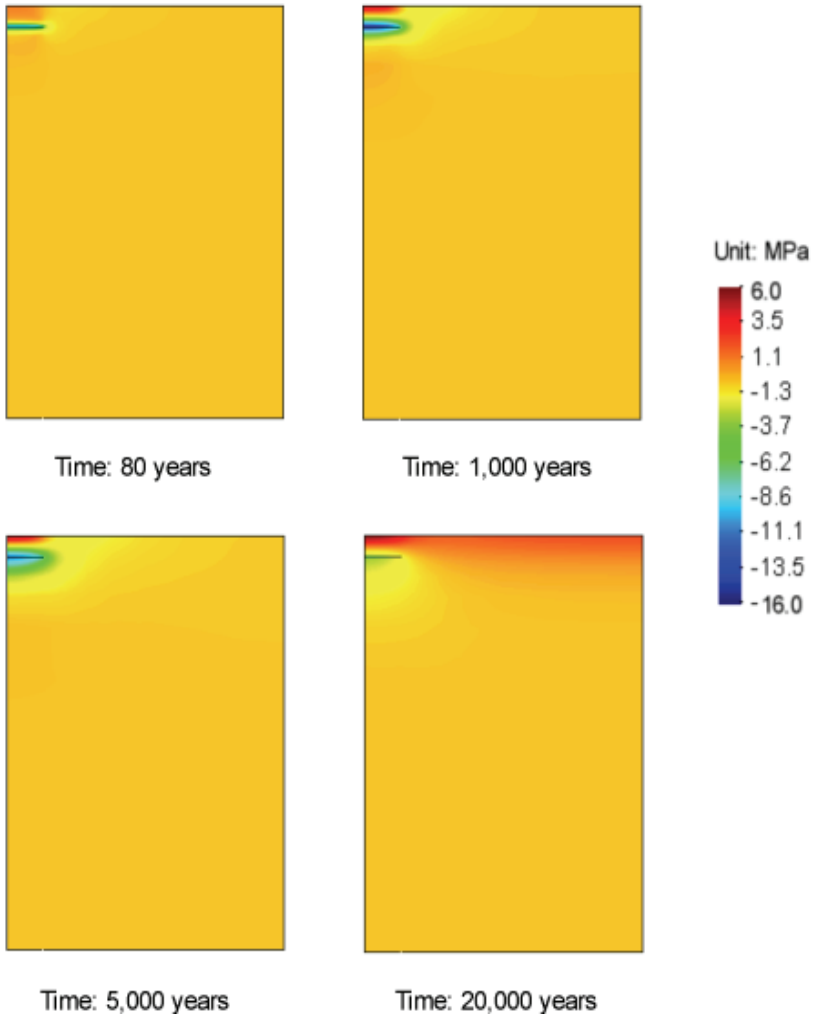


Figure 39: Distributions of Thermally Induced Stresses in the X-Direction on the Vertical Cross-Section through the Centre of the Repository at Four Different Times
(Compressive stress is negative)

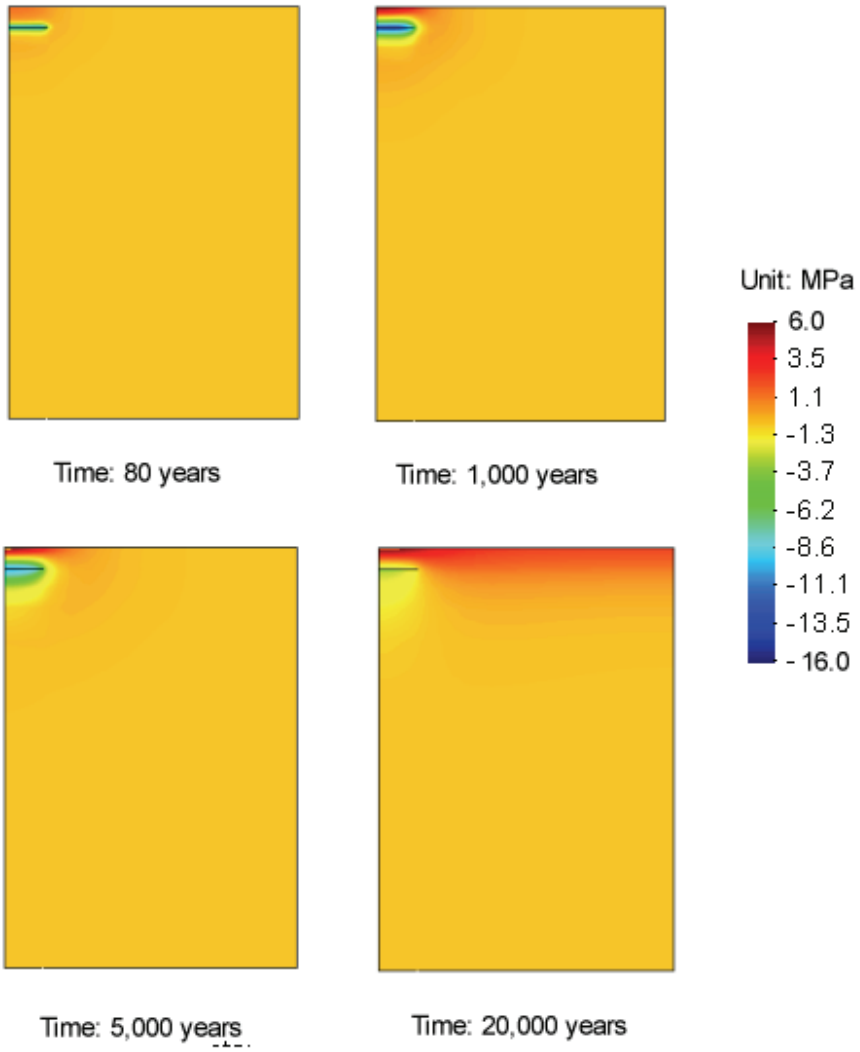


Figure 40: Distributions of Thermally Induced Stresses in the Y-Direction on the Vertical Cross-Section through the Centre of the Repository at Four Different Times
(Compressive stress is negative)

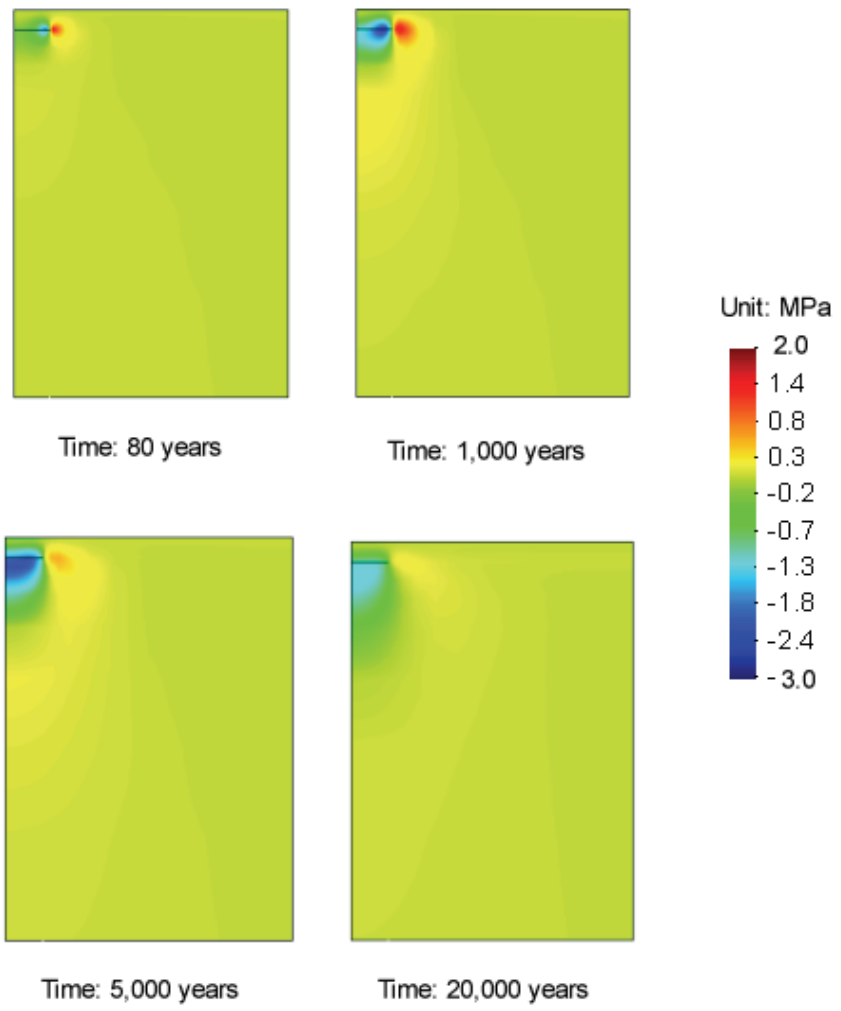


Figure 41: Distributions of Thermally Induced Stresses in the Z-Direction on the Vertical Cross-Section through the Centre of the Repository at Four Different Times
(Compressive stress is negative)

The thermally induced maximum and minimum principal stresses (σ_1 and σ_3, respectively) for four different times are shown in Figures 42 and 43, respectively. These distributions also show the reduction of thermally induced stress at the ground surface immediately above the repository during the time of from 0 to 20,000 years after waste placement, and the reduction of stress at the repository level after 5,000 years.

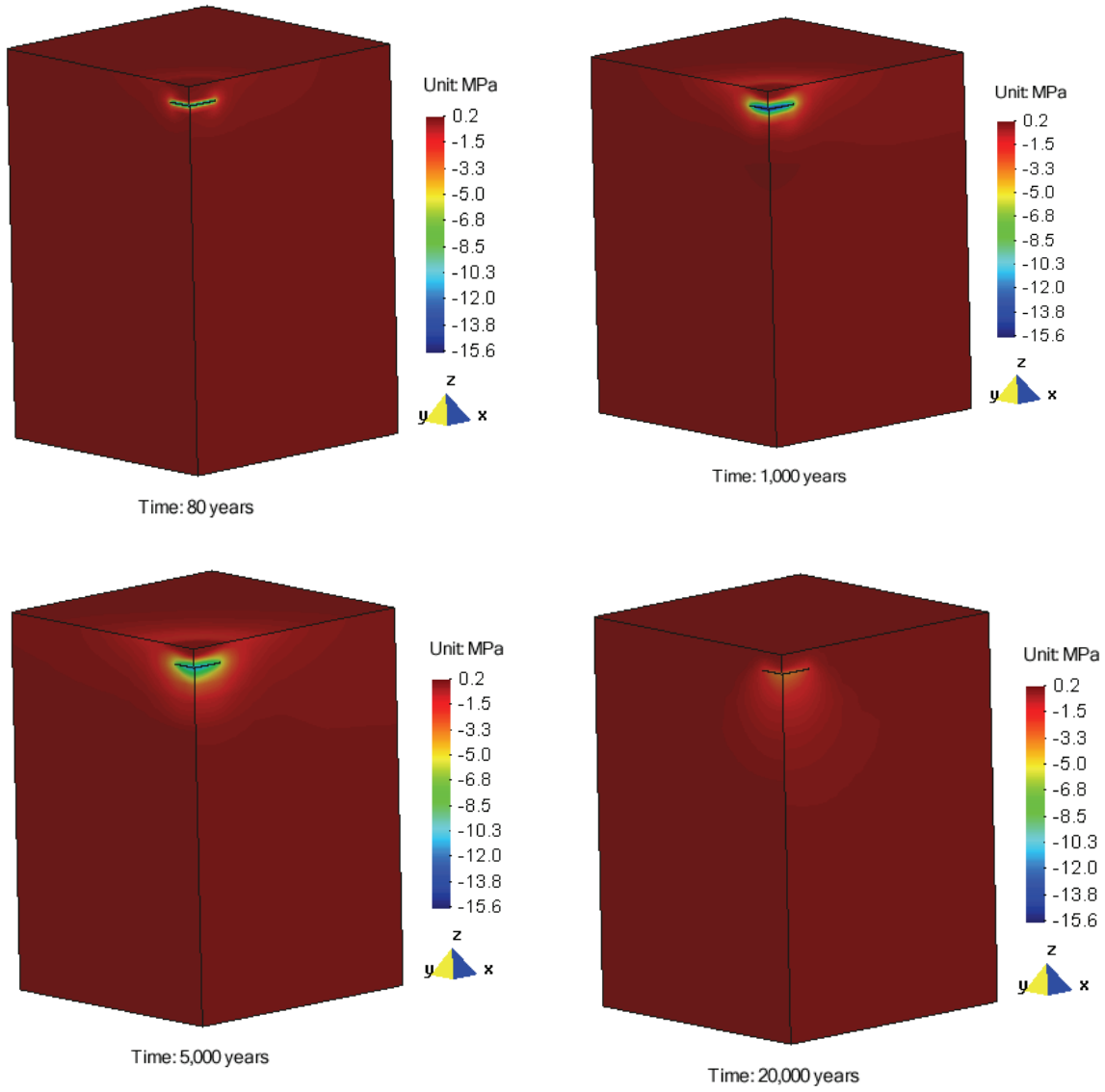


Figure 42: **Thermally Induced Maximum Principal Stresses at Different Times**
(Compressive stress is negative)

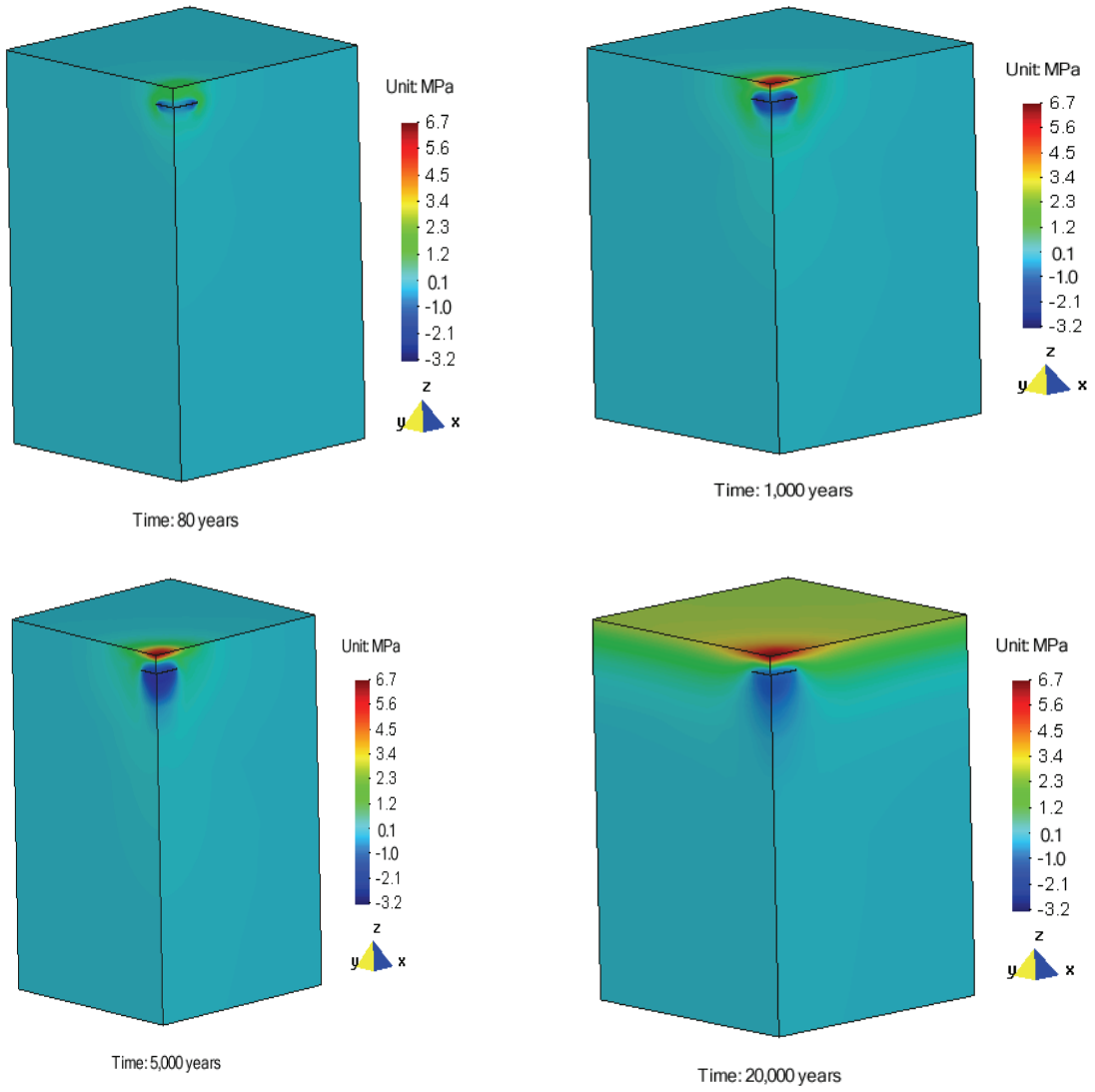


Figure 43: Thermally Induced Minimum Principal Stresses at Different Times
(Compressive stress is negative)

The thermally induced vertical displacements along the vertical line through the repository centre (Line AE in Figure 11) are illustrated in Figure 44. The relatively shallow portion of the rock mass (i.e., above 1500-m depth) displaces upwards for the first 10,000 years after waste placement and then begins to subside. After 100,000 years, the rock from the bottom of the model to the top of the model (ground surface) consistently moves down because of the thermal contact induced by temperature decrease during a period of glaciations.

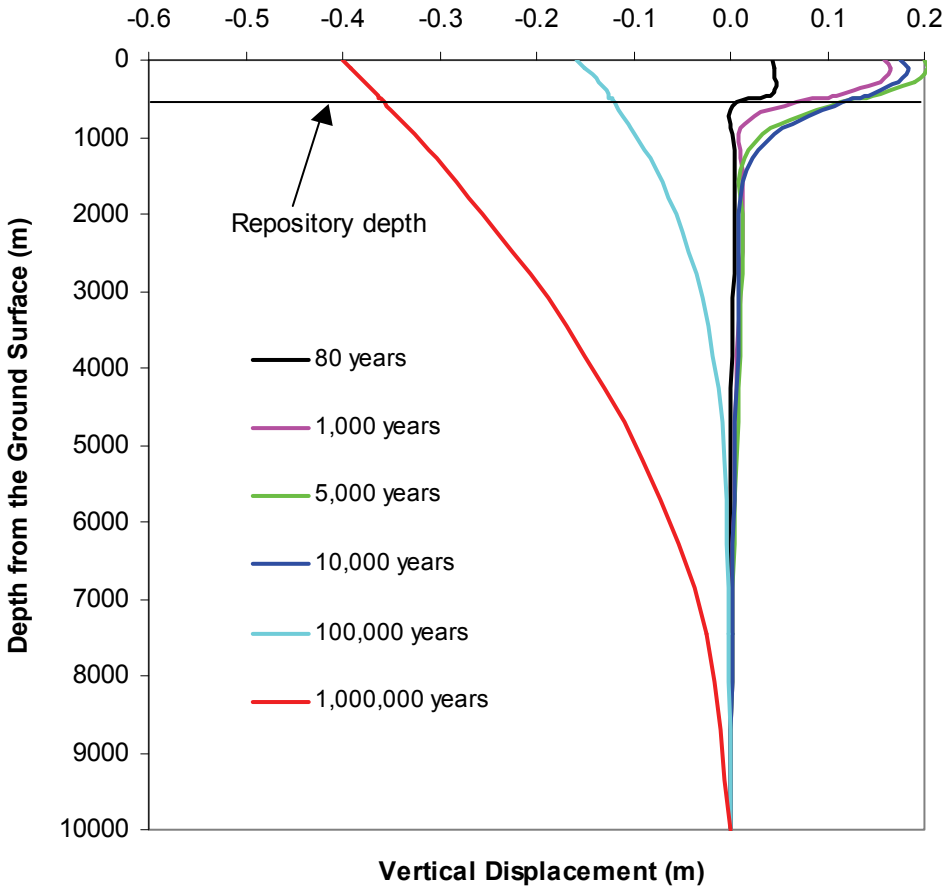


Figure 44: Thermally Induced Vertical Displacements along the Vertical Line through the Repository Centre without Considering Ice Load (Upward displacement is positive)

Figure 45 shows the comparison of the vertical displacement along the vertical line through the repository centre at 96,000 years with and without considering the ice load. Based on the boundary condition that the bottom of the model is fixed in the vertical direction, the subsidence on the top is 6.6 m with and 0.16 m without considering ice load at 96,000 years, respectively.

The vertical displacements along a horizontal line at ground surface passing over the centre of the repository (Line AB in Figure 11) are shown in Figure 46. During the first 5,000 years after waste placement, the lateral extent of thermally induced displacement at ground surface is only about 3,000 m from the vertical line through the repository centre. At 10,000 years, the rock moves down from Point A to Point B uniformly due to the temperature decrease caused by glaciation on the ground surface. At year 1,000,000, the ground surface displaces downward about 0.4 m based on the boundary condition that the bottom of model (10,000 m from the ground surface) was fixed in the vertical direction.

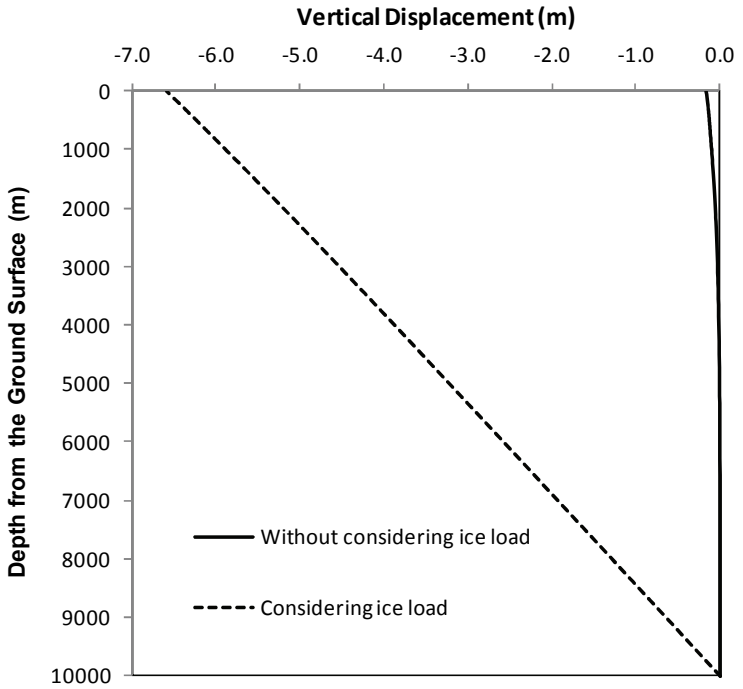


Figure 45: Comparison of Vertical Displacement along the Vertical Line through Repository Centre at 96,000 Years without and with Considering the Ice Load (Upward displacement is positive)

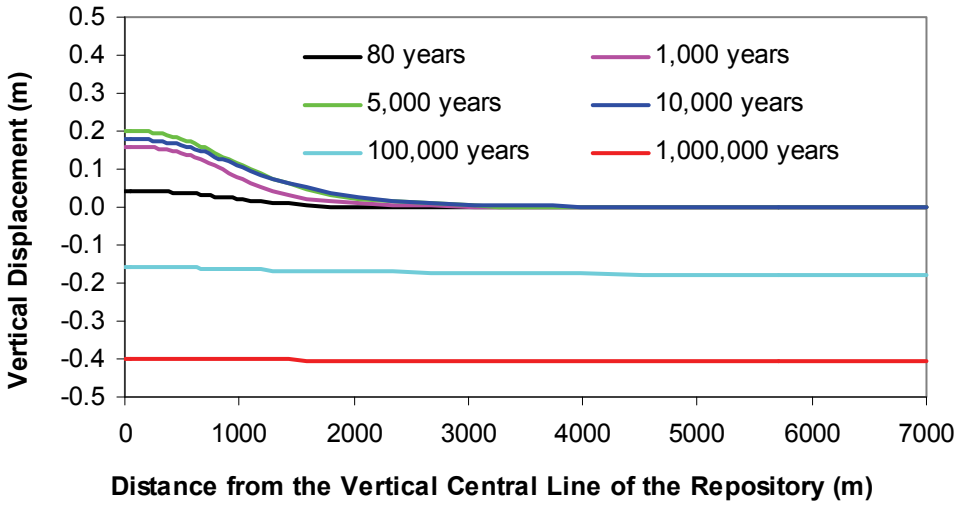


Figure 46: Thermally Induced Vertical Displacement along Ground Surface without Considering Ice Load (Upward displacement is positive)

At ground surface immediately above the repository centre, the vertical displacement as a function of time without considering ice load is shown in Figure 47. Vertical displacement increases as a function of time until it reaches a peak value and then decreases. At ground

surface above the centre of the repository, the vertical displacement peaks at 0.2 m at 5,000 years. The vertical displacement of the rock at ground surface immediately above the repository centre is 0.05 m at 60,000 years. The displacement of the rock at ground surface immediately above the repository centre peaks at 0.4 m downwards at 1,000,000 years due to thermal shrinkage during the period of glaciation.

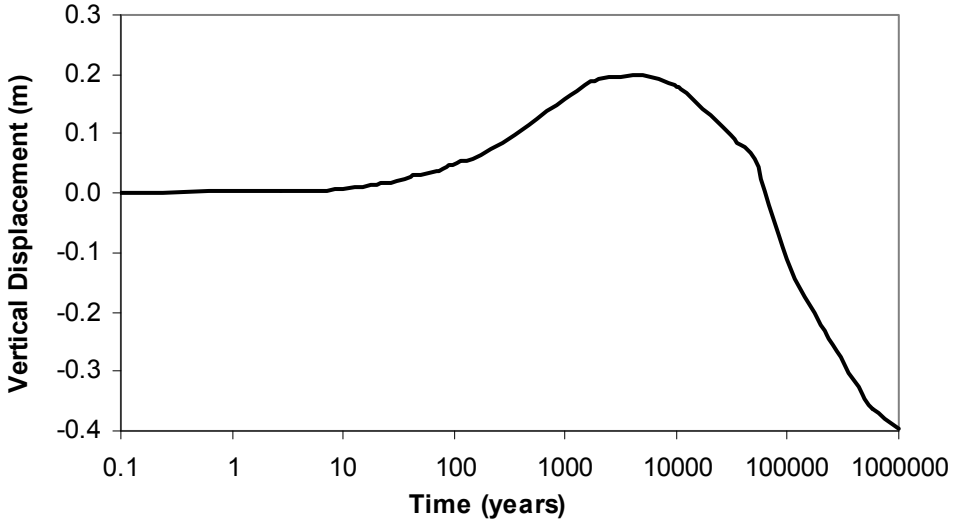


Figure 47: **Thermally Induced Vertical Displacement at Ground Surface above the Repository Centre without Considering Ice Load** (Upward displacement is positive)

Figure 48 shows vertical displacement at ground surface above the repository centre considering ice load. The difference between Figure 48 and Figure 47 is that the subsidence during the period of glaciation is much greater than that without considering ice load. The peak subsidence is 6.5 m at 96,000 years.

The vertical displacements in a three-dimensional model at a time of 5,000 years after waste placement are shown in Figure 49. The rock above and below the repository is uplifted due to thermal expansion.

Figure 50 shows the vertical displacements at repository centre as a function of time without considering ice load. Vertical displacements increase as a function of time until they reach a peak value and then decrease. The vertical displacement peaks at 0.13 m at 5,000 years. The rock at the repository centre displaces downwards by 0.045 m at 60,000 years. The rock at ground surface immediately above the repository centre displacement peaks at 0.35 m downwards at 1,000,000 years due to thermal shrinkage during the period of glaciation.

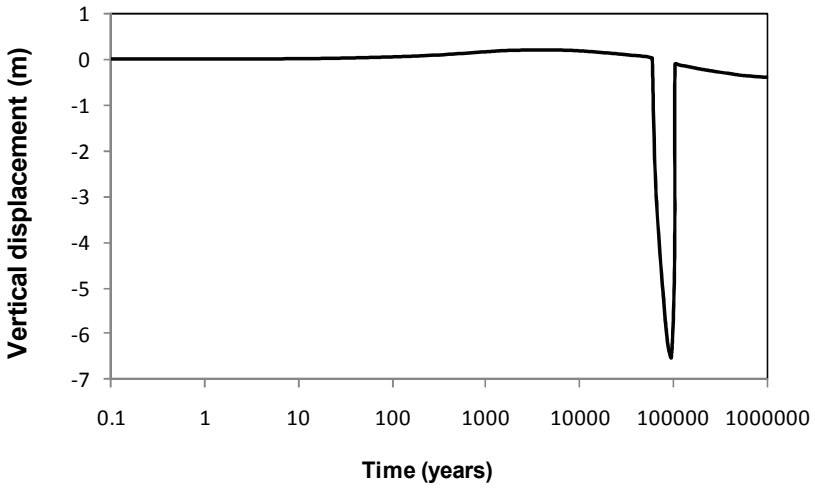


Figure 48: Vertical Displacement at Ground Surface above the Repository Centre Considering Ice Load (Upward displacement is positive)

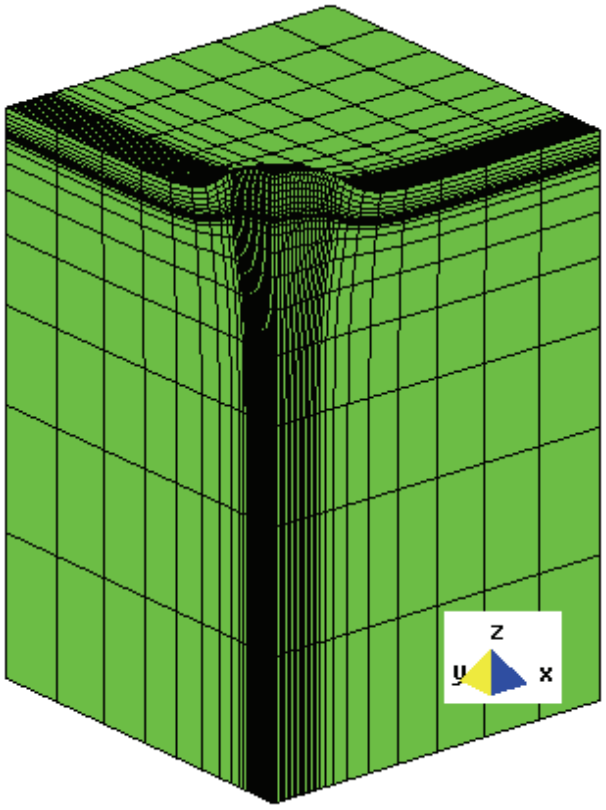


Figure 49: Thermally Induced Vertical Displacements at 5,000 Years with a Maximum Value of 0.2 m (Note: the vertical displacement scale is exaggerated (factor = 5,000) for clarity)

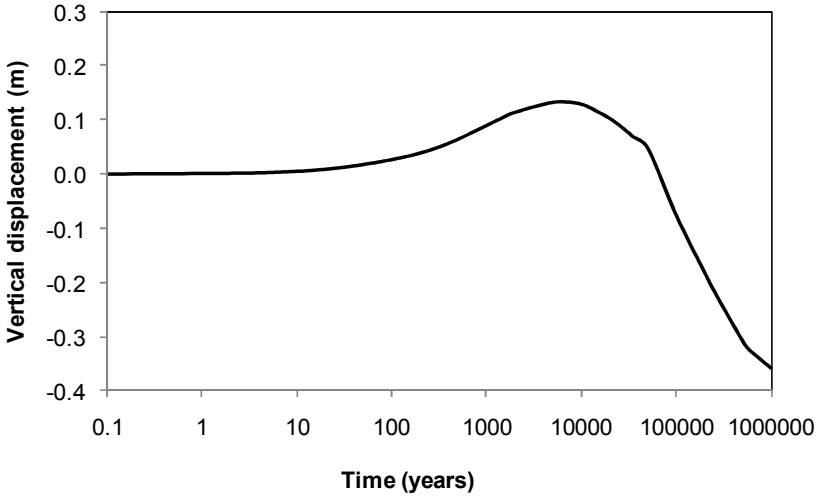


Figure 50: Thermally Induced Vertical Displacement at the Repository Centre without Considering Ice Load (Upward displacement is positive)

In summary, thermally induced stress increases in the horizontal direction at the repository level are 15.4 MPa at 80 years and 15.8 MPa at 500 years. Thermally induced vertical stress at the repository level is 2 MPa at 5,000 years. The total stress in the horizontal direction (Y direction) is 50 MPa at 80 and 500 years and 43 MPa at 96,000 years. The total stress in the vertical direction is 14 MPa at 5,000 years and 41 MPa at 96,000 years. The ice load will cause an increase of 28.9 MPa in vertical stress and an increase of 9.6 MPa in horizontal stresses in the rock at 96,000 years. .

Due to thermal expansion, there will be about 37 m of rock below the ground surface in which there is no horizontal compressive stresses. The permeability in this zone may be increased.

The rock at the ground surface above the repository centre will displace upwards about 0.2 m at 5,000 years due to thermal expansion. The subsidence will be about 6.4 m at the ground surface due to the ice load during the period of glaciation.

6. NEAR-FIELD MODELLING

This section includes two sets of numerical analyses. The first set includes the thermal modelling to analyze the detailed temperatures in the sealing materials and the rock surrounding the used-fuel container. The second set includes a series of mechanical and coupled T-M modelling exercises to obtain the mechanical response.

Due to a convergence problem with application of non-zero initial stresses in a coupled T-M model, the mechanical responses are obtained by splitting the mechanical analyses into two models.

- The first simulation is a coupled T-M model with initial stresses of zero and a thermal load shown in Table 1 to obtain the thermally induced stresses and displacements in the rock surrounding the used-fuel container. All of materials are assumed to be elastic and, therefore, the swelling pressure of sealing materials is not incorporated in this model.

- The second set calculates stresses in the rock induced by excavation of the placement room and the in-floor borehole with the initial stresses equal to the representative in situ stresses.

The total stresses are obtained by adding stress vectors in the rock induced by excavation of the placement room and the in-floor borehole with initial stresses equal to the representative in situ stresses to the stress vectors from coupled T-M model with zero initial stresses.

Stability analyses depend on the total stresses. A safety factor is used to evaluate the rock mass stability. The procedure to calculate the safety factor is described as follows.

- First, the major and minor principal stresses are calculated based on total stress vectors.
- Second, the strength (σ_{1f}) is determined using Equation 1.
- Third, safety factor (SR) is calculated using the following equation: $SR=\sigma_{1f}/\sigma_1$, where σ_1 is the major principal stress.

6.1 NEAR-FIELD THERMAL MODELLING

6.1.1 The Near-Field Thermal Model

The model geometry for the thermal near-field modelling is the same as shown in Figure 4 in which the value of b is 20 m and the value of d is 2.1 m (i.e., see Section 4.1.1, 40-m emplacement-room spacing and 4.2-m container spacing). The thermal boundary conditions are shown in Figure 5. The thermal load uses one quarter of a container heat output, which is listed in Table 1. The initial temperature in the rock is 5°C on the upper surface with a geothermal gradient of 0.012°C/m of depth. The initial stresses and displacement are set at zero. The mechanical boundary conditions are defined in Section 4.1.2 and Figure 6.

Some selected locations and lines near the placement room and in-floor borehole are marked in Figure 51. The numerical results for these selected locations are given in this section.

As discussed in Section 3.12, the results from the near-field modelling are relevant to a horizontally infinite repository and accurate only for 1,000 years for a horizontally finite repository.

6.1.2 Thermal Results from Near-Field Thermal Modelling

Figure 52 shows the temperatures along Line EI (at the mid-height of the container) from the container surface (Point D, refer to Figure 6 for location) to the model boundary (Point I) (refer to Figure 51 for locations) at seven different times. The temperatures are 33°C on the container surface and quickly drop to 15°C at the borehole surface at 0.02 years. At 10 years, the temperatures are 100°C at the container surface, 61°C at the borehole surface and 27°C at the model boundary (Point I). With time, the temperature distribution becomes more uniform.

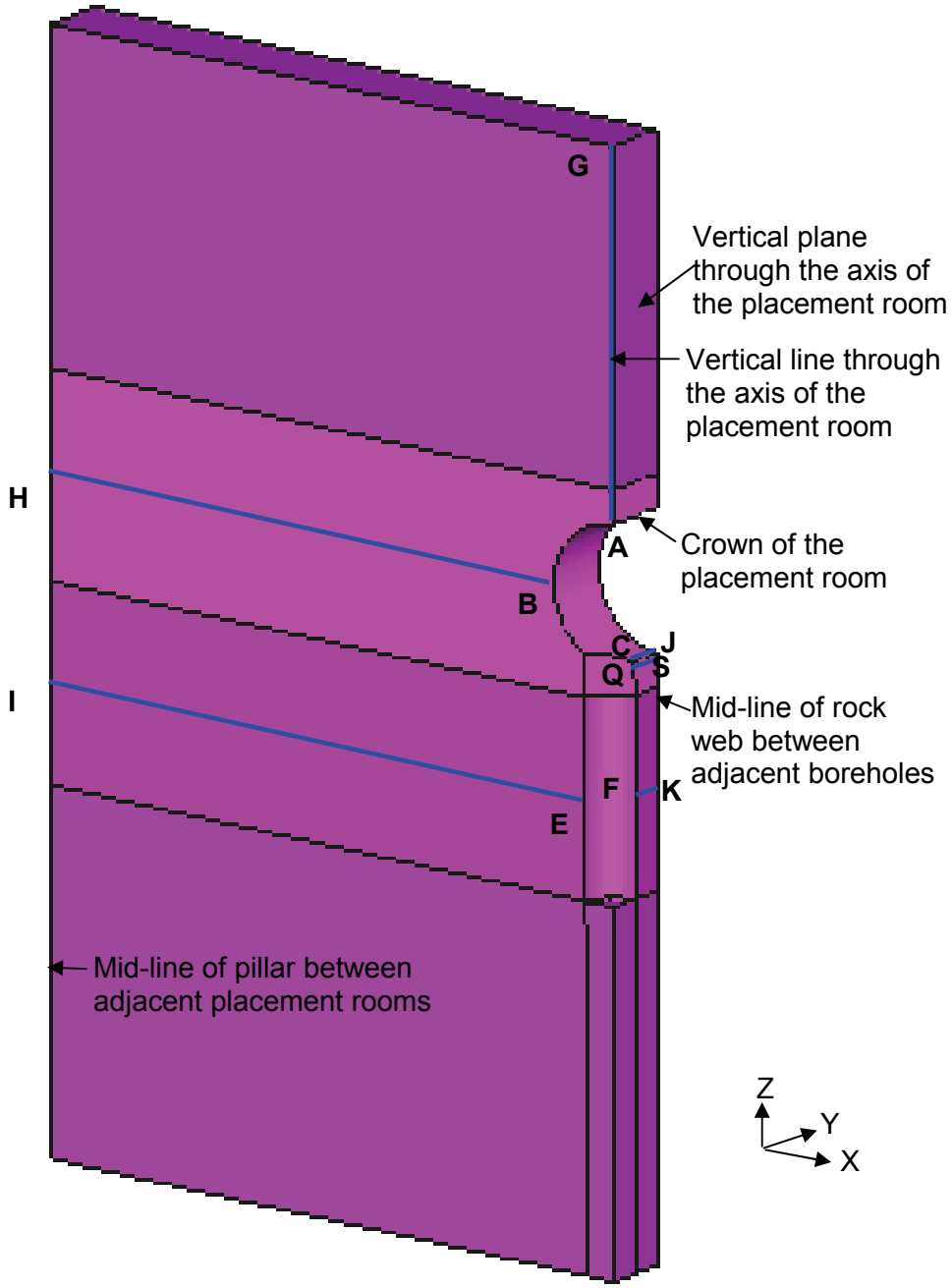


Figure 51: Locations for Presentation of Near-Field Modelling Results

6.1.3

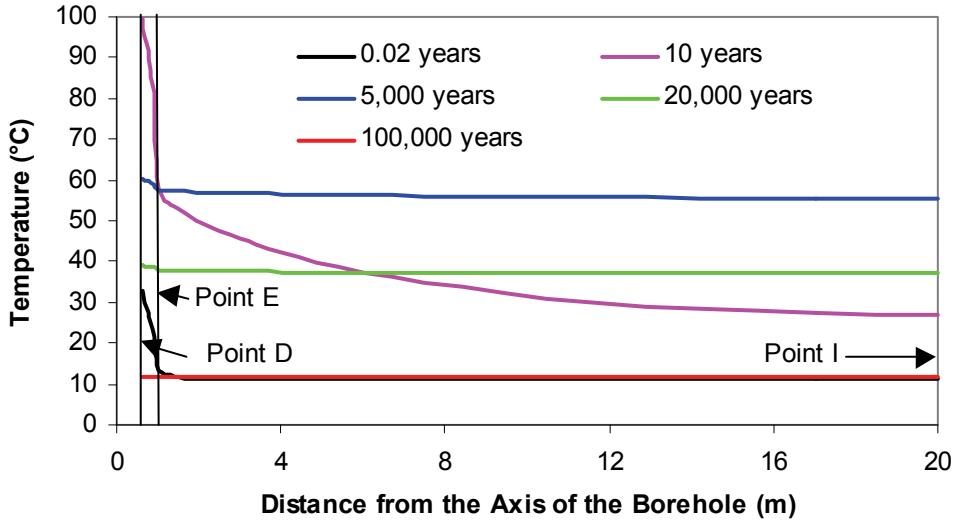


Figure 52: **Temperatures along Horizontal Line EI through the Mid-Height of the Container between Two Placement Rooms**

Figure 53 shows the temperature with time at different locations along Line EI. At different locations they show the same pattern. At 0.6235 m from the container axis (i.e., at the container surface, Point D), the temperature peaks at 100°C at 10 years, drops to 60°C at 5,000 years and 12°C at 100,000 years. At the borehole surface, the temperatures are 65°C at 30 years, 58°C at 5,000 years and 11.8°C at 100,000 years.

Figure 54 shows the temperature development with time at five different locations (Point A, B, C, D and E, refer to Figure 51 for location of Point A, B, C and E and refer to Figure 6 for location of Point D). The temperature on the crown of the placement room (Point A) is 50°C at 80 years and at 56°C at 4,500 years. The temperature on Point C is 54°C at 50 years.

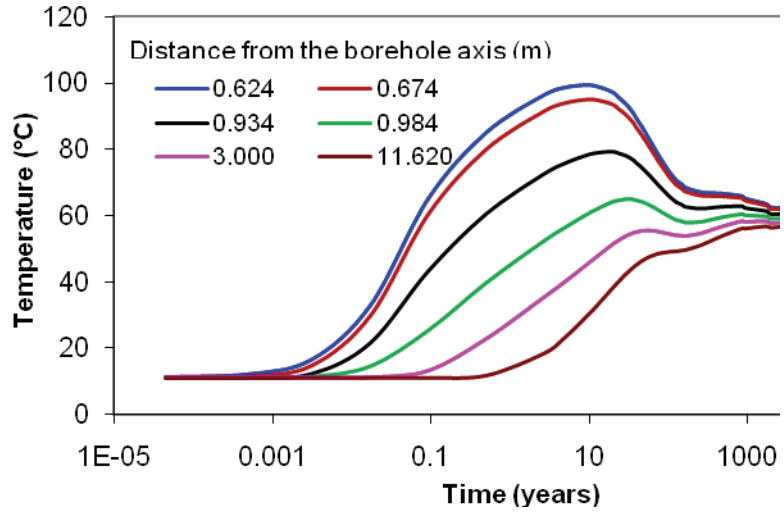


Figure 53: **Temperature versus Time at Different Locations along Horizontal Line EI**

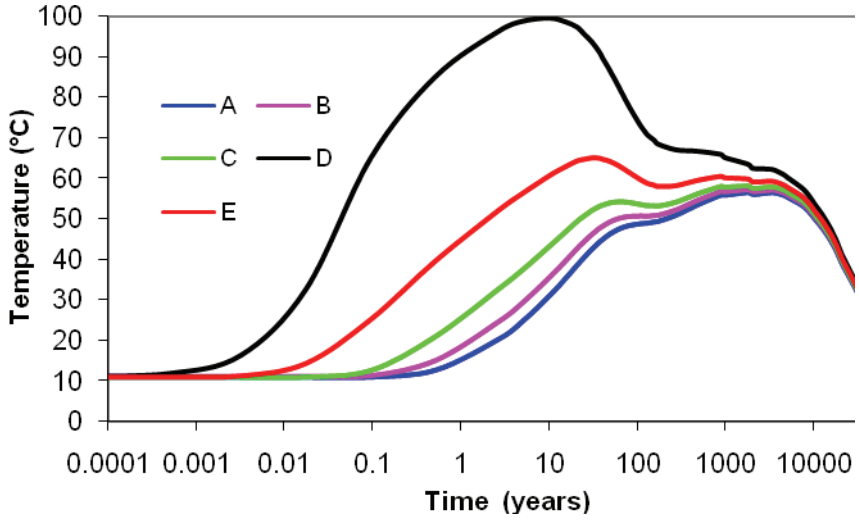


Figure 54: **Temperatures at Locations of A, B, C, D and E in the Vicinity of the Container and Placement Room**

Figure 55 shows the temperature along Line BH between placement rooms at six different times. The temperature is 29°C at the placement-room wall of Point B and gradually drops to 19°C at mid-pillar between rooms (i.e., at the model boundary) at 5 years. At 5,000 years, the temperature is 55.8°C at the placement-room wall and 55.2°C at mid-pillar (i.e., 20 m from the borehole axis).

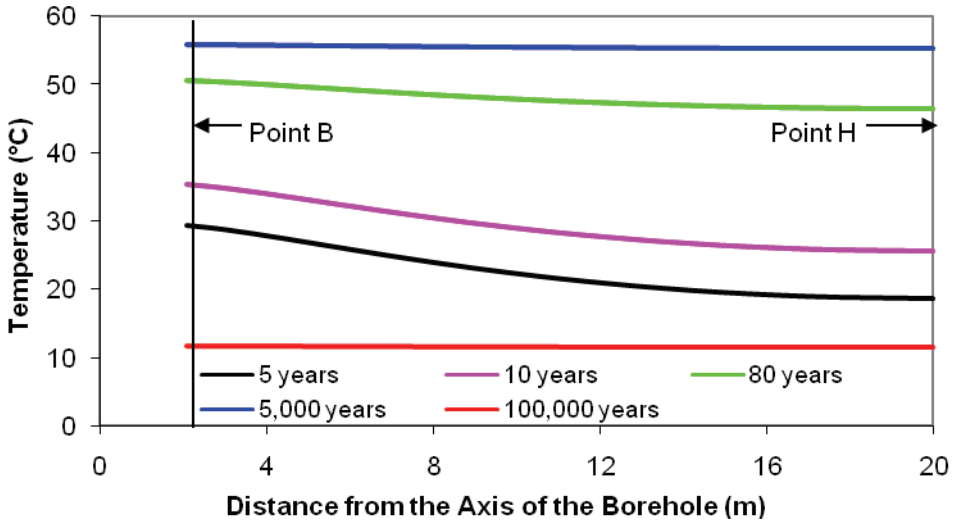


Figure 55: **Temperature along Line BH at Different Times**

Figure 56 shows the temperature distribution along vertical line through the axis of the borehole at seven different times. At earlier times, the temperatures along the vertical line are not uniform. The temperature on the container surface is much higher than that in the buffer and the surrounding rock. However, the temperatures become more uniform after 1,000 years. Finally, they approach the ambient temperature after 100,000 years.

The temperature distributions on the cross-sectional planes of symmetry through the borehole/container central axis are shown in Figure 57 at four different times. The temperature in the buffer, backfill and pellets becomes more uniform with time.

The temperature distributions in the rock around a container at four different times are shown in Figure 58. The plot again shows that the temperature in the rock becomes more uniform with time.

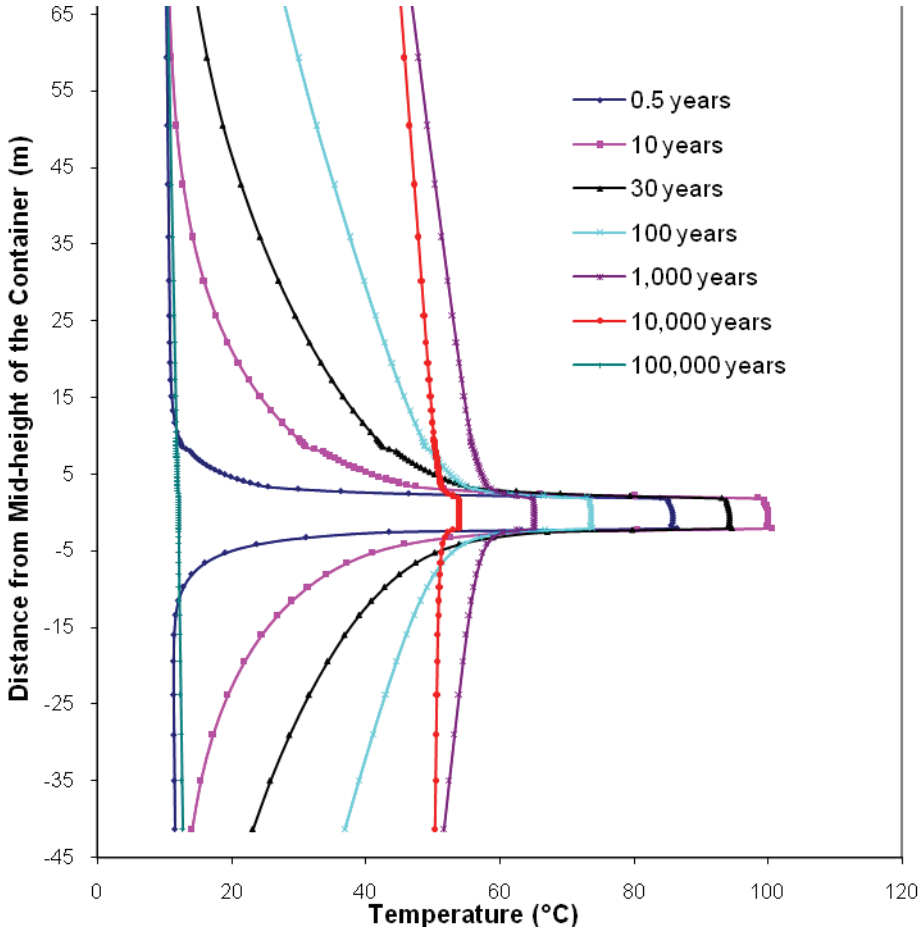


Figure 56: **Temperature along Vertical Line through the Axis of the Container at Seven Different Times**

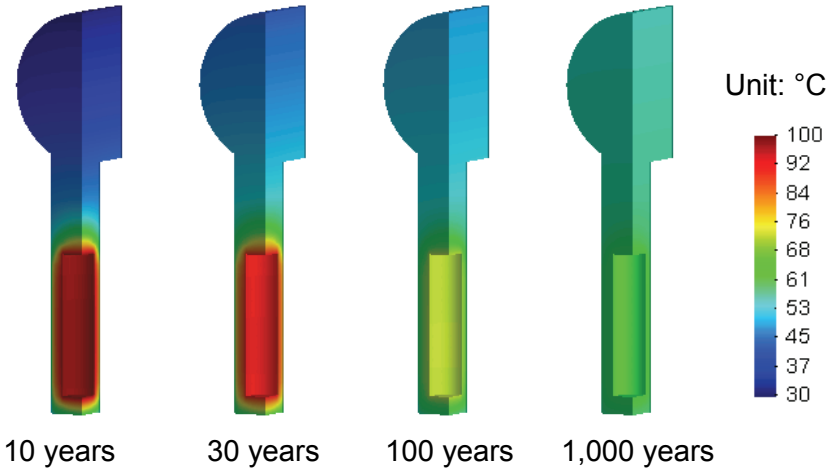


Figure 57: **Temperatures in the Buffer, Light Backfill, Dense Backfill and Pellets at Four Different Times**

6.2 NEAR-FIELD MECHANICAL AND COUPLED T-M MODELLING

6.2.1 Excavation Analyses

Based on the in-situ stresses as shown in Equations 2, 3 and 4, at the repository horizon of 500 m below ground surface, the three principal in-situ stress components are as follows:

$$\left.\begin{aligned}\sigma_1 = \sigma_y &= 35.2\ \text{MPa}\\ \sigma_2 = \sigma_x &= 23.2\ \text{MPa}\\ \sigma_3 = \sigma_z &= 12.1\ \text{MPa}\end{aligned}\right\}$$

The rock mass, prior to excavation, is in an equilibrium state based on the local in-situ stresses generated by lithostatic load and plate tectonics. Upon excavation of the placement rooms and in-floor boreholes, the stresses re-adjust to a new state of equilibrium. Regardless of the specific state of equilibrium, stress concentrations greater than the original in-situ stress magnitudes are generated at various locations around the excavation perimeters depending largely on the geometric shape of the excavation and its orientation to the in-situ stress field.

EXCAVATION MODEL

The excavation-model geometry is shown in Figure 4(a). The only material in this model is rock, and the thermal boundary conditions are all isothermal. The side surfaces are fixed in their horizontal directions as shown in Figure 7. The bottom of the model is fixed in the vertical direction. On the top of the model, a vertical stress of 12.1 MPa is applied to represent the vertical in-situ stress at 500-m depth. The walls of the placement room and the in-floor borehole are free to displace. The initial stresses in the rock are as shown above.

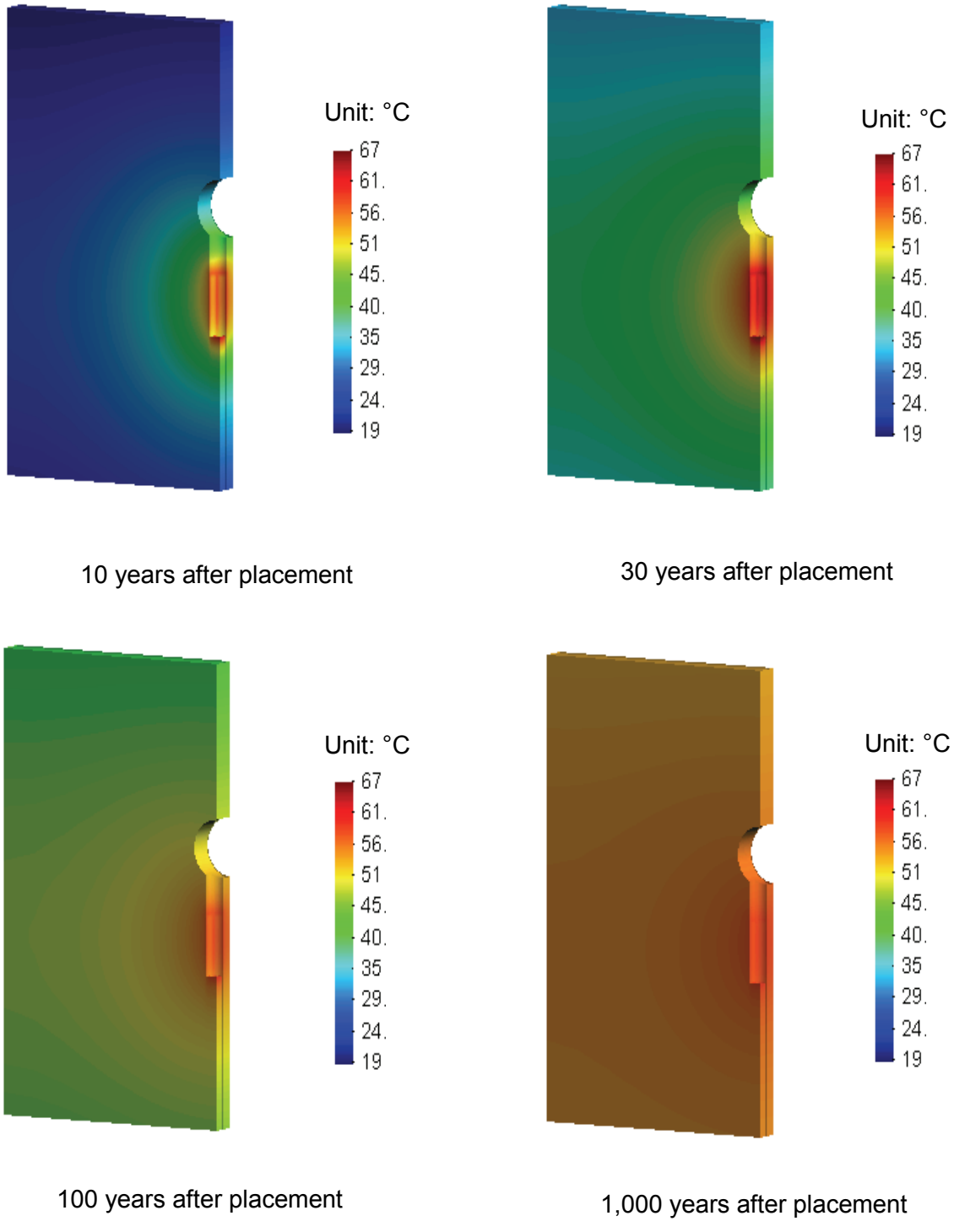


Figure 58: **Temperatures in the Rock near the Container at Four Different Times**

Two kinds of geometries were analyzed to investigate the influence of the shapes on the excavation-induced stresses in the rock. One geometry is a circular placement room with a diameter of 4.2 m. The other is an elliptical placement room being set at 4.05 m high and 6.89 m wide.

Figure 59 shows the stresses along Line AG for both the circular- and elliptical-shape placement-rooms. The tangential stress (X-direction) at the top of the circular placement room is greater than that at the top of the elliptical placement room. For example, the X-directional stress for the circular room is 59 MPa, while it is 39.5 MPa for the elliptical room. Note that the vertical stresses near Point A are not zero for both room shapes. The vertical stresses are 1 MPa for the circular room and 0.5 MPa for the elliptical room. The reason is that CODE_BRIGHT (version 23beta) can only output the stresses of elements. Therefore, the value is not the stress at Point A, but at a point 0.125 m above the room crown, which is the centre of the first element above the room.

Figure 60 shows the stresses along Line BH after room and borehole excavation for the circular- and elliptical-shape placement rooms. There is a slight difference in the Y-directional stress between the two models. There is an obvious difference in the Z-directional stress between the two models. For the elliptical-shape placement room, the Z-directional stress decreases from 29 MPa near Point B (placement-room wall) to 13 MPa at Point H (model boundary), while the Z-directional stress increases from 14 MPa near Point B (placement-room wall, 2.1 m from the placement-room axis) to 16 MPa at a location 3 m from the placement-room axis and then gradually decreases to 13 MPa at Point H.

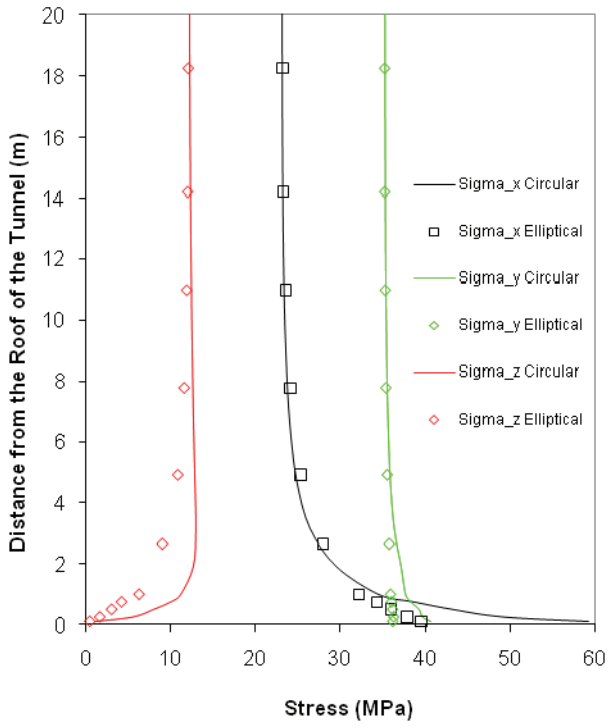


Figure 59: **Stresses along Line AG after Excavation for Two Different Placement-Room Shapes**

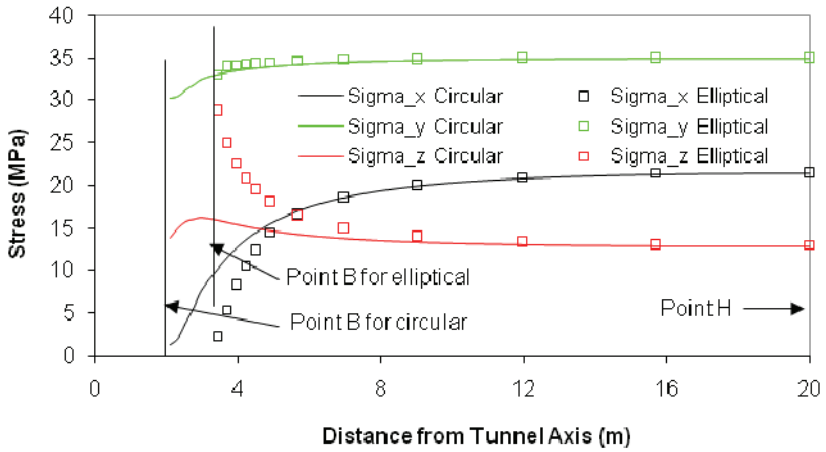


Figure 60: **Stresses along Line BH after Excavation for Two Placement-Room Shapes**

Figure 61 shows the stresses along Line EI after placement room and borehole excavation for both the circular- and the elliptical-shape placement rooms. The influence of the placement-room shapes on the stresses along Line EI is negligible.

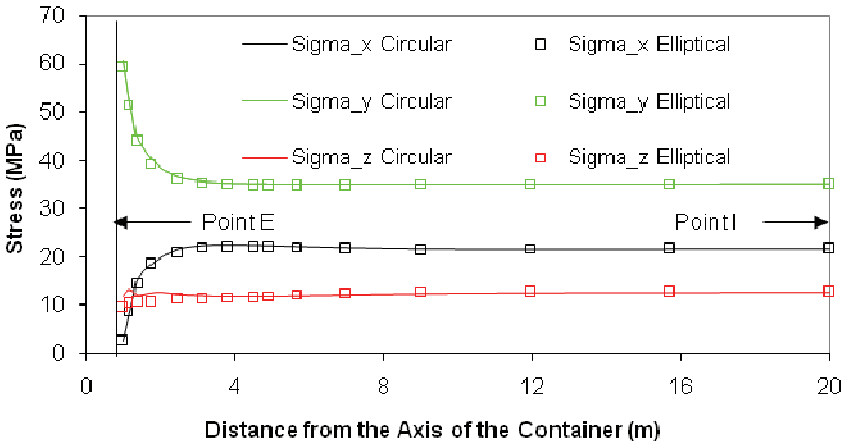


Figure 61: **Stresses along Line EI after Excavation for Two Different Placement-Room Shapes**

Figure 62 shows the stresses along Line FK from the circular placement-room model and the elliptical placement-room model. There is little apparent difference in the X- and Y-directional stresses between the two room shapes. The Z-directional stresses for the circular room are about 2 MPa greater than those for the elliptical placement room.

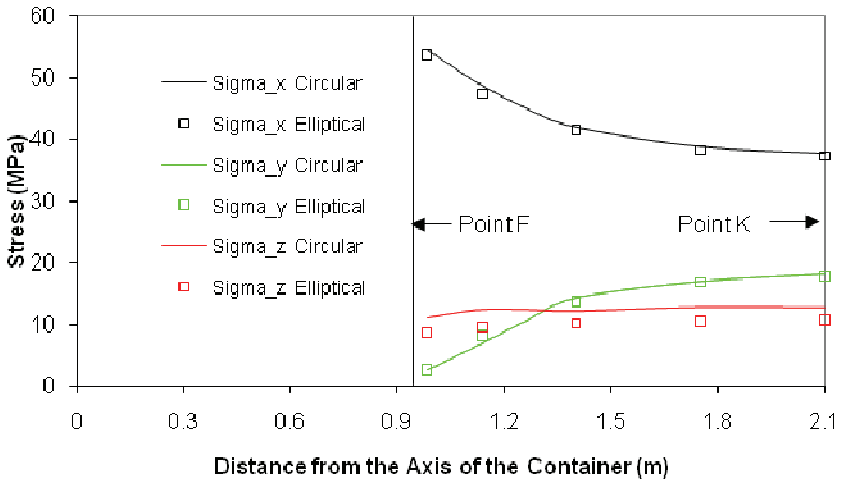


Figure 62: **Stresses along Line FK after Excavation for Two Different Placement-Room Shapes**

Figure 63 shows the stresses along Line CJ (the rock web between boreholes on the floor of the placement room) after placement room and borehole excavation for the circular placement-room model and the elliptical placement-room model. There is little difference in the Y-directional stresses and the Z-directional stresses between the circular and the elliptical placement rooms. The X-directional (tangential) stress in the circular room varies from 107 MPa at Point C to 75 MPa at Point J, whereas for the elliptical-room case, the corresponding values are about 81 and 55 MPa at C and J, respectively. The complex stress geometry at the junction of the room floor and borehole collar (Point C) generates the highest stress concentrations in all cases, as compared the tangential stress in the crown of the room.

Figure 64 shows the stresses along Line QS (i.e., 0.25 m below the placement-room floor) after placement room and borehole excavation for both the circular and the elliptical placement rooms. There are small differences in the Y-directional stresses between the circular and the elliptical placement rooms. However, the influence of the placement-room shapes on the X-directional stresses is very significant. The X-directional stress in the circular placement-room model is from 97 MPa near Point Q to 65 MPa at Point S.

The above excavation analyses show that the elliptical-shaped placement room is generally more stable than the circular-emplacement room, especially when the floor of the room is disturbed by an intersecting borehole. The next section examines the near-field thermal-mechanical stability of the rock near the placement room with a circular shape.

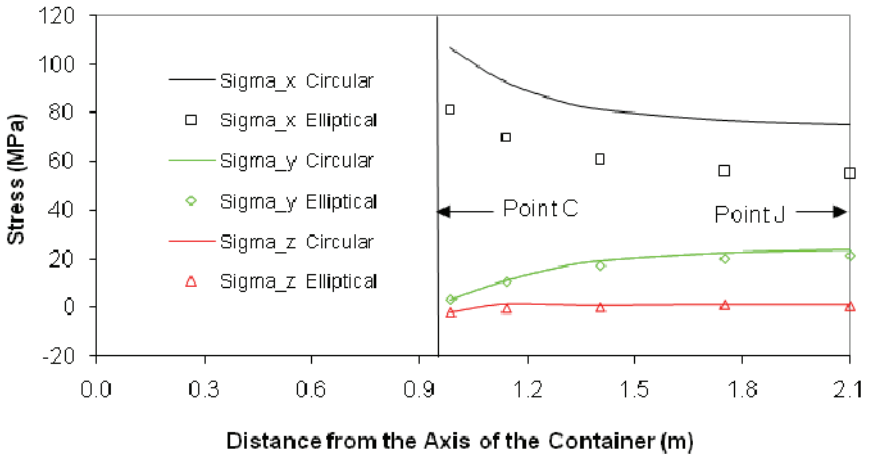


Figure 63: **Stresses along Line CJ after Excavation for Two Placement-Room Shapes**

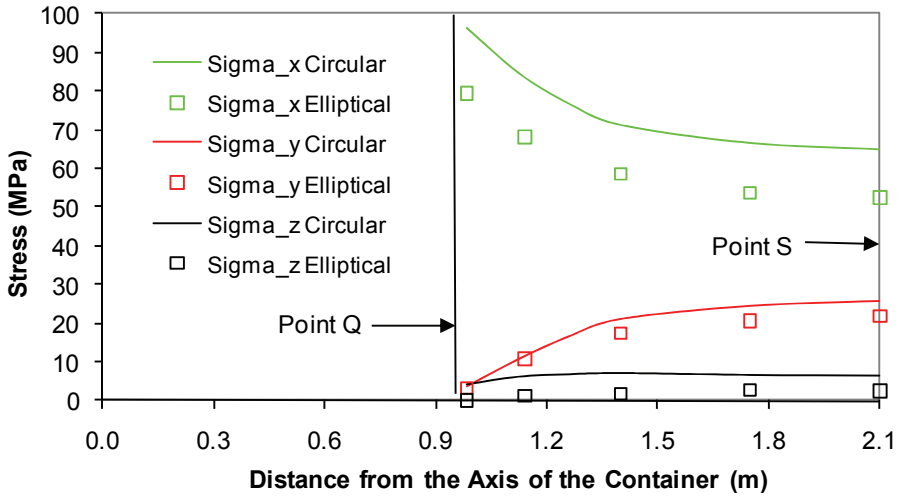


Figure 64: **Stresses along Line QS after Excavation for Two Placement-Room Shapes**

6.2.2 Coupled T-M Analyses for the Circular-Shaped Placement Room

6.2.2.1 Coupled T-M Near-Field Model

The model geometry is the same as that shown in Figure 4. Thermal and mechanical boundary conditions are the same as those described in Section 4.1.2 and Figures 5 and 6. Initial stresses are assumed to be zero.

Since the near-field model only represents a model with an infinite repository, the modelling results are not representative for a model with a finite repository after 1,000 years. In this section, the results for the first ,1,000 years after waste placement are given, which are not only representative of the results or an infinite repository but also for a finite repository, since temperatures are the similar for both in time period presented (Guo 2007).

6.2.2.2 Thermal Results from the Coupled T-M Modelling

The thermal response is the same as described in Section 6.1.

6.2.2.3 Thermally Induced Near-Field Stresses

The thermally induced stresses along Line AG through the placement-room crown are shown in Figures 65, 66 and 67 (refer to Figure 51 for locations). The peak thermally induced stress at 1,000 years in the X-direction is 71 MPa near Point A (placement-room crown) and 31 MPa at Point G (20 m above the placement-room crown). The thermally induced stress in the X-direction gradually decreases with distance from the placement-room crown. Although the pattern of the stresses in the Y-direction is different from that of the stresses in the X-direction, the peak thermally induced stress in the Y-direction also occurs at the placement-room crown with a magnitude of 41 MPa at 1,000 years. Due to the small value of Young's modulus of light backfill, the thermally induced stress in the Z-direction at the placement-room crown is only 1 MPa at 1,000 years.

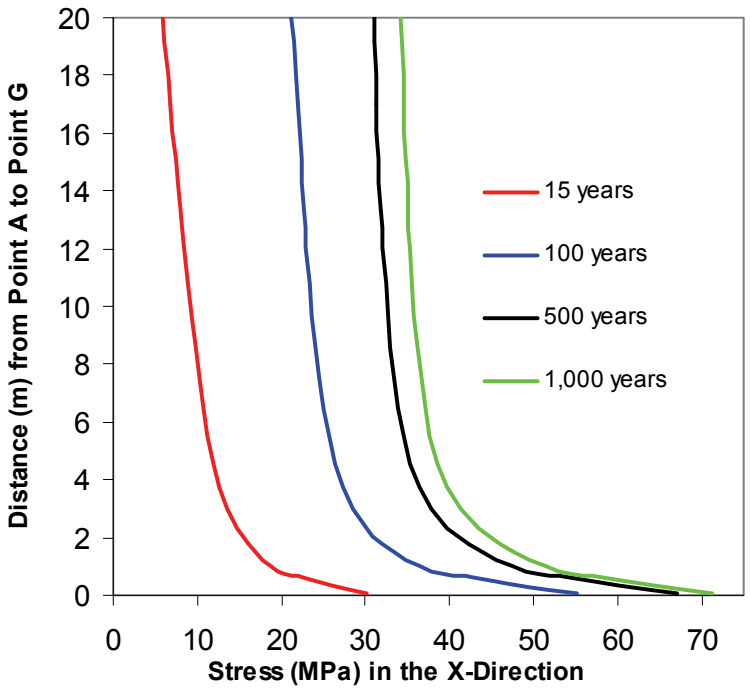


Figure 65: Thermally Induced Stresses in the X-Direction along Line AG

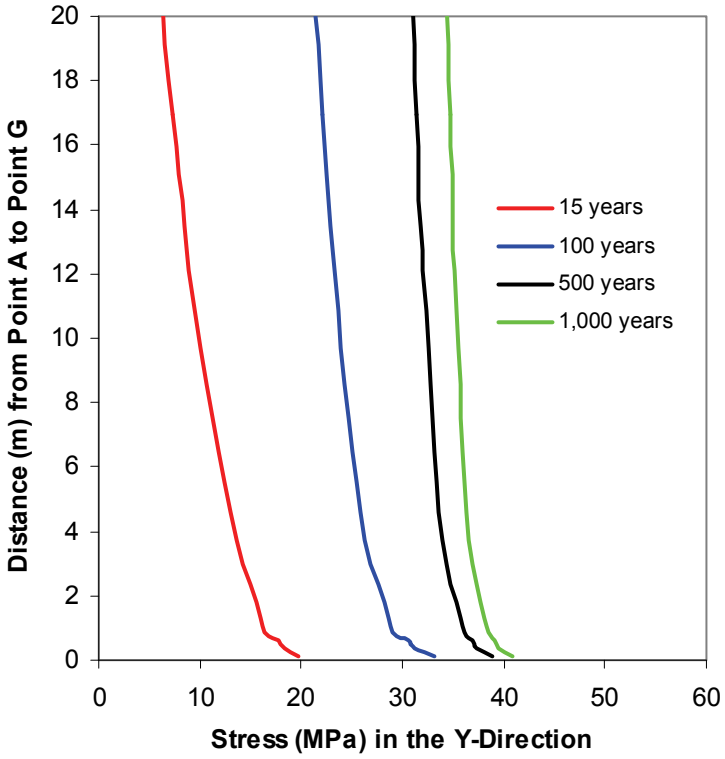


Figure 66: **Thermally Induced Stresses in the Y-Direction along Line AG**

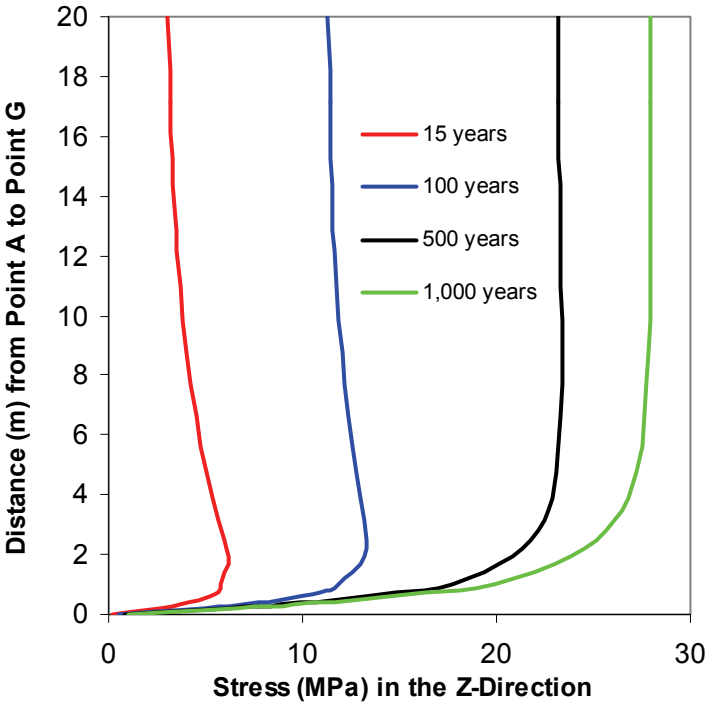


Figure 67: **Thermally Induced Stresses in the Z-Direction along Line AG**

The thermally induced stresses in the X-, Y-, and Z-directions along the horizontal Line BH extending from the placement-room mid-height to the pillar centre line (refer to Figure 51 for location) at four different times are shown in Figures 68, 69 and 70. The stresses in the X-direction at different times are 0.6 MPa, 1.1 MPa, 1.6 MPa and 1.8 MPa near Point B (i.e., the placement-room wall) at 15 years, 100 years, 500 years and 1,000 years, respectively, because the stiffness of the light backfill is very small compared to the rock. At Point H, the thermally induced stress in the X-direction increases from zero before waste placement to 34 MPa at 1,000 years. The thermally induced stress in the Y-direction increases from zero before waste placement to 22 MPa at 1,000 years near Point B. The thermally induced maximum stress in the Z-direction is not at Point B but at a location 0.225 m from Point B. The stress in the Z-direction is 32.5 MPa near Point B, increasing to 46 MPa at location 0.225 m from Point B and then drops to 29 MPa at Point H at 1,000 years.

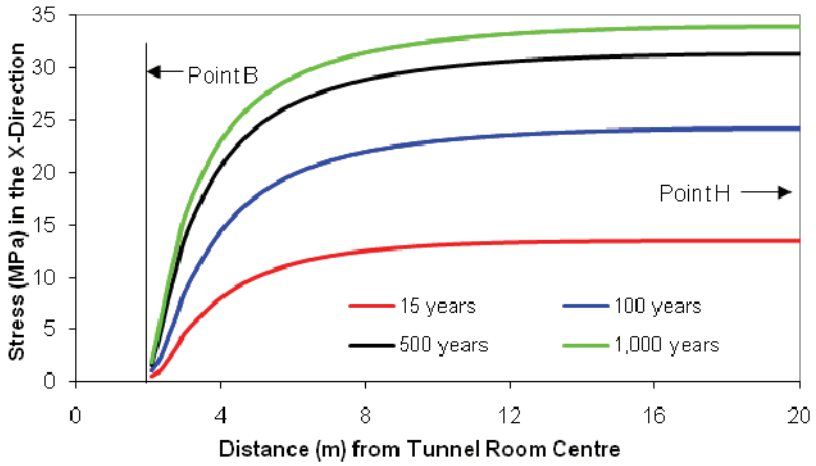


Figure 68: Thermally Induced Stresses in the X-Direction along Line BH

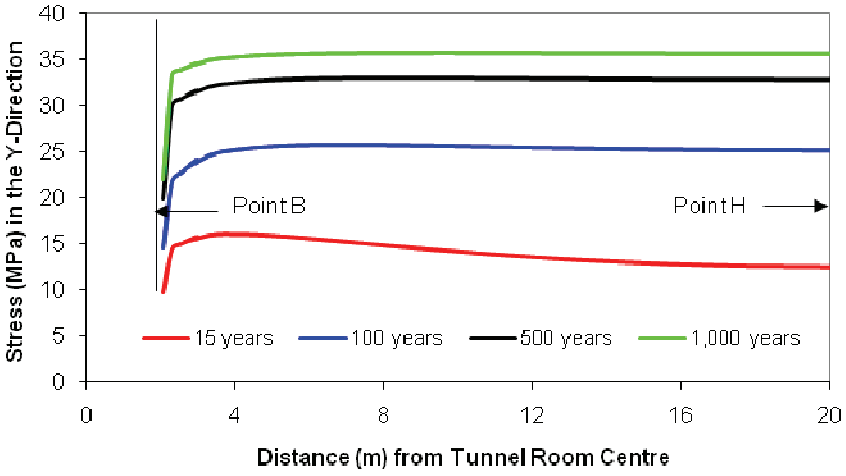


Figure 69: Thermally Induced Stresses in the Y-Direction along Line BH

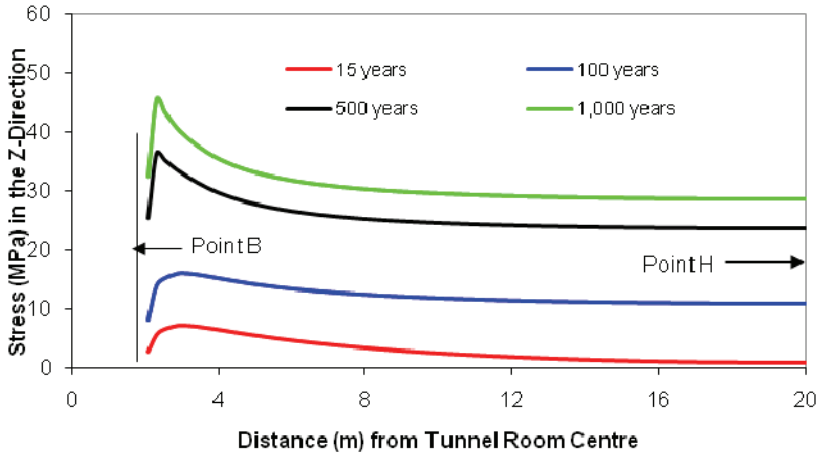


Figure 70: Thermally Induced Stresses in the Z-Direction along Line BH

The thermally induced stresses in the X-, Y-, and Z-directions along a horizontal Line EI extending from the mid-height of the container to the pillar centre line (refer to Figure 51 for location) at four different times are illustrated in Figures 71, 72 and 73. The stresses in the X-direction at different times are about 2~3.5 MPa near Point E (the borehole wall) because the stiffness of the buffer is very low compared to the stiffness of the rock. At Point I, the thermally induced stress in the X-direction increases from zero before waste placement to 34 MPa at 1,000 years. The thermally induced stress in the Y-direction along Line EI is 55 MPa near Point E and 36 MPa at Point I at 1,000 years. The thermally induced stress in the Z-direction is 11 MPa near Point E and drops to 0.5 MPa at Point I at 15 years and 25 MPa increasing to 28.5 MPa at Point I at approximately 1,000 years. The trend of decreasing thermally induced stress in the Z-direction with distance at 15 years is different from the trend of increasing stress with distance at 1,000 years.

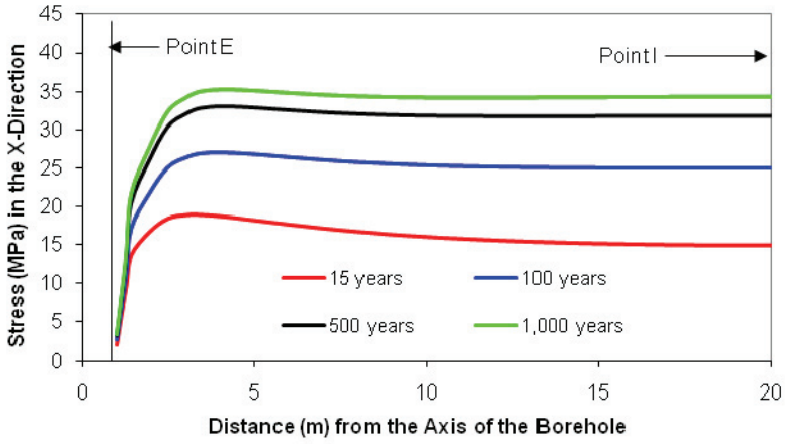


Figure 71: Thermally Induced Stresses in the X-Direction along Line EI

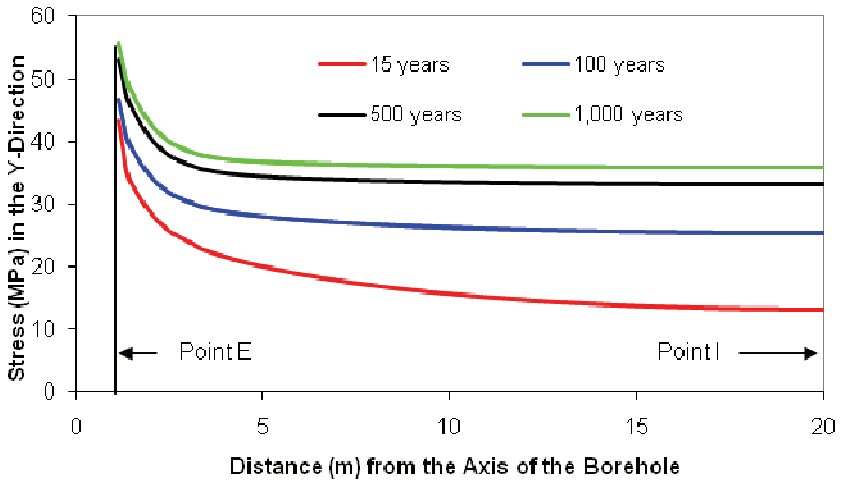


Figure 72: Thermally Induced Stresses in the Y-Direction along Line EI

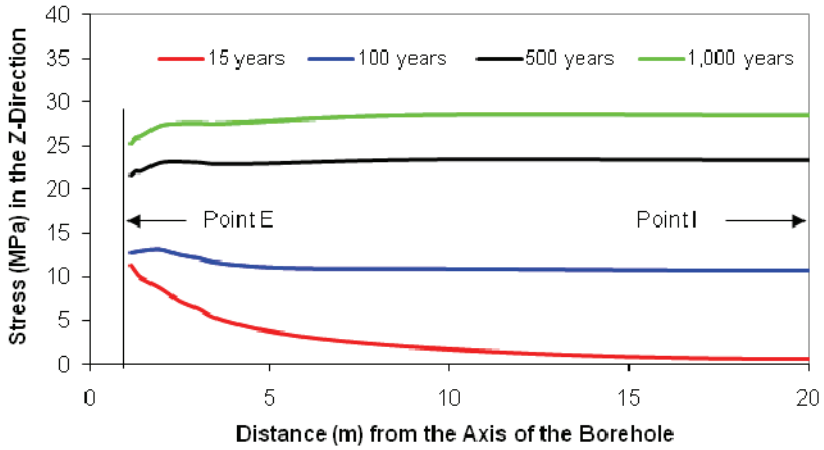


Figure 73: Thermally Induced Stresses in the Z-Direction along Line EI

The thermally induced stresses in the X-, Y-, and Z-directions along Line FK, a horizontal line at the container mid-height extending from the borehole wall to the mid line of the web between adjacent boreholes (refer to Figure 51 for location) at four different times are given in Figures 74, 75 and 76. The stresses in the X-direction are about 73 MPa near Point F and 57 MPa at Point K at 1,000 years. The peak thermally induced stress along Line FK is 83 MPa at 1,000 years occurring at location 0.139 m from Point F (the borehole wall). The thermally induced stress in the Y-direction along Line FK is about 3 MPa near Point F and 21 MPa at Point K at 1,000 years. The thermally induced stress in the Z-direction is 23 MPa near Point F, increases to a peak value of 33 MPa and then drops to 31 MPa at Point K at 1,000 years.

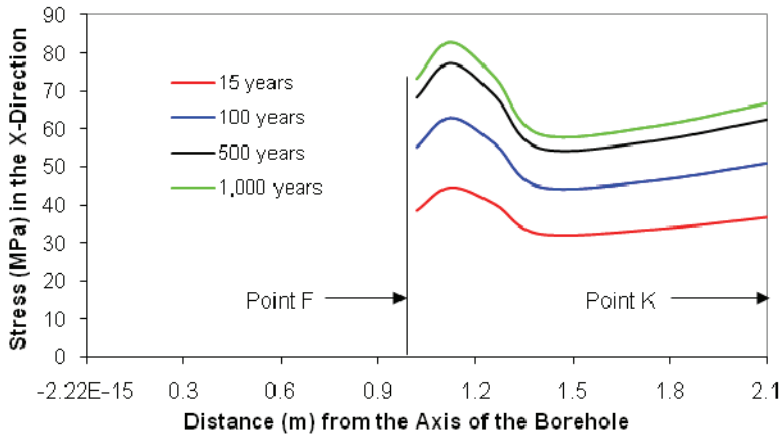


Figure 74: Thermally Induced Stresses in the X-Direction along Line FK

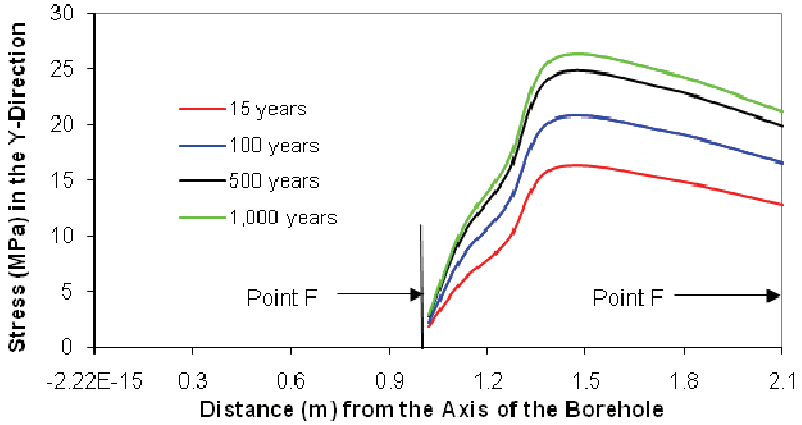


Figure 75: Thermally Induced Stresses in the Y-Direction along Line FK

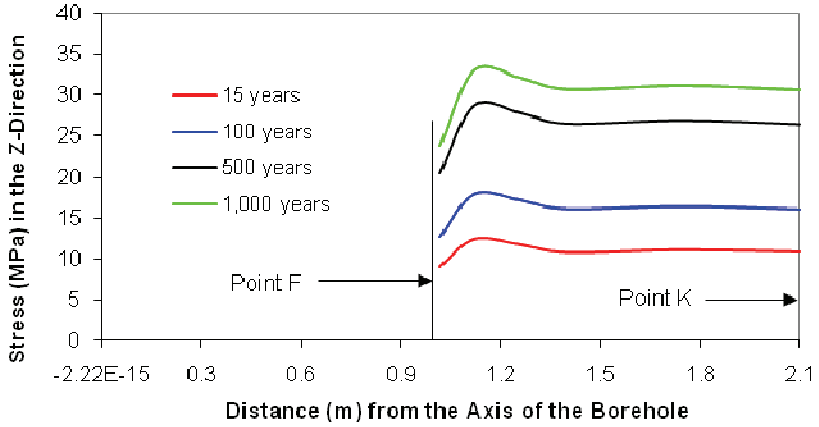


Figure 76: Thermally Induced Stresses in the Z-Direction along Line FK

The thermally induced stresses in the X- and Y-directions along Line CJ, a horizontal line from the borehole wall to the mid line of the web between adjacent boreholes along the floor of the placement room (see Figure 45 for locations), are shown in Figures 77 and 78, respectively. The thermally induced stress in the X-direction near Point C (adjacent to the borehole) is 26 MPa at 15 years and increases to 57 MPa at 1,000 years. The thermally induced stress in the Y-direction ranges from about 1.6 MPa near Point C to 14 MPa at Point J approximately at 1,000 years. The thermally induced stress in the Z-direction is 0 ~ 3 MPa at all times due to the low stiffness of the backfill relative to the rock stiffness and is not presented.

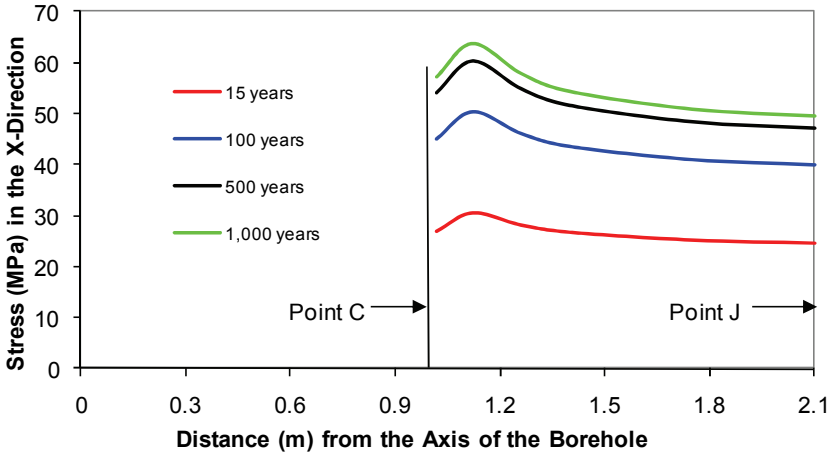


Figure 77: Thermally Induced Stresses in the X-Direction along Line CJ

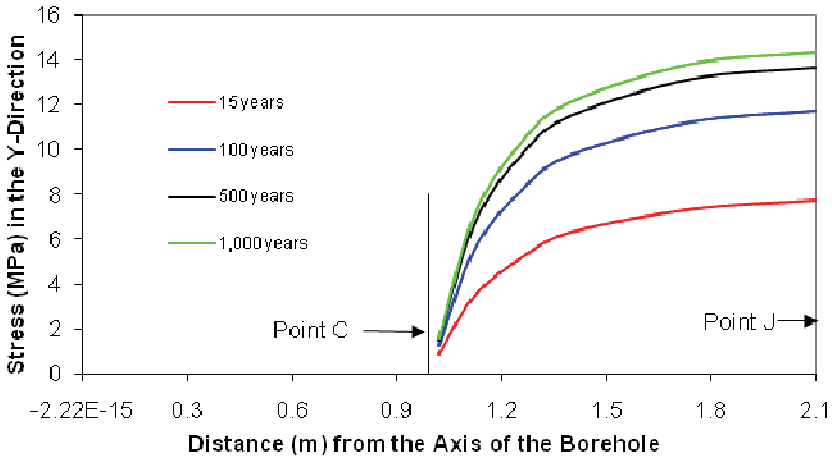


Figure 78: Thermally Induced Stresses in the Y-Direction along Line CJ

The thermally induced stresses in the X-, Y-, and Z-directions along Line QS, a horizontal line 25 cm below the bottom of the placement room extending from the borehole wall to the mid line of the web between adjacent boreholes (refer to Figure 51 for location) at four different times are given in Figures 79, 80 and 81. The stresses in the X-direction are about 115 MPa near Point Q and 93 MPa at Point S at 1,000 years. The peak thermally induced stress along Line

QS is 128 MPa at 1,000 years occurring at location 0.139 m from Point Q (the borehole wall). The thermally induced stress in the Y-direction along Line QS is about 4 MPa near Point Q and 33 MPa at Point S at 1,000 years. The thermally induced stress in the Z-direction is 5 MPa near Point Q, increases to a peak value of 11 MPa and then drops to 9 MPa at Point S at 1,000 years.

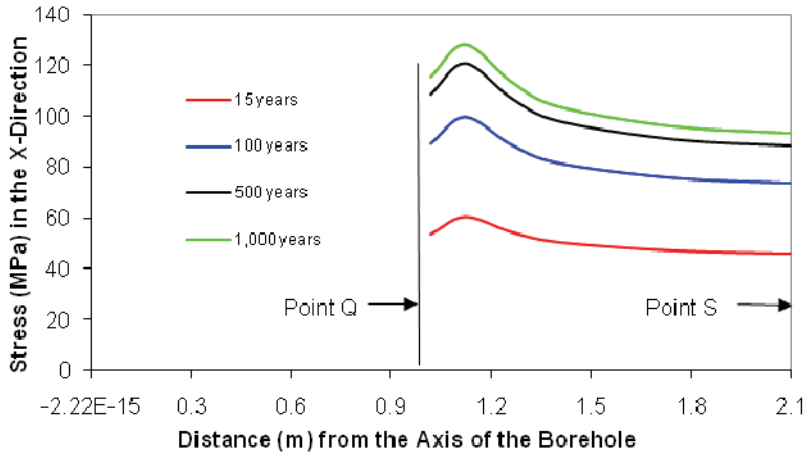


Figure 79: Thermally Induced Stresses in the X-Direction along Line QS

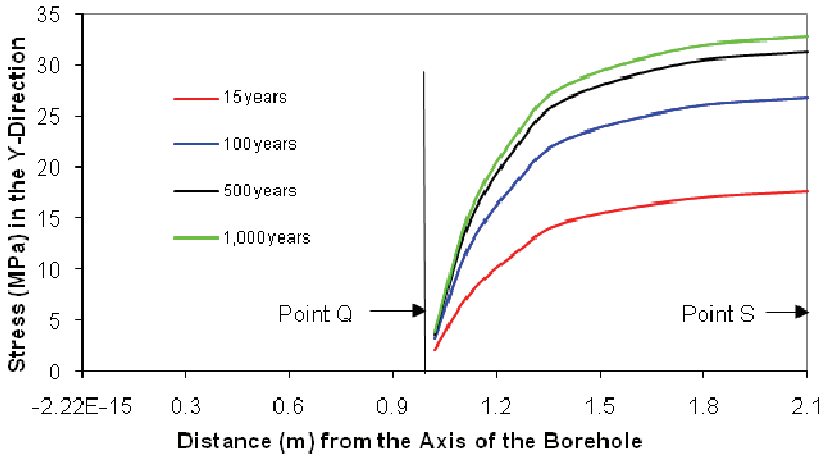


Figure 80: Thermally Induced Stresses in the Y-Direction along Line QS

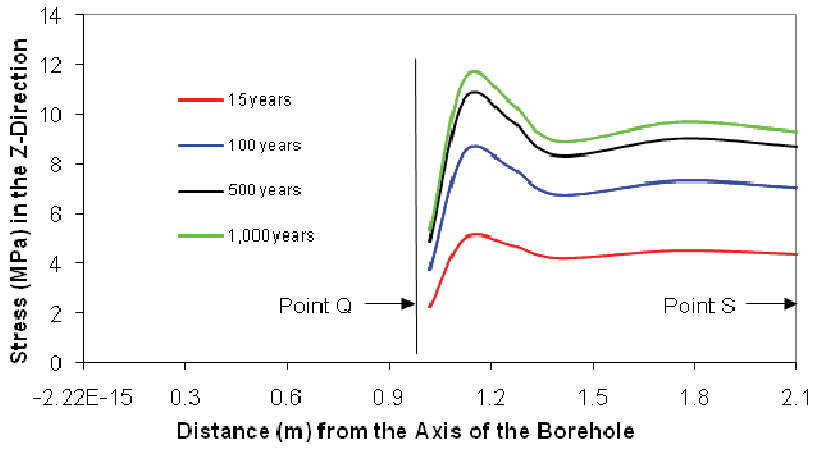


Figure 81: Thermally Induced Stresses in the Z-Direction along Line QS

6.2.2.4 Thermally Induced Near-Field Displacements

The thermally induced displacements in the Z-direction along Line AG are shown in Figure 82. Generally, the rock displaces upwards with distance from the placement-room crown. The rock moves upwards 3.3 mm at the placement-room crown and 7.5 mm at Point G at 15 years after waste placement.

Figure 83 shows thermally induced rock displacement in the vertical direction with time at four different locations along Line AG. At Point A (placement-room crown), the rock displacement increases from 0 mm immediately after waste placement to 3.9 mm at 50 years after waste placement, then decrease to 0.1 mm at 1,000 years after waste placement. At Point G, the rock displacement increases from 0 mm immediately after waste placement to 17.3 mm at 100 years after waste placement, and then decrease to 10.7 mm at 1,000 years after waste placement.

Figure 84 shows the horizontal displacement with time for four different locations along Line BH. The rock at the four different locations moves outwards (away from the placement-room centre) during the first 10 years, then moves inwards toward the placement-room centre.

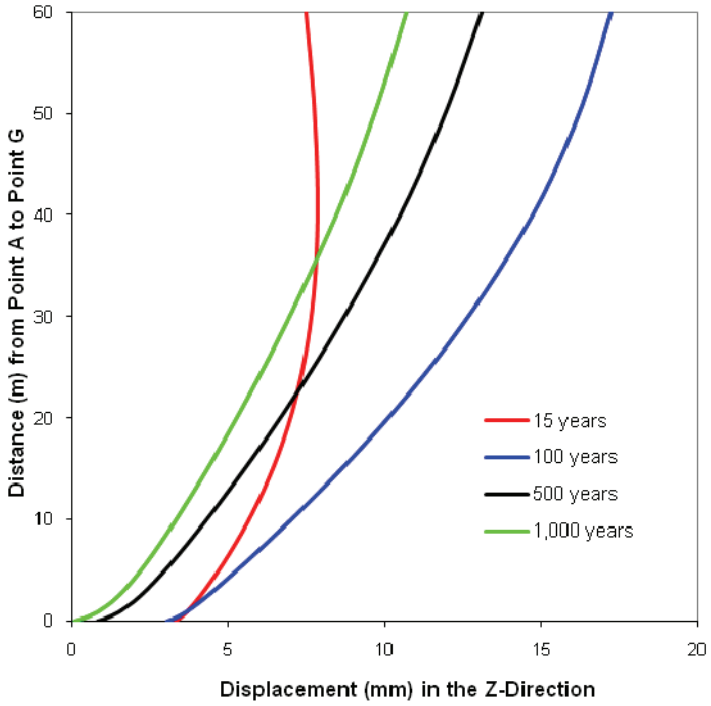


Figure 82: **Thermally Induced Displacements in the Z-Direction along Line AG**

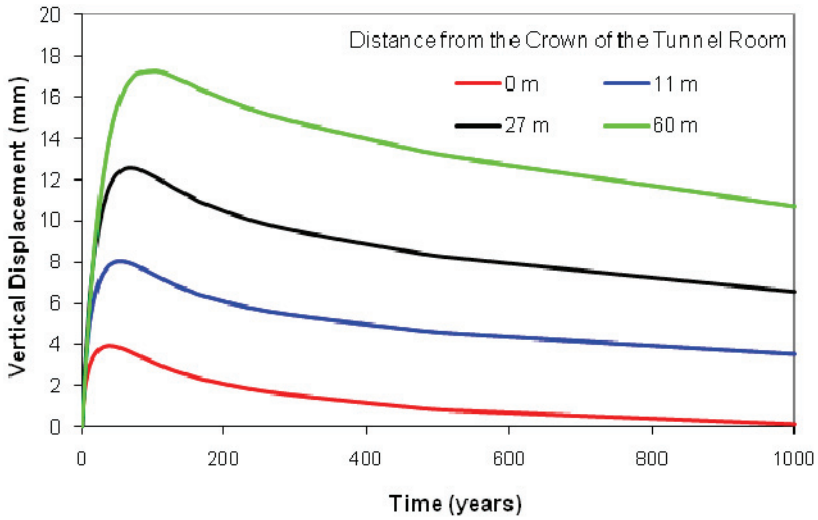


Figure 83: Vertical Displacement vs. Time at Four Different Locations along Line AG

The thermally induced displacements in the X-direction along Line BH are shown in Figure 85. The rock at Point B (the placement-room wall) moves outwards by 0.1 mm at 1.3 years, then moves inwards by 1.1 mm at 15 years, and 2.6 mm at 100 years. The displacement value gradually drops with distance away from the placement room until the displacement is zero at Point H (as required by the model boundary conditions). The displacements are 0.3 mm, 0.6 mm, 1.6 mm and 2.6 mm at 2.1 m, 4.0 m, 9.4 m and 14.2 m from the placement-room centre, respectively.

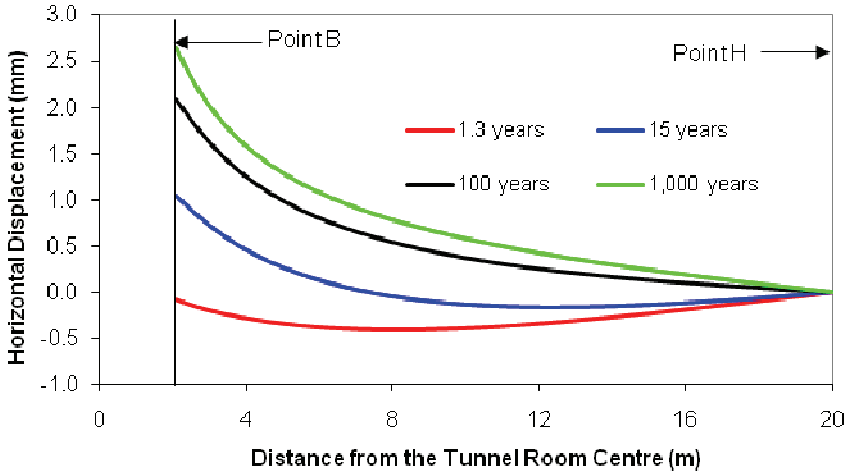


Figure 84: Thermally Induced Displacements in the X-Direction along Line BH

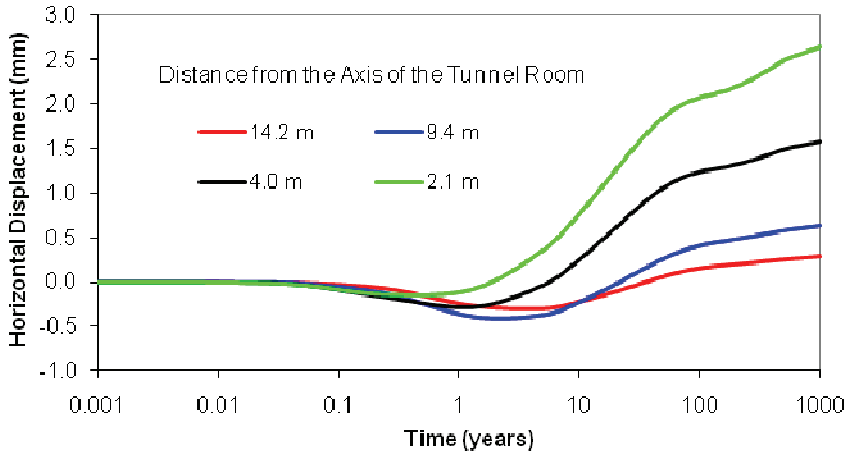


Figure 85: **Thermally Induced Displacement in the X-Direction at Different Locations along Line BH**

The thermally induced horizontal displacements along Line EI are shown in Figure 86. The thermally induced horizontal displacement at the borehole wall (Point E) is inwards towards the borehole and is less than 0.1 mm at 1.3 years, 0.5 mm at 15 years, 1.0 mm at 100 years and about 1.4 mm at 1,000 years.

Figure 87 shows the horizontal displacement with time for five different locations along Line EI. The rock at the four different locations (2.0 m, 4.0 m, 9.4 m, and 14.2 m from the borehole axis) moves outwards (away from the borehole axis) during the first 10 years, then moves inwards toward the borehole centre. The displacements are 0.3 mm, 0.5 mm, 0.8 mm, 1.0 mm and 1.4 mm at distances of 1.0 m, 2.1 m, 4.0 m, 9.4 m and 14.2 m from the placement-room centre, respectively.

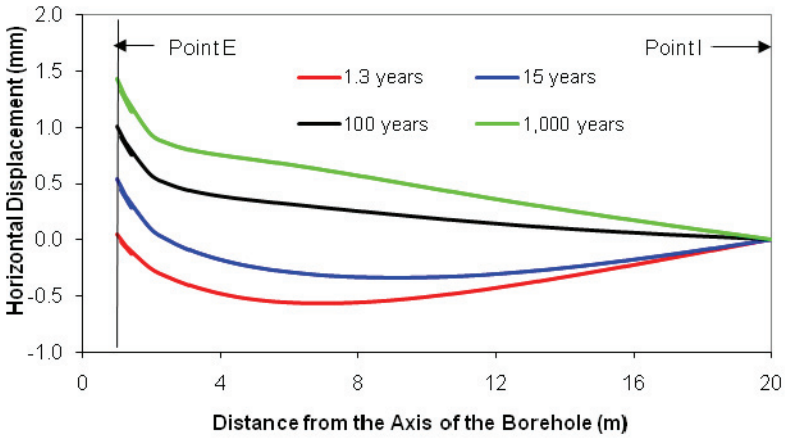


Figure 86: Thermally Induced Displacements in the X-Direction along Line EI

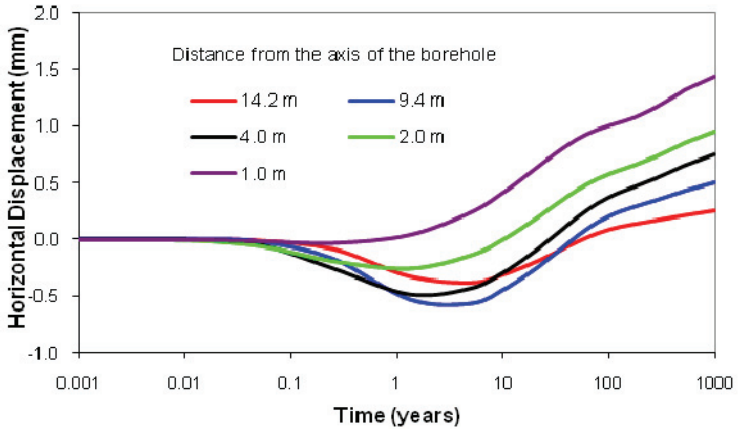


Figure 87: **Thermally Induced Displacement in the X-Direction at Different Locations along Line EI**

The thermally induced horizontal displacements along Line FK, a line between the container axis and the mid-line of the web between the adjacent boreholes at the container mid-height, are shown in Figure 88. At Point F (the borehole wall), the thermally induced horizontal displacement is about 0.66 mm at 1,000 years towards the in-floor borehole.

Figure 89 shows the horizontal displacement with time for five different locations along Line FK. The rock at the five different locations moves inwards toward the borehole centre. The displacements are 0.1 mm, 0.3 mm, 0.4 mm, 0.5 mm and 0.7 mm at distances of 1.75 m, 1.4 m, 1.26 m, 1.12 m and 0.98 m from the borehole axis, respectively.

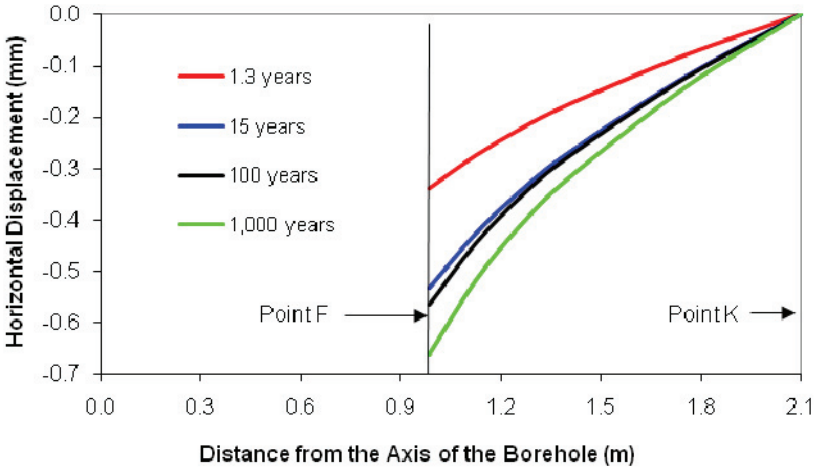


Figure 88: Thermally Induced Displacements in the Y-Direction along Line FK

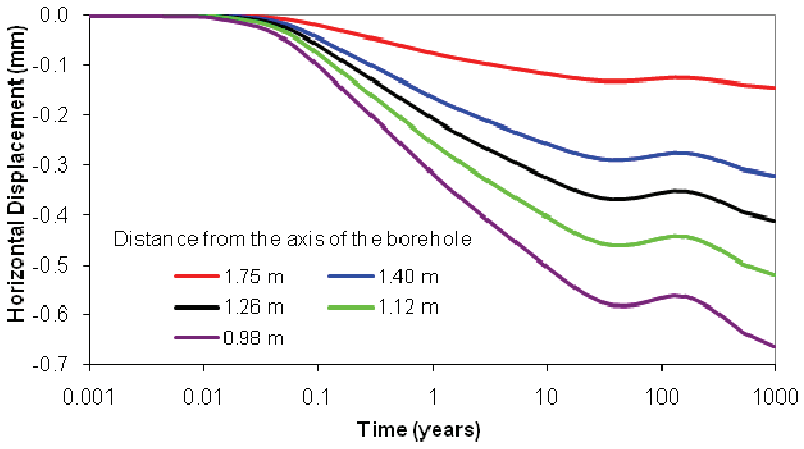


Figure 89: **Thermally Induced Displacement in the Y-Direction at Different Locations along Line FK**

Figure 90 shows the thermally induced vertical displacements along Line CJ. The rock on Line CJ moves upwards uniformly.

Figure 91 shows the thermally induced vertical displacement at Point C. The thermally induced vertical displacement at Point C is from 0 mm immediately after waste placement to 2.25 mm at 50 years after waste placement, and then gradually decreases to 1.91 mm at 1,000 years.

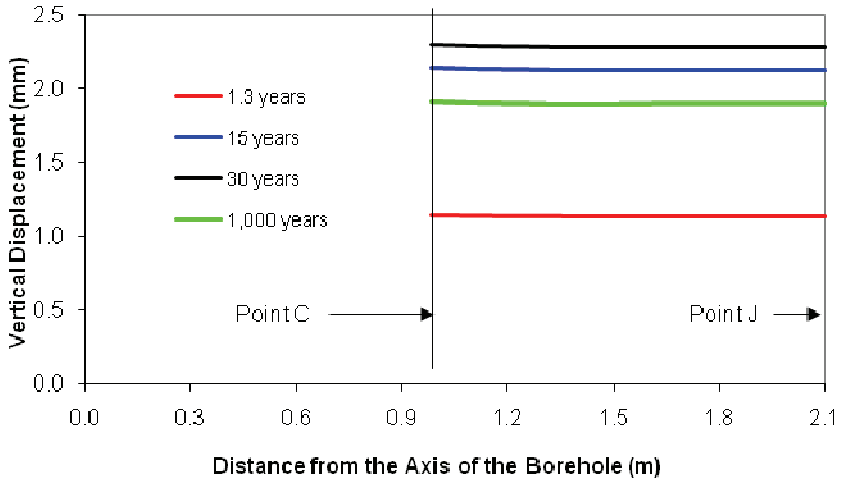


Figure 90: Thermally Induced Displacements in the Z-Direction along Line CJ

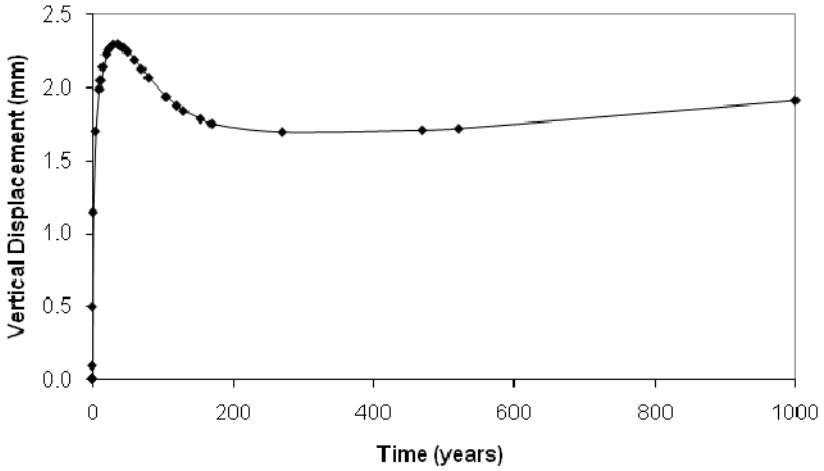


Figure 91: **Thermally Induced Vertical Displacement at Point C**

Figure 92 shows the thermally induced displacements in the horizontal direction (Y-direction) along Line CJ. The rock along line CJ moves inwards toward the borehole centre. The maximum thermally induced horizontally displacement is 0.6 mm at Point C at 1,000 years.

Figure 93 shows the horizontal displacement with time for five different locations along Line CJ. The rock at the five different locations moves inwards toward the borehole centre. The displacements are 0.1 mm, 0.27 mm, 0.35 mm, 0.45 mm and 0.6 mm at distances of 1.75 m, 1.4 m, 1.26 m, 1.12 m and 0.98 m from the borehole axis, respectively.

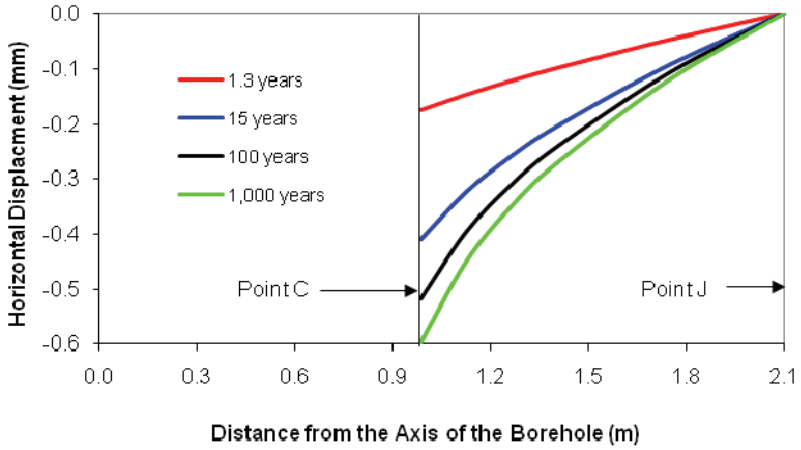


Figure 92: Thermally Induced Displacements in the Y-Direction along Line CJ

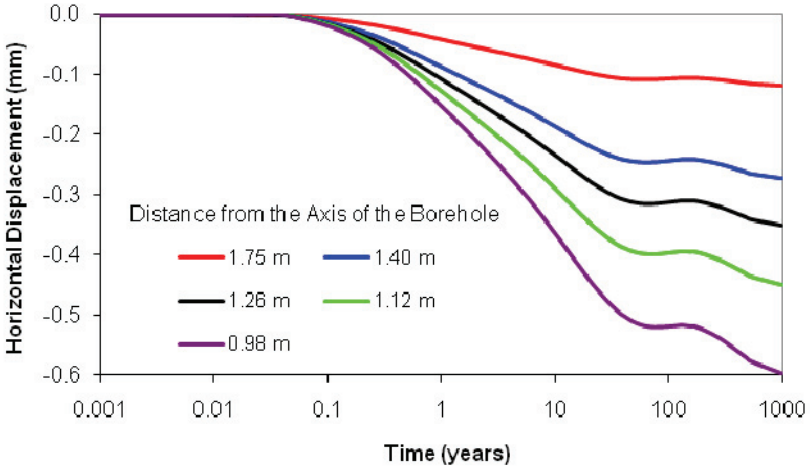


Figure 93: **Thermally Induced Displacement in the Y-Direction at Different Locations along Line CJ**

6.2.3 Combination of Excavation-Mechanical and Thermally Induced Stresses

The total stresses, calculated as the vector sum of the excavation-induced stresses and the thermally induced stresses, determine the stability of the rock along the perimeters of the in-floor borehole and placement room.

The total stresses in the X-, Y-, and Z-directions along Line AG (see Figure 45 for locations) at four different times are shown in Figures 94, 95 and 96. The peak total stress in the X-direction near Point A increases to 120 MPa at 1,000 years. The total stress in the X-direction at Point G (at 20 m above the crown of the placement room) is 57 MPa at 1,000 years. The total stress in the Y-direction is 81 MPa at the placement-room crown and 69 MPa at Point G at 1,000 years. The stress in the Z-direction at the placement-room crown is from 0 after placement room and borehole excavation to 2 MPa at 1,000 years. The Z-direction stress increases to 40 MPa at Point G at 1,000 years. Compared to the stresses from far-field model, the stresses at point G are much greater. One reason is that panel-thermal load (PTL) is used in the near-field modelling, while gross thermal load (GTL) is used in the far-field model. Using GTL in the far-field model produces lower temperature change; therefore, lower thermally induced stresses are produced. Another reason may be that the mechanical boundary conditions on the side vertical surface in the near-field model will cause higher thermally induced stresses.

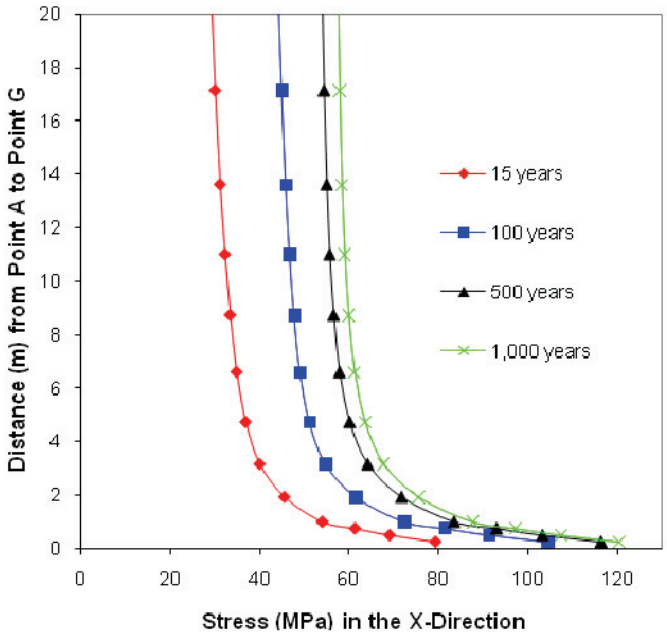


Figure 94: Profiles of Total Stresses in the X-Direction along Line AG

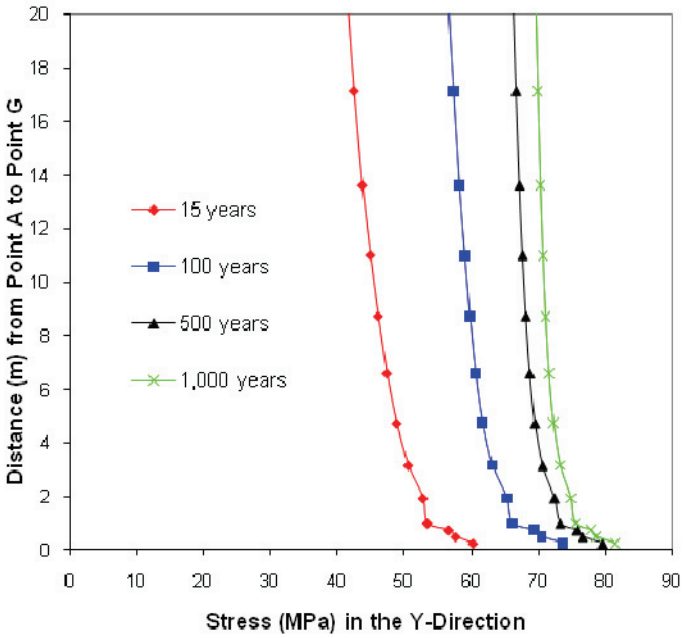


Figure 95: Profiles of Total Stresses in the Y-Direction along Line AG

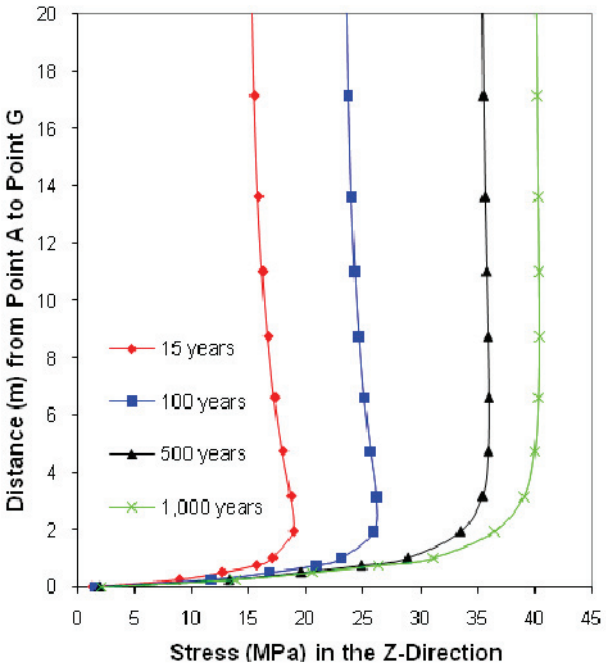


Figure 96: Profiles of Total Stresses in the Z-Direction along Line AG

The total stresses in the X-, Y-, and Z-directions along Line BH, a horizontal line from the placement room wall to the centre line of the pillar between adjacent rooms at placement room

mid-height, at different times are shown in Figures 97, 98 and 99, respectively. The stress in the X-direction is 2 MPa near Point B and increases to 35 MPa at Point H (model boundary) at 15 years. The total stress in the X-direction is about 2 MPa near Point B (the placement-room wall) and increases to 55 MPa at Point H at 1,000 years. The stress in the Y-direction is 40 MPa near Point B and increases to 47 MPa at Point H at 15 years. The total stress in the Y-direction is 52 MPa near Point B and increases to 71 MPa at Point H at 1,000 years. The stress in the Z-direction is 17 MPa near Point B, increases to 23 MPa 0.7 m from Point B and then drops to 14 MPa at Point H at 15 years. The total stress in the Z-direction is 46 MPa near Point B, increases to 61 MPa at 0.225 from Point B and then drops to 41 MPa at Point H at 1,000 years.

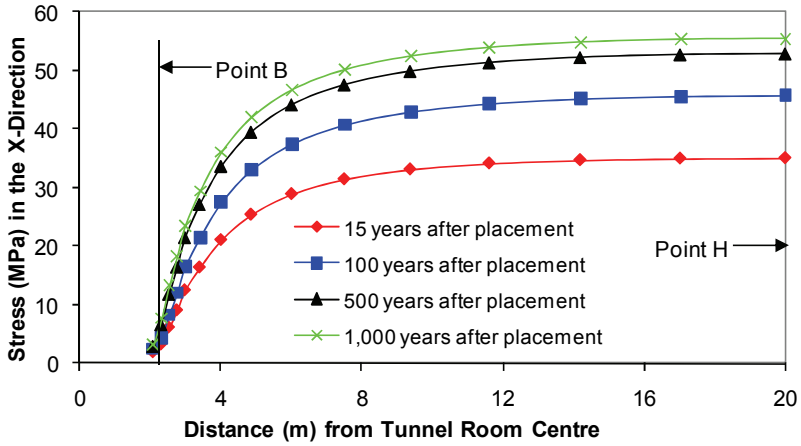


Figure 97: Profiles of Total Stresses in the X-Direction along Line BH

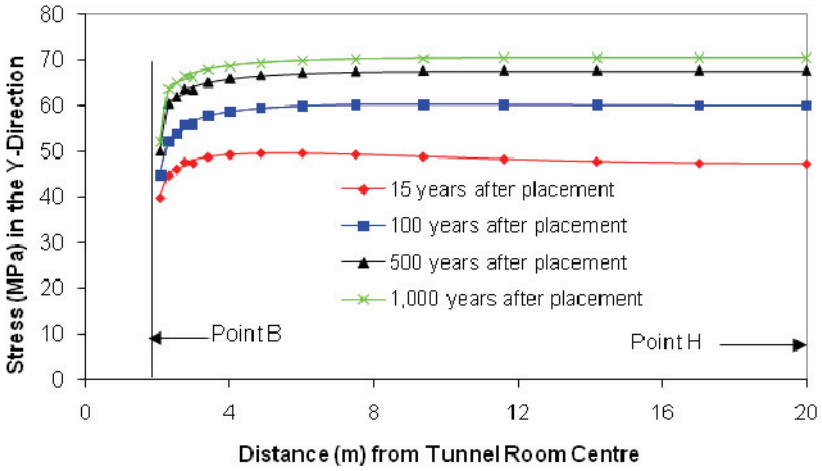


Figure 98: Profiles of Total Stresses in the Y-Direction along Line BH

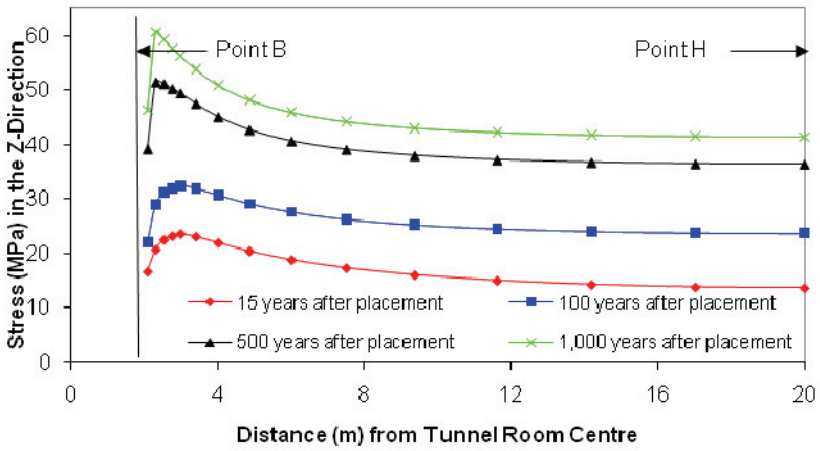


Figure 99: Profiles of Total Stresses in the Z-Direction along Line BH

The total stresses in the X-, Y-, and Z-directions along Line EI, a horizontal line between the in-floor borehole wall and the centre line of the pillar between adjacent placement rooms at the container mid-height at four different times are shown in Figures 100, 101 and 102, respectively. The stress in the X-direction is 4.5 MPa near Point E (in-floor borehole wall), increases to 41 MPa at a distance of 3.42 m from the in-floor borehole axis and then slowly drops to 36.5 MPa at Point I (model boundary) at 15 years. The total stress in the X-direction is 6 MPa near Point E, increases to 58 MPa at a distance of 4.0 m from the in-floor borehole axis, and then slowly drops to 56 MPa at Point I at 1,000 years.

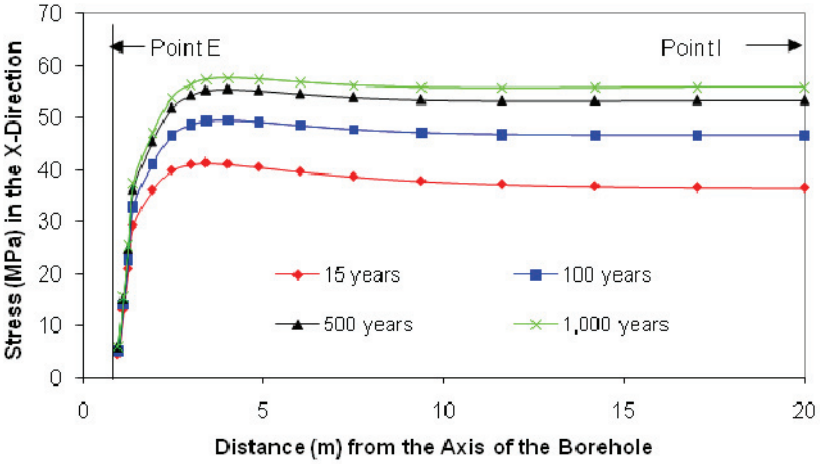


Figure 100: Profiles of Total Stresses in the X-Direction along Line EI

The stress in the Y-direction is 97 MPa near Point E and drops to 48 MPa at Point I at 15 years. The total stress in the Y-direction is 109 MPa near Point E and drops to 71 MPa at Point I at 1,000 years. The stress in the Z-direction is 25 MPa near Point E and increases to 13 MPa at

Point I at 15 years. The total stress in the Z-direction is 38 MPa near Point E and increases to 41 MPa at Point I at 1,000 years.

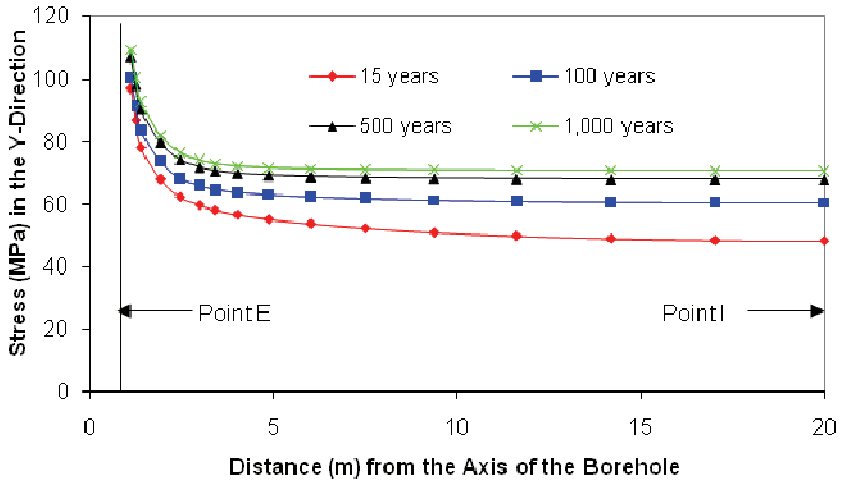


Figure 101: Profiles of Total Stresses in the Y-Direction along Line EI

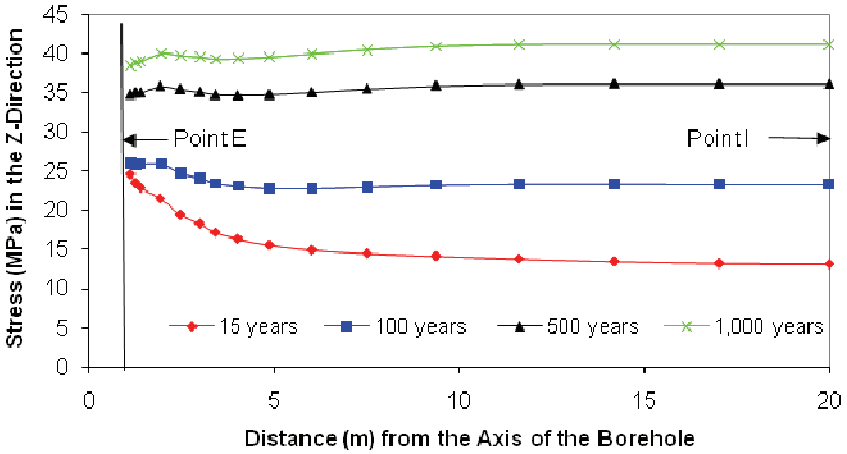


Figure 102: Profiles of Total Stresses in the Z-Direction along Line EI

Profiles of the total stresses in the X-, Y-, and Z-directions along Line FK, a horizontal line between the container axis and the mid-line of the web between adjacent boreholes at the container mid-height at four different times are shown in Figures 103, 104 and 105, respectively. The stress in the X-direction is 93 MPa near Point F (the borehole wall) and drops to 74 MPa at Point K at 15 years. The total stress in the X-direction is 128 MPa near Point F and 104 MPa at Point K at 1,000 years.

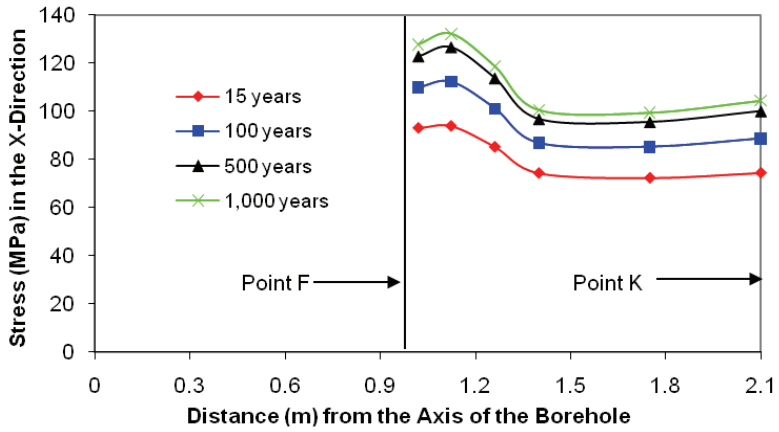


Figure 103: Profiles of Total Stresses in the X-Direction along Line FK

The stress in the Y-direction is 4.5 MPa near Point F and increases to 31 MPa at Point K at 15 years. The total stress in the Y-direction is 5.5 MPa near Point F and 40 MPa at Point K at 1,000 years. The stress in the Z-direction is 20 MPa near Point F and increases to 25 MPa at a distance of 0.14 m from Point F, and then drops to 24 MPa at Point K at 15 years. The total stress in the Z-direction is 35 MPa near Point F, increases to 45 MPa at a distance of 0.14 m from Point F and then drops to 43 MPa at Point K at 1,000 years.

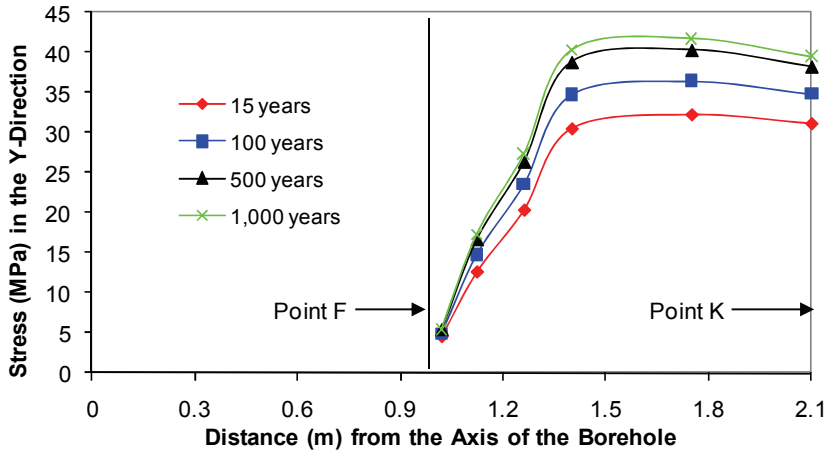


Figure 104: Profiles of Total Stresses in the Y-Direction along Line FK

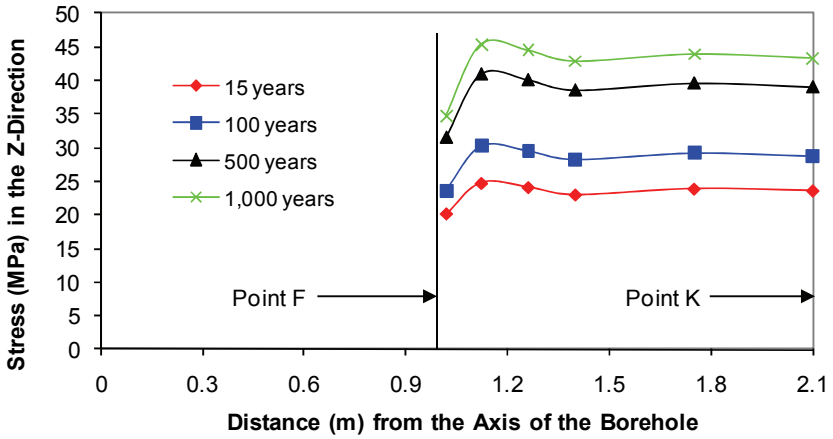


Figure 105: Profiles of Total Stresses in the Z-Direction along Line FK

Profiles of the total stresses in the X- and Y-directions along Line CJ, a horizontal line between the container axis and the mid-line of the web between adjacent boreholes along the placement-room floor are illustrated in Figures 106 and 107. The stress in the X-direction along Line CJ ranges from 134 MPa at Point C (the borehole wall) to 100 MPa at Point J at 15 years. The total stress in the X-direction along Line CJ ranges from 164 MPa at Point C to 125 MPa at Point J at 1,000 years. The stress in the Y-direction along Line CJ ranges from 4 MPa at Point C to 32 MPa at Point J at 15 years. The total stress in the Y-direction along Line CJ ranges from 5 MPa at Point C to 38 MPa at Point J at 1,000 years

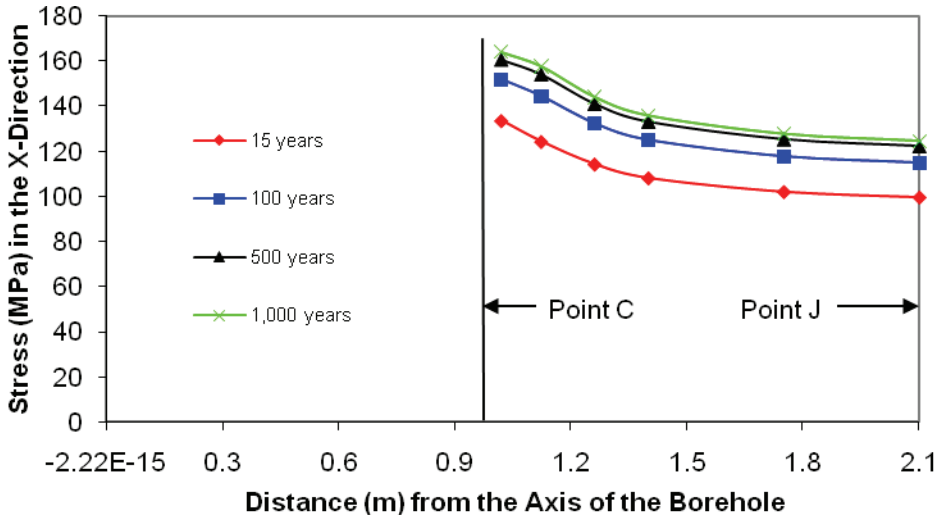


Figure 106: Profiles of Total Stresses in the X-Direction along Line CJ

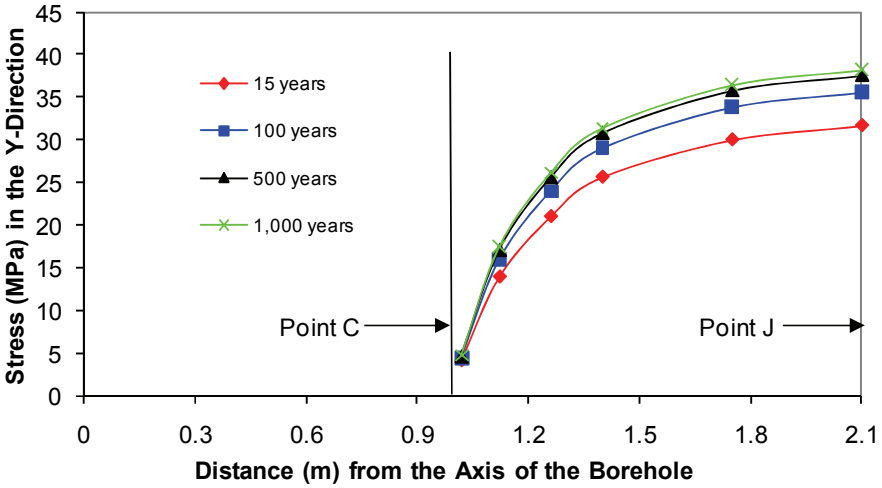


Figure 107: Profiles of Total Stresses in the Y-Direction along Line CJ

Profiles of the total stresses in the X-, Y-, and Z-directions along Line QS, a horizontal line between the container axis and the mid-line of the web between adjacent boreholes at a depth of 0.25 m from the floor of the placement room at four different times are shown in Figures 108, 109 and 110, respectively. The stress in the X-direction is 149 MPa near Point Q (the borehole wall) and drops to 110 MPa at Point S at 15 years. The total stress in the X-direction is 211 MPa near Point Q and 159 MPa at Point S at 1,000 years.

The stress in the Y-direction is 6 MPa near Point Q and increases to 43 MPa at Point S at 15 years. The total stress in the Y-direction is 8 MPa near Point Q and 59 MPa at Point S at 1,000 years. The stress in the Z-direction is 6 MPa near Point Q, increases to 11 MPa at a distance of 0.14 m from Point Q and then drops to 10 MPa at Point S at 15 years. The total stress in the Z-direction is 9 MPa near Point Q, increases to 17 MPa at a distance of 0.14 m from Point Q and then drops to 15 MPa at Point S at 1,000 years.

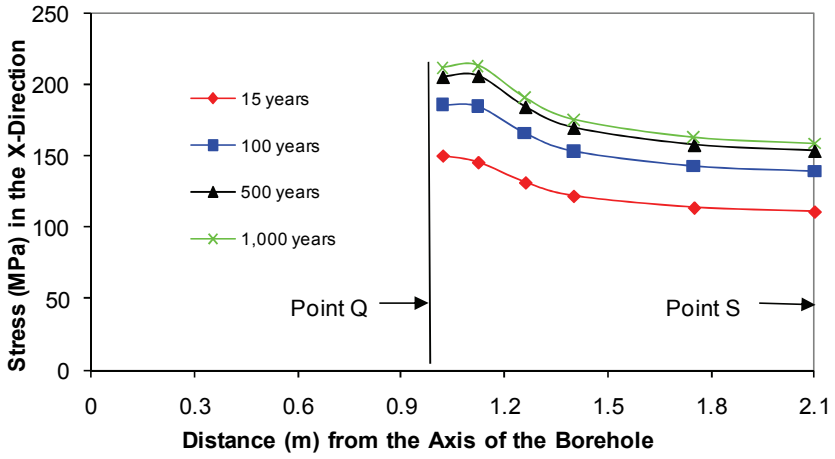


Figure 108: Profiles of Total Stresses in the X-Direction along Line QS

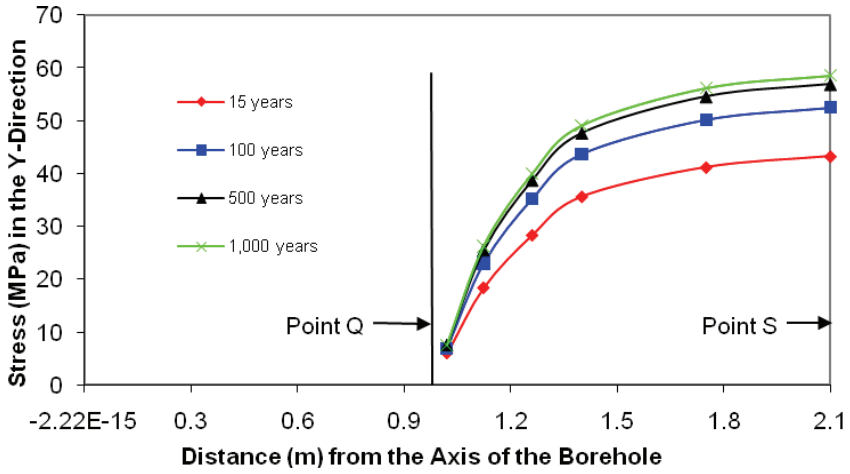


Figure 109: Profiles of Total Stresses in the Y-Direction along Line QS

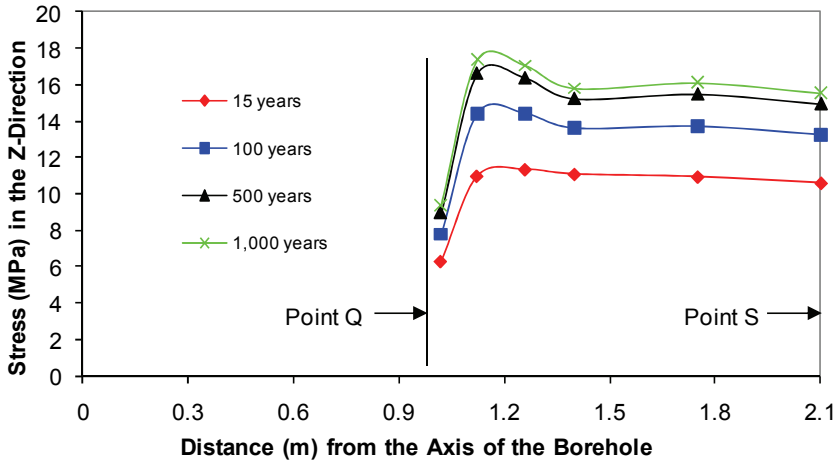


Figure 110: Profiles of Total Stresses in the Z-Direction along Line QS

6.2.4 Near-Field Stability Analyses

The lowest safety factor near the placement-room crown (0.125 m from the room crown, the centre of the element above the room crown) is 1.07 immediately upon excavation as shown in Figure 111. At Point A, the strength of the rock mass is 44 MPa due to $\sigma_3 = \sigma_r = 0$ and the tangential stress should be more than 59 MPa, the safety factor should be less than 1. However, the thickness of the failure zone is less than 0.125 m without considering progressive failure. Higher safety factors are caused by using higher "strength" values during heating of the rock for location where the rock has not exceeded a lower "strength" value during excavation, as described in Section 3.3.

The safety factors along Line BH at four different times are shown in Figure 112. The lowest safety factor is 2.2 at the wall of the placement room immediately after excavation. At 15 years, the safety factor is greater than 2.5 at all locations along this line.

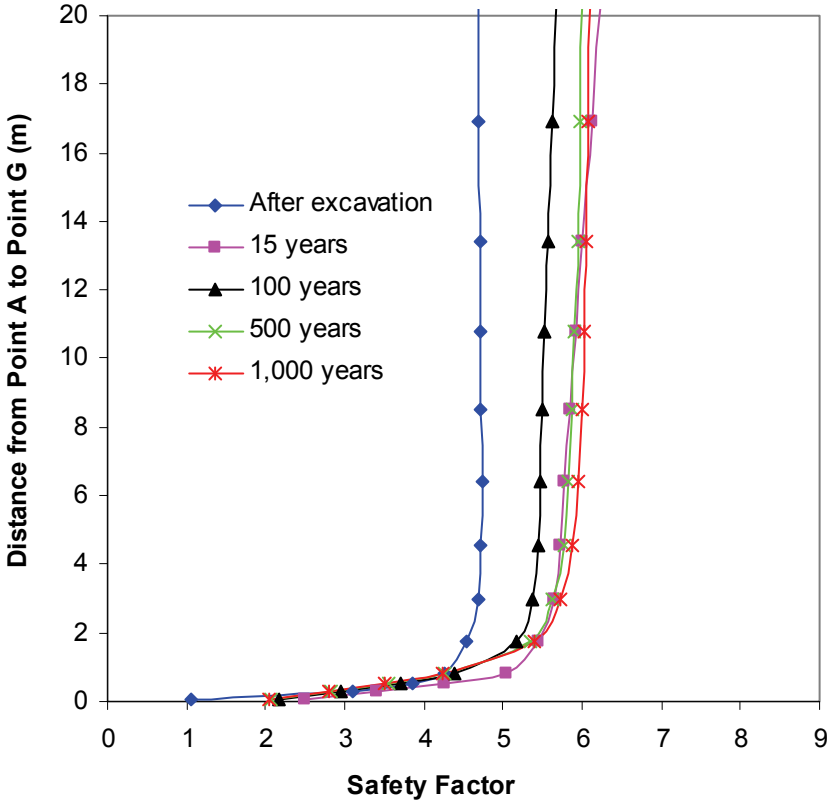


Figure 111: Safety Factors along Line AG at Four Different Times

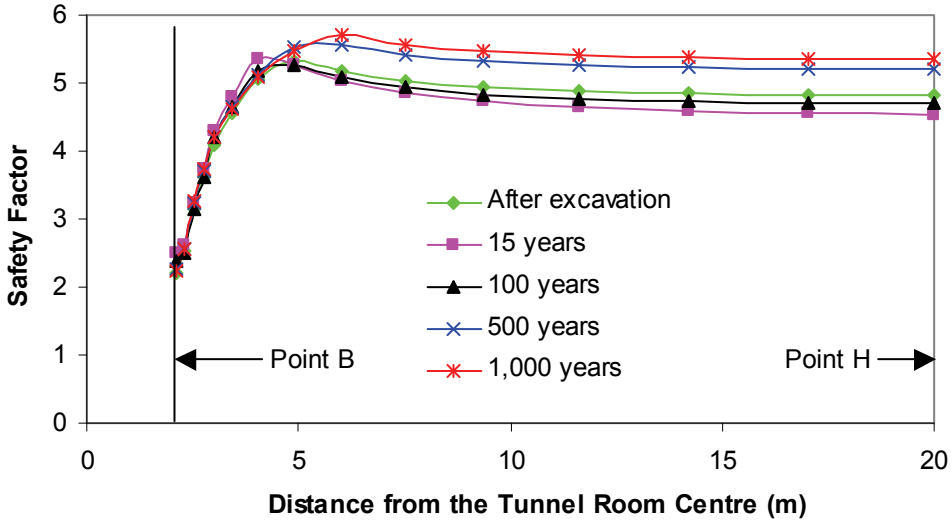


Figure 112: Safety Factors along Line BH at Four Different Times

The safety factors along Line EI at four different times are illustrated in Figure 113. The safety factor is 1.38 near the in-floor borehole wall (0.07 m from the borehole wall) immediately after excavation. The safe factors near the in-floor borehole wall are 1.07, 1.11, 1.12 and 1.07 at 15 years, 100 years, 500 years and 1,000 years, respectively. At Point E, due to $\sigma_3 = \sigma_r = 0$ and the tangential stress is more than 60 MPa as shown in Figure 61, there is a layer of excavation-induced damage zone. The thickness of the damage zone is less than 0.07 m without considering progressive failure.

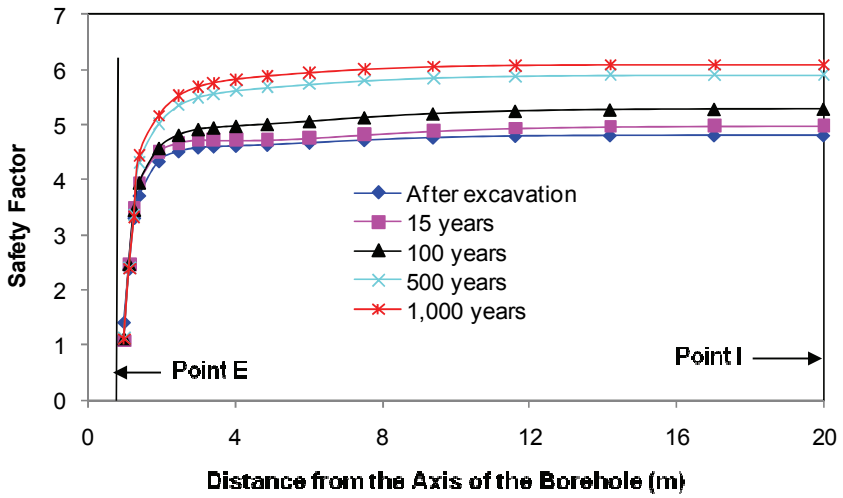


Figure 113: Safety Factors along Line EI at Four Different Times

The safety factors along Line FK at four different times are shown in Figure 114. The safety factor near the borehole wall (0.07 m from the borehole wall) is 1.5 immediately after excavation. At 15 years, the safety factor near the borehole wall (0.07 m from the borehole wall) is 1.6. After 15 years, the safety factor near the wall of borehole (0.07 m from the borehole wall) is lower than that at 15 years, but greater than 1.25. Like at Points A and E, there is layer of excavation-induced damage zone at Point F. The thickness of the damage zone is less than 0.07 m without considering progressive failure.

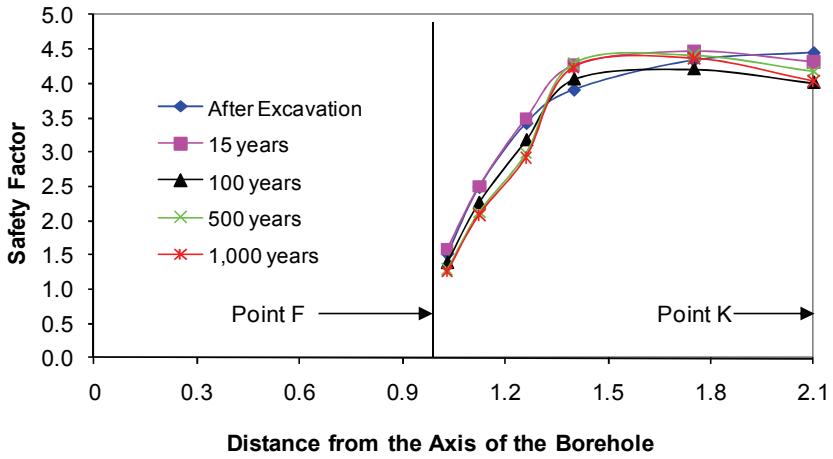


Figure 114: Safety Factors along Line FK at Four Different Times

The safety factors along Line CJ after excavation are shown in Figure 115. The safety factors after excavation at all different locations along Line CJ are less than 0.91. This implies that there is a certain thickness of rock, which is not stable. Due to symmetry, stresses at the floor of the placement room before borehole drilling would be similar to stresses at the crown of the placement room. Figure 59 shows that the rock at the floor of the placement room is not overstressed before excavation of the in-floor boreholes. Excavation of the in-floor borehole would cause the rock on the floor between two in-floor boreholes to be unstable, which would cause progressive failure in the rock along the placement-room bottom. The analysis suggests that, for the stress and strength parameters and placement geometry used, a connected zone of damaged and fractured rock would exist along the length of the placement-room floor between the adjacent in-floor boreholes. The excavation-induced yielding in the web rock will cause redistribution of the stresses in the rock. However, due to the yielding area being very small, the influence of the redistribution of the stress in the rock caused by local rock yielding is ignored in this modelling.

Safety factors along Line QS at five different times are shown in Figure 116. The safety factor near the borehole wall (0.07 m from the borehole wall) is 1.06 after excavation, 1.1 at 15 years and 1.0 at 100 years. At 1,000 years a 0.03-m thick slab of rock near the borehole wall will have a safety factor of between 0.9~1.0. The safety factor of 98% of the rock along Line QS is much greater than 1.0.

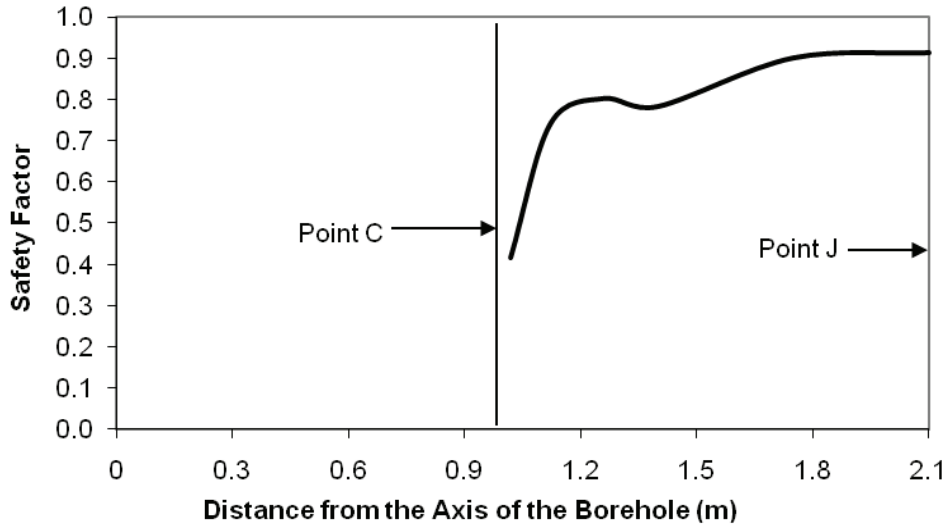


Figure 115: Safety Factors along Line CJ after Excavation

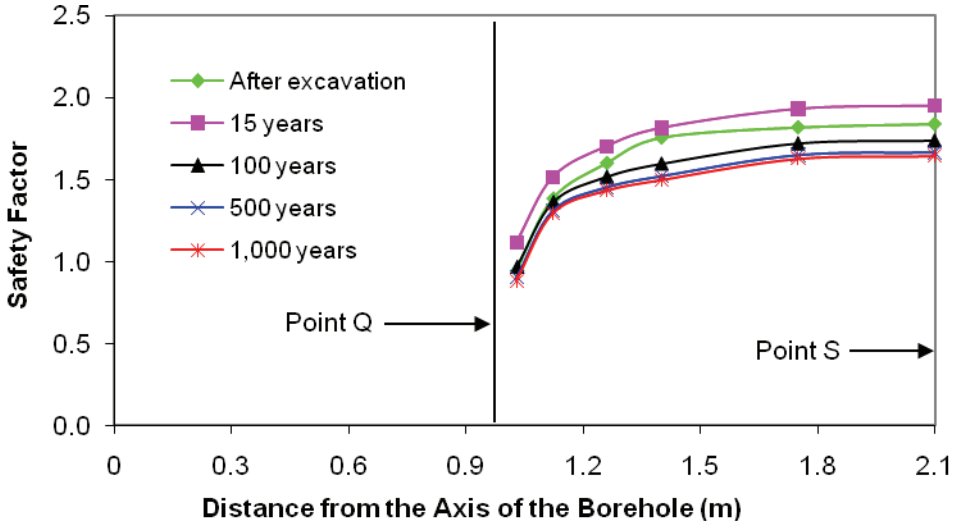


Figure 116: Safety Factors along Line QS at Five Different Times Time

Figure 117 shows the thickness of excavation-induced damage zone (EDZ) at the floor of the placement room without considering progressive failure. The greatest thickness is 0.24 m at location 0.07 m from the borehole. The thickness of the EDZ is only 0.02 m at the midpoint of the rock web between two boreholes.

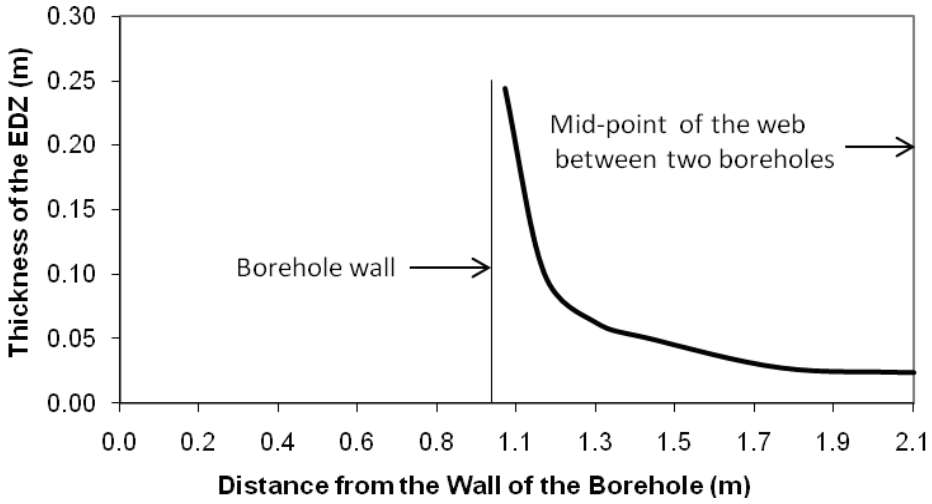


Figure 117: Thickness of the EDZ at the Floor of the Placement Room

In summary, although the safety factors along Line AG (more than 0.125 m from Point A), along Line EI (more than 0.07 m from Point E) and along FK (more than 0.07 m from Point F) are greater than 1, there will still be some failure at the roof of the placement room (at Point A) and at the borehole wall (at Point E and Point F). If there is no progressive failure happening, the thickness of the failure zone is less than 0.125 m at the roof of the placement room, 0.07 m at the borehole wall and 0.24 m at the bottom of the placement room between two adjacent boreholes. There is no damage on the wall of the placement room after excavation and during heating.

7. SUMMARY AND CONCLUSIONS

A series of three-dimensional finite-element thermal-transient and T-M structural analyses has been performed to gain a better understanding of the behaviour of the rock mass in the near-field and far-field of a DGR for used nuclear fuel using an in-floor borehole placement method.

A coupled T-M far-field three-dimensional model using the dimensions (horizontal dimensions for one quarter of a DGR are 695 m x 725 m) for an in-floor borehole placement method has been performed. Based on this modelling, the following conclusions can be drawn.

- Given an initial temperature of 11°C for a DGR at a 500-m depth, the calculated peak average rock temperature is 42°C at the centre of a repository, 27°C at the mid-point of an edge, and 19°C at the corner of a repository. Peak temperature is reached 1,500 years after waste placement.
- The maximum thermally induced uplift at the ground surface above the centre of the repository is 0.2 m. Peak uplift is reached 5,000 years after waste placement. There will be 0.4 m of subsidence caused by the rock contracting due to the decrease of the temperature by glaciation in a repository 1,000,000 years after waste placement.
- The maximum subsidence induced by ice load on the ground surface is 6.4 m at 96,000 years. The effect of ice surload on the stability of the placement rooms and boreholes was not investigated since this was beyond the scope of the near-field model out to 1,000 years.

- There will be a depth of about 37 m of rock below the ground surface in which there is no compressive stresses in the horizontal direction due to thermal expansion. Accordingly, the permeability of the rock in this region will increase.

Thermal sensitivity analyses and some preliminary coupled T-M simulations were conducted for selecting placement-room spacing and container spacing. Based on these analyses, a repository with a placement-room spacing of 40 m and a container spacing of 4.2 m was chosen as the case for further study.

Excavation-induced mechanical stresses in the rock around the placement room and the placement borehole were studied for two kinds of placement-room shapes. Although the vertical stresses at the wall of the placement room for the elliptical placement room are much greater than those for the circular placement room, they do not cause the rock to be in a yield state. The tangential stress in the rock web between the two adjacent boreholes at the floor of the placement room from the circular placement-room model is about 20~25 MPa greater than that from the elliptical placement-room model. Some damage in the inter-borehole rock web is expected from borehole drilling into the placement-room floor.

A near-field model (i.e., representing a repository of infinite horizontal extent (this means that the results are accurate only for the first 1,000 years)) is used to simulate the temperatures for 100,000 years following waste placement. The results show that the container surface has a peak temperature of 100°C at 10 years. The temperatures for other selected points near the container are also obtained. On the roof of the placement room, the temperature is 50°C after 80 years of waste placement and 56°C after 4,500 years of waste placement. The temperature at the bottom of the placement room near the borehole is 54°C after 50 years of waste placement.

A coupled near-field T-M model is also conducted for the first 1,000 years after waste placement. The stability of the rock mass is evaluated using the Hoek and Brown empirical failure criterion. Excavation of the placement room will not cause any failure in the rock surrounding the placement room. Some localized damage would occur at the roof of the placement room. The drilling of the in-floor boreholes within the placement room could cause some localized failure around the boreholes and in the rock web between two adjacent boreholes. The thickness of the damage zone is estimated to be less than 0.125 m at the roof of the placement room, about 0.24 m near the borehole and decreases to 0.02 m at the mid-point of the rock web between two boreholes and less than 0.07 m around the boreholes.

Due to the speciality of this model (lengths of the model are 5,000 m in the vertical direction and 2.1 m in the horizontal direction), the aspect ratio of the meshed elements is very great. This may have affected the simulated thermal and stress results and may have caused many of the analyses to fail due to the inability of the model calculation to converge. Possible corrective actions for solving these problems need to be investigated including the use of different programs and different type of mesh elements.

ACKNOWLEDGEMENTS

AECL technical reviews from P. Baumgartner and D. Priyanto are appreciated.

REFERENCES

Acres Consulting Services Limited in conjunction with RE/SPEC Ltd. 1985. A feasibility study of the multilevel vault concept. Atomic Energy of Canada Limited Technical Report, TR-297.**

Acres Consulting Services Ltd. 1993. A preliminary study of long-hole emplacement alternatives. Atomic Energy of Canada Limited Technical Report, TR-346.**

Baumgartner, P., D.M. Bilinsky, C. Onofrei, Y. Ates, F. Bilsky, J.L. Crosthwaite and G.W. Kuzyk. 1995. The in-room emplacement method for a used fuel disposal facility – preliminary design considerations. AECL Technical Record TR-655, COG-94-533.**

Baumgartner, P. 2005. Scoping analyses for the design of a deep geologic repository in sedimentary rock. Ontario Power Generation, Nuclear Waste Management Division Report No: 06819-REP-01300-10093-R00.*

Birgersson, L., K. Pers and M. Wilborgh. 2001. Project Jade: Long-term function and safety comparison of repository systems. Prepared by Kemakta Konsult AB for the Swedish Nuclear Fuel and Waste Management Company. SKB Technical Report TR-01-18. Stockholm Sweden.

CTECH. 2002. Deep geologic repository design update. CTECH Report 1106/MD18085/REP/01, Issue 1. (available at www.nwmo.ca)

Garisto, F., A. D'Andrea, P. Gierszewski and T. Melnyk. 2004. Third Case Study - Reference Data and Codes Ontario Power Generation Report 06819-REP-01200-10107-R00, Toronto, Ontario

Golder Associates Ltd. 1993. Used-Fuel Disposal Vault Far-Field Thermal and Thermalmechanical Analysis. Atomic Energy of Canada Limited Report, TR-M-015.**

Guo, R. 2007. Numerical modelling of a deep geological repository using the in-floor borehole placement method. Nuclear Waste Management Organization NWMO TR-2007-14. (available at www.nwmo.ca)

Guo, R. 2008. Sensitivity analyses to investigate the influence of the container spacing and tunnel spacing on the thermal response in a deep geological repository. Nuclear Waste Management Organization NWMO TR-2008-24. (available at www.nwmo.ca)

Hoek, E. and E.T. Brown. 1980. Underground excavation in rock. The Institute of Mining and Metallurgy, London.

Hoek, E. and E.T. Brown. 1988. The Hoek-Brown failure criterion – a 1988 update. 15th Canadian Rock Mechanics Symposium, Toronto, Canada.

Joint Statement. 1978. Canada/Ontario radioactive waste management program. Joint Statement by the Minister of Energy, Mines and Resources Canada and the Ontario Energy Minister, 1978 June 05. Printing and Publishing, Supply and Services Canada, Ottawa K1A 0S9 (also *In* Unpublished Documents Cited in the EIS and Primary References. Atomic Energy of Canada Limited Technical Record, TR-567, COG-92-27).

Joint Statement. 1981. Canada/Ontario joint statement on the nuclear fuel waste management program. Joint Statement by the Minister of Energy, Mines and Resources Canada and the Ontario Energy Minister, 1981 August 04. Printing and Publishing, Supply and Services Canada, Ottawa K1A 0S9 (also *In* Unpublished Documents Cited in the EIS

and Primary References. Atomic Energy of Canada Limited Technical Record, TR-567, COG-92-27).

Kaiser, P.K. and S. Maloney. 2005. Review of ground stress database for the Canadian Shield. Ontario Power Generation, Nuclear Waste Management Division Report 06819-REP-01300-10107-R00 Toronto, Canada.

Maak, P. and G.R. Simmons. 2001. Summary report: A screening study of used-fuel container geometric designs and emplacement methods for a deep geologic repository. Ontario Power Generation, Nuclear Waste Management Division Report 06819-REP-01200-10065-R00.*

Martin, C.D. 1993. The strength of massive Lac du Bonnet granite around underground openings. Ph.D. Thesis, Department of Civil and Geotechnical Engineering, University of Manitoba, Winnipeg, Manitoba, Canada.

NRCan (Natural Resources Canada). 2007. Canada's Nuclear Future: Clean, safe responsible. Natural Resources Canada news release 2007/50, June 14, 2007. (Available at www.nrcan-rncan.gc.ca/media/newsrelease/2007/200750.e.htm).

NWMO. 2005. Choosing a way forward. The Future Management of Canada's Used Nuclear Fuel. Final study. Nuclear Waste Management Organization report submitted to the Minister, Natural Resource Canada. (Available at www.nwmo.ca).

Olivella, S., A. Gens, J. Carrera and E.E. Alonso. 1996. Numerical modelling for a simulator (CODE_BRIGHT) for the coupled analysis of saline media. In Engineering Computions, Vol. 13, No. 7, pp. 87-112.

RWE NUKEM Limited. 2003a. Deep geologic repository in-floor borehole emplacement – Design changes from the in-room emplacement concept. RWE NUKEM Report 89125/REP/02.*

RWE NUKEM Limited. 2003b. Deep geologic repository in-floor borehole design update – Finite element analyses. RWE NUKEM Report 80115/REP/01.*

Tsai, A. 1986. Far-field thermal transient analyses for a used fuel disposal vault. Report No. GHED-DR-8612, Geotechnical and Hydraulic Engineering Dept., Ontario Hydro.***

Tsui, K.K. and A. Tsai. 1982. Near-field thermal and stress analyses for immobilized waste and irradiated fuel disposal vaults in crystalline hard rock. Ontario Hydro Report No. 82575.***

Tsui, K.K. and A. Tsai. 1985. Thermal analyses for different options of nuclear fuel waste placement. Atomic Energy of Canada Limited Report, AECL-7823.**

Tsui, K.K. and A. Tsai. 1994a. Three dimensional thermal and thermomechanical analyses for the near-field of a disposal vault with the borehole emplacement option. Ontario Hydro Nuclear, Report No: N-03788-940014 (UFMED).***

Tsui, K.K. and A. Tsai. 1994b. Three-dimensional thermal and thermomechanical analyses for the near-field of a disposal vault with an in-room emplacement option. Ontario Hydro Nuclear, Report No: N-03788-940015 (UFMED).***

Tsui, K.K. and A. Tsai. 1994c. The effects of sequential excavation during the construction of a disposal vault with the borehole emplacement option. Ontario Hydro Nuclear, Report No: N-03788-940016 (UFMED).***

* Available from Nuclear Waste Management Organization, 6th Floor, 22 Clair Avenue East, Toronto, Ontario M4T 2S3.
** Available from SDDO, Atomic Energy of Canada Limited, Chalk River Laboratories, Chalk River, Ontario K0J 1J0.
*** Available from Ontario Power Generation, Nuclear Waste Management Division, 17th Floor, 700 University Avenue, Toronto, Ontario M5G 1X6